CYPRUS UNIVERSITY OF TECHNOLOGY
FACULTY OF GEOTECHNICAL SCIENCES AND ENVIRONMENTAL MANAGEMENT

PhD Thesis

WATER RESOURCES OF CYPRUS UNDER CHANGING CLIMATIC CONDITIONS

Niki Cleridou

Lemesos 2014

CYPRUS UNIVERSITY OF TECHNOLOGY
FACULTY OF GEOTECHNICAL SCIENCES AND ENVIRONMENTAL MANAGEMENT
DEPARTMENT OF AGRICULTURAL SCIENCES, BIOTECHNOLOGY AND FOOD SCIENCE

WATER RESOURCES OF CYPRUS UNDER CHANGING CLIMATIC CONDITIONS

by
Niki Cleridou

Lemesos 2014

Advisory Committee

Professor V. Gkekas (Advisor)

Professor D. Hadjimitsis (Member)

Associate Professor I.M. Vardavas (External Advisor)

Πνευματικά δικαιώματα

Η έγκριση της διδακτορικής διατριβής από το Τμήμα Γεωπονικών Επιστημών, Βιοτεχνολογίας και Επιστήμης Τροφίμων του Τεχνολογικού Πανεπιστημίου Κύπρου δεν υποδηλώνει απαραιτήτως και αποδοχή των απόψεων του συγγραφέα εκ μέρους του Τμήματος.

Acknowledgements

First and foremost I would like to thank my external supervisor, Prof. Ilias Vardavas. His guidance and support from the initial to the final stage of this research enabled me to develop an understanding of the subject. Without his help, the accomplishment of this study could not be possible.

I would also like to express my deep gratitude to my supervisor, Prof. Vasilis Gkekas, for his substantial help in the progress of my work, especially at the final stage of the study.

Besides my advisors, I would like to thank Prof. Diofantos Hadjimitisis, member of the advisory comittee for his help and encouragement.

My special thanks to Dr. Barry Croke for his valuable and constructive suggestions during all the years of this research work. His willingness to give his time so generously has been very much appreciated.

Furthermore, I would like to thank Dr. Christos Matsoukas for the provision of the GCM climatic data, Dr. Nikos Benas for the calculations he did on estimating the potential evaporation and Dr. Christos Mathioudakis for technical support.

I would also like to thank the staff of the Cyprus Meteorological Service and the Cyprus Water Development Department for their provision of data. My special thanks to Dr. Georgios Petrides, former director of the Geological Survey Department, for providing me with information on the geology of the study area at the initial stage of my research.

I would like to acknowledge all academic and administrative staff of the Cyprus University of Technology who offered me their help at the various stages of my research.

Finally, I wish to thank my parents and my family for their support, love and encouragement throughout my study.

Περίληψη

Εξετάσαμε τις επιπτώσεις της κλιματικής αλλαγής στους υδάτινους πόρους της Κύπρου, στα τέλη του 21^{ου} αιώνα, μελετώντας το υδατικό ισοζύγιο της λεκάνης απορροής του ποταμού Κούρη, που αποτελεί και την πιο σημαντική λεκάνη απορροής της Κύπρου. Χρησιμοποιήθηκε ένα απλό μαθηματικό μοντέλο ημερήσιας βροχόπτωσης - απορροής σε συνδυασμό με μοντέλα υπολογισμού της ηλιακής ακτινοβολίας για τον υπολογισμό της επιφανειακής απορροής, της πραγματικής εξατμισοδιαπνοής και της κατείσδυσης του ύδατος στον υπόγειο υδροφορέα, σε ιστορικούς χρόνους και μέχρι τα τέλη του 21^{ου} αιώνα. Ο υπολογισμός της επιφανειακής απορροής της λεκάνης σε ιστορικούς χρόνους βασίστηκε σε δεδομένα από επίγειους σταθμούς καθώς και από δορυφορικά δεδομένα υψηλής ανάλυσης από το δορυφόρο MODIS, πάνω από την λεκάνη απορροής. Για τον υπολογισμό της επιφανειακης απορροής μέχρι και το τέλος του 21^{ου} αιώνα χρησιμοποιήθηκαν κλιματικά δεδομένα, όπως βροχόπτωση, θερμοκρασία κ.λ.π. από το κλιματικό μοντέλο GCM ECHAM6 του οποίου οι προβλέψεις για την εξέλιξη του κλίματος είναι ενδιάμεσες, συγκρινόμενο με άλλα παρόμοια μοντέλα. Χρησιμοποιήθηκαν κλιματικά δεδομένα από δύο ακραία σενάρια κλιματικής αλλαγής, το RCP2.6, το οποίο προβλέπει χαμηλώτερες των σημερινών εκπομπές αερίων θερμοκηπίου και το RCP8.5 που προβλέπει αυξημένες εκπομπές αερίων θερμοκηπίου μέχρι το τέλος του 21^{ου} αιώνα. Τα δύο αυτά σενάρια καλύπτουν όλο το φάσμα κλιματικών σεναρίων που υπάρχουν. Τα κλιματικά αυτά δεδομένα προσαρμόστηκαν στις διαστάσεις της υπό μελέτη περιοχής και αποτέλεσαν δεδομένα εισόδου του υδρολογικού μοντέλου. Τα αποτελέσματα έδειξαν ότι οι τιμές της μέσης ετήσιας βροχόπτωσης θα ελαττωθούν από 174 Mm^3 που είναι σήμερα στο 162 Mm^3 και 132 Mm^3 αντίστοιχα για τα δύο σενάρια μέχρι το τέλος του 21^{ου} αιώνα. Η σημερινή μέση ετήσια επιφανειακή απορροή της λεκάνης στο φράγμα του Κούρη είναι 21.5 Mm^3 και προβλέπεται να ελαττωθεί στο 16.6 Mm^3 και 6.9 Mm ^{3} για τα δύο σενάρια αντίστοιχα. Η μέση ετήσια θερμοκρασία προβλέπεται να αυξηθεί από 0.3 °C έως και 3.8 °C ενώ η μέση ετήσια δυνητική εξάτμιση προβλέπεται να αυξηθεί, από 1600 mm που είναι σήμερα, στα 1700 mm, μέχρι τα τέλη του αιώνα. Σήμερα, 31 Mm^3 ή 18% της βροχόπτωσης διατίθεται για επιφανειακή απορροή ή καταλήγει στον υπόγειο υδροφορέα. Αυτή η τιμή προβλέπεται να

ελαττωθεί στο 25 Mm^3 ή 15% και 15 Mm^3 ή 11% αντίστοιχα για τα δύο σενάρια. Η συνολική ροή στο φράγμα του Κούρη αποτελεί το 31% της συνολικής ροής σε όλα τα φράγματα της Κύπρου και μια ελάττωση της τάξης του 30% όπως προβλέπεται από το χειρότερο σενάριο, μεταφράζεται σε δραματική μείωση των υδάτινων πόρων της Κύπρου η οποία θα πρέπει να αντιμετωπιστεί με ορθολογικότερη διαχείριση των υδάτινων πόρων.

Abstract

We estimate future water resources of Cyprus by examining the water fluxes of its most important catchment, that of Kouris. Water fluxes such as surface runoff, actual evaporation and recharge are calculated by a combination of a daily rainfall-runoff model, and radiation transfer models, run with historical and predicted future climatic data. We compute the catchment discharge for historical periods based on ground-based measurements and MODIS satellite climatic data at high resolution over the catchment. Climatic change impacts on the water resources are predicted by ECHAM6, a middle range General Circulated Model. We used climatic data as input to our models, downscaled to the catchment resolution from two climate scenarios: the mild RCP2.6 and the extreme RCP8.5, to estimate water resources by the end of the 21^{st} century. The models show that the present mean annual rainfall resource of 174 Mm^3 will be reduced to 162 Mm^3 and 132 Mm^3, for the mild and extreme scenario, respectively. The present mean discharge of 21.5 Mm^3 into the Kouris dam from the catchment will decrease to 16.6 Mm^3 and 6.9 Mm^3 under the mild and extreme scenario, respectively. The present mean annual potential evaporation of about 1600 mm will increase by about 100 mm under the extreme scenario. Today an average of 31 Mm^3 of rainfall goes to surface water and groundwater resources; this will decrease to 25 Mm^3 and 15 Mm^3 under the corresponding scenarios. Given that inflow to the Kouris dam represents a significant fraction of all current inflows to the dams of Cyprus, then an almost 2/3 reduction in these inflows under the extreme scenario translates to a significantly reduced future water storage on Cyprus that will require the planning of larger engineering projects for desalination and recycling, for example, to meet its future water resource demands.

Contents

Introduction **1**

1 Cyprus Profile **9**
1.1 Cyprus geography 9
1.2 Climate 10
1.3 Water resources 13

2 Kouris Catchment **17**
2.1 Location and flows 17
2.2 Cultivation and population 19
2.3 Geology 20

3 Historical Input Data **27**
3.1 Rainfall 27
3.1.1 Spatial variability 27
3.1.2 Temporal variability 36
3.2 Discharge data 36
3.2.1 Temporal variability 38
3.3 Pan and potential evaporation 41
3.3.1 Pan evaporation 41
3.3.2 Potential evaporation 43

4 The Daily Rainfall-Runoff Model **49**
4.1 Model description 49
4.1.1 Wetting phase 50
4.1.2 Infiltration-runoff phase 52
4.1.3 Drying phase 56
4.2 Model calibration 58

5 Model Validation **63**
5.1 Graphical analyses: time-series plots . . . 63
5.2 Graphical analyses: flow duration curves . . . 67
5.3 Numerical analyses: objective function χ^2, relative error ε and Nash-Sutcliffe efficiency . . . 68
5.4 Numerical analyses: correlation criteria . . . 70
5.5 Fourier analysis of daily runoff coefficients . . . 73

6 Model Application - Kouris Catchment Hydrology **77**
6.1 Catchment evaporation . . . 77
6.2 Simulated discharge . . . 81
6.3 Recharge . . . 87
6.4 Groundwater . . . 87
6.5 Water balance . . . 88

7 Historical Observed Climate Change **95**
7.1 Representative station . . . 95
7.2 Historical trends . . . 95
7.2.1 Rainfall . . . 95
7.2.2 Temperature . . . 101
7.2.3 Discharge . . . 101

8 GCM Climate Projections **105**
8.1 Historical GCM trends . . . 107
8.2 Future GCM projections . . . 110
8.2.1 Rainfall . . . 110
8.2.2 Temperature . . . 112
8.2.3 Potential evaporation . . . 116

9 Climate Change Impact on the Water Resources **123**
9.1 Downscaling the rainfall . . . 123
9.2 Downscaling the potential evaporation (PE) . . . 125
9.3 Future catchment water balance . . . 131

10 Discussion & Conclusions **139**
10.1 Study limitations . . . 139
10.2 Recommendations for further work . . . 143

10.3 Conclusions 144

Appendices **147**

A Penman Potential Evaporation **149**

List of Figures **155**

List of Tables **161**

Introduction

The depletion of water resources in many parts of the world is a major environmental problem of this century (Hoekstra et al. 2012). Cyprus, an island in the East Mediterranean has a semi-arid climate and limited water resources, entirely depended on precipitation. The frequent droughts of the last decades together with the increase in water demand have reduced water resources considerably and Cyprus is already confronted with severe water deficit problems. In 2008, after four consecutive years of low rainfall, the available water reached a critical level and the government resorted to importing water from Greece using ship tankers. Almost all aquifers show a depleting trend and coastal aquifers have been degraded by sea water intrusion. Surface water also shows a declining trend. The government, realizing the water deficit problem early, constructed dams at the outlet of all major rivers in an effort to increase water supply. The total dam capacity increased from 6 Mm^3 in 1960 to 332 Mm^3 today including three desalination units that have been constructed since 1997.

World-wide, many studies have assessed the impact of climate change on water resources. Vaze and Teng (2011a) studied the potential impact of climate change by 2030 across New South Wales and the Australian Capital Territory, using 15 GCMs (General Circulation Models) and 2 hydrological models. Bergstrom et al. (2001) used GCM scenarios, regional climate models and hydrological runoff models to assess the impact of climate change on water resources of the Nordic area on a time scale of 50 to 100 years. Menzel and Bürger (2002) investigated the impact of climate change on the hydrology of a catchment in Eastern Germany, by the end of the 21^{st} century, using one GCM scenario and a conceptual rainfall-runoff model. Christensen et al. (2004) studied the effects of climate change on the water resources of the Colorado River basin, North America, during the 21^{st} century. The above are just a few examples of the studies that can be found in the scientific literature on climate change impacts on water resources. According to the latest IPCC (Intergovernmental Panel on Climate Change) 2013 report, by the end of this century, the planet′s climate will change in such a way that some regions will experience greater amounts of precipitation whilst others such as the Mediterranean region will experience less amounts of precipitation.

Mediterranean countries have already experienced the consequences of decreased precipitation and increased temperatures on their water resources (EEA 2012) and these consequences are expected to worsen as the climate continues to change to a drier one. Several studies have looked at the impact of a drier climate on the water resources of Mediterranean countries, such as those of Sanchez-Gomez et al. (2009), Dubois et al. (2012), Estrela et al. (2012), but few attempts have been made to describe the potential impact of climate change on the Cyprus water resources. The interest, so far, has focused on the future trends of certain climatic parameters, such as precipitation and temperature. Giannakopoulos et al. (2010) investigated the impact of climate change on precipitation and temperature over Cyprus. Lelieveld et al. (2012) used a regional climatic model to predict precipitation and temperature changes by the end of the 21^{st} century in the Eastern Mediterranean and the Middle East with a reference to Cyprus. Ragab et al. (2010) used simple climate change scenarios such as the per cent change in precipitation and temperature to predict the change in the water resources of two catchments (one being the Kouris) in Cyprus by 2050.

In the present work, for the first time to our knowledge, we calculate future water fluxes for the most important catchment in Cyprus, that of Kouris, by combining a well-tested and validated conceptual daily rainfall-runoff model (CREEK, Vardavas 1988; Croke et al. 2000) and detailed radiation transfer models (Vardavas and Taylor 2011) to generate daily discharge at the catchment outlet that feeds the Kouris dam. The climatic data, such as the daily rainfall and the monthly potential evaporation needed by the model, are obtained for the catchment from a ground-based network of rain gauges and satellite climatic data at high resolution provided by MODIS (Moderate Resolution Imaging Spectroradiometer), to generate the historical water resources. We focus on the estimation of seasonal and annual values of rainfall, surface runoff, actual evaporation and recharge of the catchment in order to first understand its hydrology and secondly to predict the potential impact of climatic changes on the water cycle of the catchment and thus on the future water resources of Cyprus. In order to assess the climatic impact on the catchment's hydrology we compare water fluxes of the catchment using both historical model input data and future GCM climatic data over Cyprus downscaled to the catchment resolution and used to generate model water fluxes up to the end of the 21^{st} century. For this purpose, we chose the middle range GCM ECHAM6 predictions for two emission scenarios for greenhouse gases (RCP2.6 and RCP8.5), which cover the range of the expected climate change.

Modeling catchment hydrology and the climatic parameters that affect it, is a process that involves inevitably uncertainties, especially when modeling future catchment hydrology. First, there is the uncertainty in the hydrological model due to its structure and its calibrated

parameters (Wilby 2005; Vaze et al. 2010; Bastola et al. 2011; Merz et al. 2011; Coron et al. 2012). Secondly, there is the uncertainty in downscaling climate parameters, such as the rainfall and the potential evaporation (Chiew et al. 2009; Chen et al. 2011), from a coarser GCM resolution to the catchment scale. Thirdly, there is the uncertainty associated with the GCM models and the scenarios of future emissions of greenhouse gases and other forcing agents, and this is the largest uncertainty according to many scientists (Prudhomme et al. 2003; Minville et al. 2008; Kay et al. 2009; Teng et al. 2012). GCMs are the best tools we have so far to describe the evolving climate system and even though a big improvement has been made in climate modeling (IPCC 2013) there is still the question of how well the climate models reproduce the chaotic climate system and how well they respond to external forcing.

In this study, and being aware of the uncertainties in our assessment of future water resources, we do not attempt to make stringent predictions about future water resources on Cyprus, but rather to assess the range of the likely impact of climate change on the future water resources, keeping in mind the worst case scenario of RCP8.5.

In the following chapters, an overview of Cyprus geography, climate and water resources is given in Chapter 1 and details of the Kouris catchment in Chapter 2. In Chapter 3 we examine the historical data on rainfall, discharge, and potential evaporation, both on a seasonal and inter-annual basis. In Chapter 4 a detailed description of the daily rainfall-runoff model, its adaptation and calibration is given. The rigorous validation of the model is covered in Chapter 5 and the application of the model to the Kouris catchment is given in Chapter 6. Historical climate change of the catchment in terms of the ground-based rainfall record since 1916 is presented in Chapter 7 while historical GCM rainfall trends and future GCM climate projections in terms of temperature, potential evaporation and rainfall are examined in Chapter 8. We look at future climate change impact on the water resources of the catchment in terms of rainfall, discharge, actual evaporation and recharge in Chapter 9. Discussion on the uncertainties involved, recommendations for further work and our conclusions are finally presented in Chapter 10.

Bibliography

Bastola, S., Murphy, C., and Sweeney, J.: The role of hydrological modelling uncertainties in climate change impact assessments of Irish river catchments, Advances in Water Resources, 34, 562-576, 2011.

Bergstrom, S., Carlsson, B., Gardelin, M., Lindstrom, G., Pettersson, A., and Rummukainen, M.: Climate change impacts on runoff in Sweden-assessments by global climate models, dynamical downscaling and hydrological modelling, Climate research, 16, 101-112, 2001.

Chen, J., Brissette, F. P., and Leconte, R.: Uncertainty of downscaling method in quantifying the impact of climate change on hydrology, Journal of Hydrology, 401, 190-202, 2011.

Chiew, F. H. S., Teng, J., Vaze, J., Post, D. A., Perraud, J. M., Kirono, D. G. C., and Viney, N. R.: Estimating climate change impact on runoff across southeast Australia: Method, results, and implications of the modeling method, Water Resources Research, 45, W10 414, doi:http://dx.doi:10.1029/2008WR007338, 2009.

Christensen, N. S., Wood, A. W., Voisin, N., Lettenmaier, D. P., and Palmer, R. N.: The effects of climate change on the hydrology and water resources of the Colorado River basin, Climatic Change, 62, 337-363, 2004.

Coron, L., Andreassian, V., Perrin, C., Lerat, J., Vaze, J., Bourqui, M., and Hendrickx, F.: Crash testing hydrological models in contrasted climate conditions: An experiment on 216 Australian catchments, 48, doi:http://dx.doi:10.1029/2011WR011721, 2012.

Croke, B., Cleridou, N., Kolovos, A., Vardavas, I., and Papamastorakis, J.: Water resources in the desertification-threatened messara valley of Crete: estimation of the annual water budget using a rainfall-runoff model, Environmental Modelling and Software, 15, 387-402, 2000.

Dubois, C., Somot, S., Calmanti, S., Carillo, A., Déqué, M., Dell'Aquilla, A., Elizalde, A., Gualdi, S., Jacob, D., L'Hévéder, B., et al.: Future projections of the surface heat and water

budgets of the Mediterranean Sea in an ensemble of coupled atmosphere-ocean regional climate models, Climate dynamics, 39, 1859-1884, 2012.

EEA: Climate change, impacts and vulnerability in Europe 2012. An indicator-based report, 2012.

Estrela, T., Pérez-Martin, M., and Vargas, E.: Impacts of climate change on water resources in Spain, Hydrological Sciences Journal, 57, 1154-1167, 2012.

Giannakopoulos, C., Hadjinicolaou, P., Kostopoulou, E., Varotsos, K., and Zerefos, C.: "Precipitation and temperature regime over Cyprus as a result of global climate change", Advances in Geosciences, 23, 17-24, 2010.

Hoekstra, A. Y., Mekonnen, M. M., Chapagain, A. K., Mathews, R. E., and Richter, B. D.: PLoS One, 7, e32 688, 2012.

IPCC: Climate Change 2013: The Physical Science Basis. Contribution of Working Group I to the Fifth Assessment Report of the Intergovernmental Panel on Climate Change [Stocker, T. F., D. Qin, G.-K. Plattner, M. Tignor, S. K. Allen, J. Boschung, A. Nauels, Y. Xia, V. Bex and P. M. Midgley (eds.)], Cambridge University Press, Cambridge, United Kingdom and New York, NY, USA, 2013.

Kay, A., Davies, H., Bell, V., and Jones, R.: Comparison of uncertainty sources for climate change impacts: flood frequency in England, Climatic Change, 92, 41-63, 2009.

Lelieveld, J., Hadjinicolaou, P., Kostopoulou, E., Chenoweth, J., El Maayar, M., Giannakopoulos, C., Hannides, C., Lange, M., Tanarhte, M., Tyrlis, E., and Xoplaki, E.: Climate change and impacts in the Eastern Mediterranean and the Middle East., Climatic Change, 114, 667-687, doi:10.1007/s10584-012-0418-4, 2012.

Menzel, L. and Bürger, G.: Climate change scenarios and runoff response in the Mulde catchment (Southern Elbe, Germany), Journal of hydrology, 267, 53-64, 2002.

Merz, R., Parajka, J., and Blöschl, G.: Time stability of catchment model parameters: Implications for climate impact analyses, Water Resources Research, 47, 2011.

Minville, M., Brissette, F., and Leconte, R.: Uncertainty of the impact of climate change on the hydrology of a nordic watershed, Journal of hydrology, 358, 70-83, 2008.

Prudhomme, C., Jakob, D., and Svensson, C.: Uncertainty and climate change impact on the flood regime of small UK catchments, Journal of Hydrology, 277, 1-23, 2003.

Ragab, R., Bromley, J., Dorflinger, G., and Katsikides, S.: IHMS—Integrated Hydrological Modelling System. Part 2. Application of linked unsaturated, DiCaSM and saturated zone, MODFLOW models on Kouris and Akrotiri catchments in Cyprus, Hydrological Processes, 24, 2681-2692, 2010.

Sanchez-Gomez, E., Somot, S., and Mariotti, A.: Future changes in the Mediterranean water budget projected by an ensemble of regional climate models, Geophysical Research Letters, 36, 2009.

Teng, J., Vaze, J., Chiew, F. H., Wang, B., and Perraud, J.-M.: Estimating the Relative Uncertainties Sourced from GCMs and Hydrological Models in Modeling Climate Change Impact on Runoff, Journal of Hydrometeorology, 13, 2012.

Vardavas, I.: A simple water balance daily rainfall-runoff model with application to the tropical Magela Creek catchment, Ecological Modelling, 42, 245-264, 1988.

Vardavas, I. and Taylor, F.: Radiation and Climate: Atmospheric Energy Budget from Satellite Remote Sensing, International Series of Monographs on Physics, OUP Oxford, 2011.

Vaze, J. and Teng, J.: Future climate and runoff projections across New South Wales, Australia: results and practical applications, Hydrological Processes, 25, 18-35, 2011a.

Vaze, J., Post, D., Chiew, F., Perraud, J.-M., Viney, N., and Teng, J.: Climate non-stationarity-validity of calibrated rainfall-runoff models for use in climate change studies, Journal of hydrology, 394, 447-457, 2010.

Wilby, R. L.: Uncertainty in water resource model parameters used for climate change impact assessment, Hydrological Processes, 19, 3201-3219, 2005.

Chapter 1

Cyprus Profile

1.1 Cyprus geography

Cyprus is an island in the East Mediterranean (Figure 1.1) lying between 34°33′ and 35°41′ North and between 32°20′ and 34°35′ East. It is the third largest island of the Mediterranean after Sicily and Sardinia. It has a maximum length of 240 km from east to west and a maximum width of 100 km from north to south. It covers an area of 9251 km^2 of which 9240 km^2 is land and 10 km^2 is water. According to the World Bank report published in 2009 the agricultural land is 1247 km^2 or 13.5% of total land area and 20.8% of it is irrigated. Forests cover an area of 1730 km^2 or 18.7% of the total land area and has a coastline of 772 km. All statistics and data that follow refer to the Cyprus government controlled area.
Cyprus is traversed by two mountain ranges: Troodos, the main massif in the central and southwest part of the island and Pendadaktylos, a narrow massif, lying along the northern coast (Figure 1.2). Troodos highest mountain is Olympus, at 1953 m elevation and Pen-

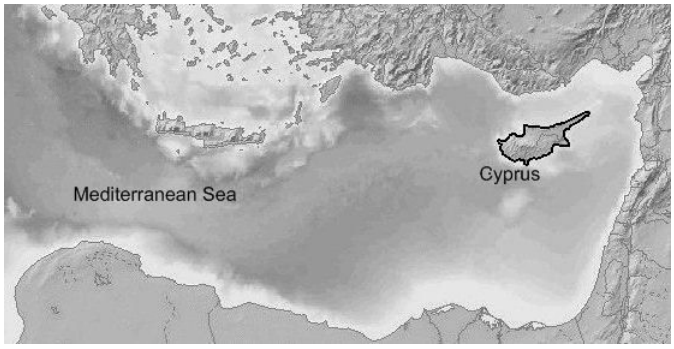

Figure 1.1: The East Mediterranean with the island of Cyprus shown near the Middle East coast.

Figure 1.2: A geological map of Cyprus.

dadaktylos highest point is at 1019 m. The Troodos massif plays an important role in the water resources of Cyprus. It controls the climate of Cyprus and the major groundwater resources of Cyprus are related to it. The main rivers of Cyprus originate in the Troodos extending radially to feed the plains and the aquifers. Around the Troodos mountain the region is hilly. Between the two massifs there is Mesaoria, the central plain. Along the coast there are narrow fertile plains.

1.2 Climate

The island has a semi-arid climate (according to FAO) with cool wet winters from November to March and dry hot summers from May to September. Snow falls only in the Troodos mountains. Most of the snow falls in January and February, but it has snowed as early as October (24/10/2000) and as late as May (17/05/1992). The average number of days per year with snow for the period 1976-1991 was 38.

Temperature

Air temperature shows great diversity. It depends on the altitude, the season and whether it is day or night. The mean annual daily temperature (1991-2005) of Lefkosia, the capital of Cyprus, at elevation of 162 m (Athalassa station) is 19.7 °C but in January the mean daily value is 10.6 °C and in July it is 29.7 °C. However, the daily temperature may climb up to 45 °C in the summer (recorded value 45.6 °C in August 2010) and may fall to a few degrees

below zero in winter (recorded value -2.9 °C in February 1997). At Prodromos, elevation 1380 m, the mean annual daily temperature (1991-2005) is 13 °C but in January the mean daily value is 3.5 °C and in July it is 23.3 °C. However, a minimum temperature of -10.2 °C in February and a maximum temperature of 35.4 °C in July have been recorded. There are also big differences between daytime and nighttime temperatures that can be as high as 20 °C. Since the beginning of the 20 th century, there is an increasing trend in the mean annual temperature, ranging from 1 °C to 1.3 °C, statistically significant at the 99.9% level (Price et al. 1999). This local warming is approximately twice the observed globally averaged warming over the last century (Houghton et al. 1996).

Precipitation

Normal annual precipitation is 503 mm (normal value refers to the mean of period 1961/62-1990/91) but it is very much dependent on the altitude, varying from about 300 mm at the coasts to over 1000 mm at the highest regions of Troodos. There is also great variability with time. There were dry years with a mean annual precipitation less than 400 mm and very wet years with more than 600 mm. Within a year, on average, 90% of annual precipitation falls from October to April.

Since the beginning of the 20th century there is a declining trend in precipitation, by about 1 mm per year. Regression analysis on the diagram of annual rainfall with time (Figure 1.3) gives a decreasing trend of -1.02 ± 0.66 mm per year at the 95% confidence level. The reduction is also evident in the long-term averages of annual precipitation. The mean annual rainfall for the thirty-year period 1916/17-1945/46 was 548 mm and that for the period 1980/81-2009/10 was 464 mm, implying a reduction of about 15%.

Evaporation

About 86% of annual precipitation is lost to evaporation, which exhibits seasonal and regional variability. It is low in winter, the minimum value occuring in January and high in summer, with the maximum in July. Evaporation decreases with altitude. Mean daily class A pan evaporation for the period 1991-2005 gives for January 1 mm/day at Prodromos station at 1380 m elevation and 2.6 mm/day at Larnaca station at 1 m elevation. The July values are 7.4 mm/day and 9.9 mm/day, respectively.

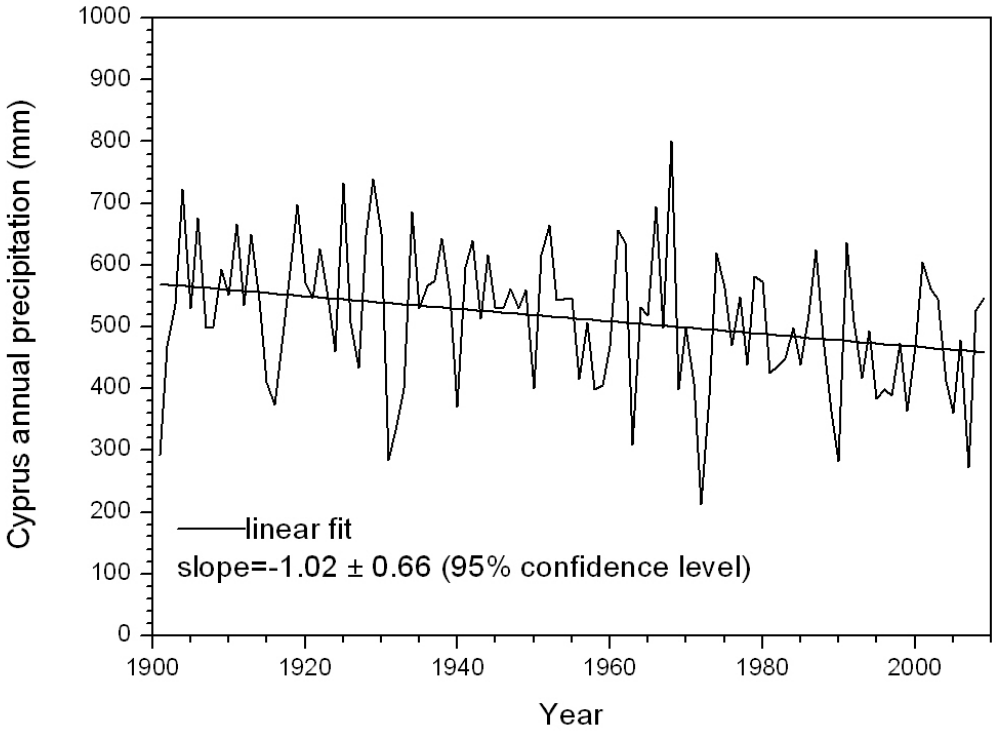

Figure 1.3: Cyprus annual precipitation since the beginning of the 20th century. The regression line is also shown.

1.3 Water resources

Water resources can be divided into surface water and groundwater bodies.

Surface water

Surface water includes the lakes and the rivers. There are 5 lakes which are saline or brackish that dry up regularly. The rivers are small and almost all of them flow only in winter, with their flow controlled by precipitation. Only sections of few rivers flow all year round. The Water Development Department (WDD) of the republic of Cyprus measures the flow of 31 rivers since 1970 (Georgiou 2002). All of them originate from the Troodos mountains. They drain almost all in an area with an elevation more than 500 m and since this area is the most productive we may say that their total surface runoff is essentially the total surface runoff of the island.

Groundwater

There are 66 aquifers which are grouped into 20 groundwater bodies. Most of the aquifers are found below river beds and coastal alluvial deposits. There is also the complex system of Troodos fractured aquifers with water trapped in cracks, joints, fractures and faults. Most of the springs with a substantial flow are related to the Troodos igneous aquifers. The biggest has daily flows from 1500 m^3 to 7000 m^3. All coastal aquifers are over exploited and their water level is below the sea level, so there is a problem of sea intrusion. Ten are connected to the sea. The construction of dams upstream of several aquifers has deprived them of the riverbed recharge.

Water Balance

The mean annual precipitation of Cyprus for the period 1970/71-1999/2000 is 463 mm, of this 86% is lost to evaporation and only 14% of precipitation goes to surface water and groundwater. Water demand was estimated to be 215 Mm^3 in 1994, 265.9 Mm^3 in 2000 and 313.7 Mm^3 by 2020, i.e. an increase of about 46% in a 27- year period (Savvides et al. 2001). On the other hand, according to regional GCM scenarios, the future climate in the region of Cyprus will be even drier. Considering that water resources replenishment depends entirely on precipitation and that most of the consumed water comes from groundwater and surface resources, with only a small portion covered by desalination units, the prospects of the future water supply are very grim.

Bibliography

Georgiou, A.: Reassessment of the island's water resources and demand, Objective 1 - Output 1.4.2, Assesssment of Groundwater Resources of Cyprus, Ministry of Agriculture, Natural Resources and Environment of the Republic of Cyprus, 2002.

Houghton, J. T., Meira Filho, L., Callander, B. A., Harris, N., Kattenberg, A., and Maskell, K.: Climate change 1995: The science of climate change. Contribution of working group I to the second assessment report of the IPCC, Cambridge University Press, Cambridge, 1996.

Price, C., Michaelides, S., Pashiardis, S., and Alpert, P.: Long term changes in diurnal temperature range in Cyprus, Atmospheric Research, 51, 85-98, 1999.

Savvides, L., Dorflinger, G., and Alexandrou, K.: The assessment of water demand of Cyprus. Report, objective 1- output 1.5.1, Ministry of Agriculture, Natural Resources and Environment, Water Development Department and Food and Agriculture Organization of the United Nations (FAO) Land and Water Development Division. TCP/CYP/8921, FAO, Rome., p. 12, 2001.

Chapter 2

Kouris Catchment

2.1 Location and flows

The Kouris catchment is the major drainage system of Cyprus and it is thus selected as the study area. It has an area of about 300 km^2, lying on the southern slopes of the Troodos massif, the main massif of Cyprus. It extends from an elevation of 1978 m north to sea level in the south, along a distance of about 30 km, giving thus rise to very high slopes. It has an extensive network of streams and it is drained by three major rivers, Kouris, Limnatis and Kryos (Figure 2.1). Limnatis and Kryos meet Kouris (the river with the biggest flow in Cyprus) upstream of the Kouris dam, the biggest dam of Cyprus with a 110 Mm^3 capacity (Figure 2.2). The drained area upstream of Kouris dam is about 278 km^2. Kouris river has a mean annual flow of 9.7 Mm^3 (over the period 1989/90-2008/09) and rarely flows all year, with summer flow when it occurs sustained by spring water. The mean annual flow of Limnatis and Kryos for the same period was 9.3 Mm^3 and 2.5 Mm^3, respectively, giving a total of 21.5 Mm^3 annually while the average annual inflow to all Cyprus dams for the same period was 69.9 Mm^3, implying that 31% of this inflow comes from the rivers Kouris, Limnatis and Kryos. The catchment gives the largest contribution, among all other catchments, to the total surface runoff of the island. Since 1998, water from Arminou dam, lying outside the catchment, is also transferred to the Kouris dam. Since the construction of the Kouris dam in 1988, the dam has overflowed only twice: in the winter of 2004 (2003/04 hydrological year which begins on 1^{st} October and ends 30^{th} September) and in the winter of 2012 (2011/12 hydrological year). In most years its water level is low, the lowest occurring in October 2008 corresponding to 0.1 Mm^3 water storage.

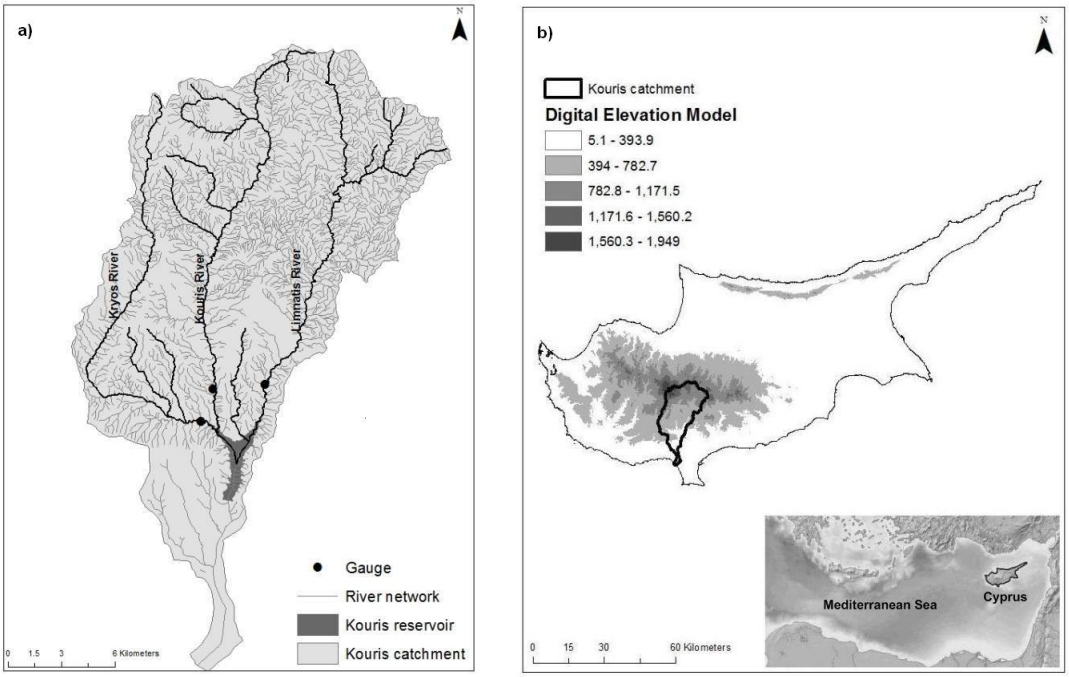

Figure 2.1: The Kouris catchment with the river network and a map of Cyprus with an outline of the catchment boundary. Also shown is the location of Cyprus in the Eastern Mediterranean region.

Figure 2.2: The Kouris dam

Figure 2.3: Wild vegetation of Troodos.

Figure 2.4: Troodos cedar forest.

2.2 Cultivation and population

The Kouris catchment is sparsely populated. The northern part is not cultivated at all and has coniferous trees (Figures 2.3 and 2.4). In the south it is partly cultivated mainly with vineyards, deciduous trees and some seasonal crops (Figure 2.5). The irrigated area upstream of Kouris dam is about 17 km^2.

Figure 2.5: Vineyards on the south slopes of Troodos.
(http://www.libertasperpetuum.wordpress.com/2013/01/14/cyprus/)

2.3 Geology

The Troodos massif occupies the central part of the island and plays an important role in the water resources of Cyprus. It controls the climate of Cyprus and the major groundwater resources of Cyprus are related to it. The main rivers of Cyprus originate in the Troodos, extending radially to feed the plains and the aquifers. Troodos is part of the ophiolite sequence that stretches from the Alps to the Himalayas through Greece, Cyprus, Turkey etc. and is considered to be the best exposed ophiolite in the world. Ophiolites are composed of hard rocks (basalt, dolerite, gabbro and peridotite) formed in the mid-oceanic ridges after tectonic fracturing and hydrothermal alteration (Dewandel et al. 2005).

The catchment consists of the upper mountainous ophiolite complex and the lower overlying sedimentary complex. The ophiolite complex comprises harzburgites, dunites, serpentines and gabbros (Figure 2.6) on the highest elevations followed by sheeted dykes (Figure 2.7) and pillow lavas (Figure 2.8). Hartzburgites and gabbros are very thick bodies (up to kilometers) and highly fractured. Joints and faults are open to the surface and are the main pathways for infiltration. Dykes have a thickness of up to 500 m, are less fractured and infiltration is lower. Pillow lavas have a thickness varying from 50 m to 200 m, are even less fractured than dykes and have low permeability. Borehole records show that gabbros are the most productive aquifers followed by dunites, serpentites and sheeted dykes. Pillow lavas are very poor aquifers. Groundwater circulation takes place mostly at a depth of up to 100 m and to a lesser degree in the tectonic fractures. The sedimentary complex is made of limestone, marls and chalks of low permeability (Figure 2.9). The marls fill the faults and block the recharge and the movement of groundwater. In the places where there are chalks, limited

Figure 2.6: Outcrop of harzburgite (background) and gabbro (foreground) in a tectonic contact at the Troodos ophiolite.
(http://www.cyprusgeology.org/english/EN/index.htm/)

karstic phenomena were developed and the circulation of groundwater is allowed (Georgiou 2002). The thickness of the sediments varies from a few tens of meters to more than 600 m. It is a poor aquifer with 70% of boreholes drilled being unsuccessful in finding adequate water. Details of the geology and hydrogeology of the catchment are given in the work of Boronina et al. (2003b). The hydrogeology of the area of Troodos is very complicated (Georgiou 2002) and thus, for the purposes of this study, we consider the whole catchment as one complex aquifer.

Figure 2.7: Sheeted dykes of Troodos ophiolite.
(http://www.sandatlas.org/2012/06/sheeted-dikes-of-the-troodos-ophiolite/)

Figure 2.8: Outcrop of pillow lavas of Troodos ophiolite.
(http://www.sandatlas.org/2012/04/pillow-lava-in-cyprus/)

Figure 2.9: Chalks and marls in the sedimentary complex.
(http://www.cyprusgeology.org/english/EN/index.htm/)

Bibliography

Boronina, A., Renard, P., Balderer, W., and A., C.: Groundwater resources in the Kouris catchment(Cyprus): data analysis and numerical modelling, Journal of Hydrology, 271(1-4), 130-149, 2003b.

Dewandel, B., Lachassagne, P., Boudier, F., Al-Hattali, S., Ladouche, B., Pinault, J., and Al-Suleimani, Z.: "Evaluation of approaches for estimation of rainfall and the Unit Hydrograph", Hydrogeology Journal, 13, 708-726, 2005.

Georgiou, A.: Reassessment of the island's water resources and demand, Objective 1 - Output 1.4.2, Assesssment of Groundwater Resources of Cyprus, Ministry of Agriculture, Natural Resources and Environment of the Republic of Cyprus, 2002.

Chapter 3

Historical Input Data

3.1 Rainfall

3.1.1 Spatial variability

Mean daily rainfall data are obtained from 16 stations (their characteristics are shown in Table 3.1) at various elevations (highest at 1380 m and lowest at 220 m) for the period 1989/90 to 2008/09. The rainfall increases with elevation and the difference in annual rainfall between

Table 3.1: Characteristics of rainfall stations

Station Number	Station Name	Elevation (m)	Lat. North	Long. East
313	KOURIS (DAM)	220	$34^o\ 43'$	$32^o\ 55'$
311	ALASSA (E.S.)	340	$34^o\ 46'$	$32^o\ 56'$
347	APESIA (E.S.)	470	$34^o\ 47'$	$32^o\ 59'$
295	DOROS	480	$34^o\ 49'$	$32^o\ 55'$
321	LANEIA	580	$34^o\ 50'$	$32^o\ 55'$
325	AGIOS MAMAS	580	$34^o\ 51'$	$32^o\ 57'$
320	SAITTAS (N.G.)	640	$34^o\ 52'$	$32^o\ 55'$
232	AGIOS THERAPON	675	$34^o\ 48'$	$32^o\ 50'$
400	KALO CHORIO (P.S.)	730	$34^o\ 51'$	$33^o\ 01'$
260	KOILANI (P.S.)	820	$34^o\ 51'$	$32^o\ 52'$
207	OMODOS (E.S.)	840	$34^o\ 51'$	$32^o\ 48'$
410	AGIOS THEODOROS	995	$34^o\ 53'$	$33^o\ 02'$
377	AGROS	1015	$34^o\ 55'$	$33^o\ 01'$
250	PANO PLATRES	1115	$34^o\ 53'$	$32^o\ 52'$
337	KYPEROUNTA (E.S.)	1135	$34^o\ 56'$	$32^o\ 58'$
301	PANO AMIANTOS	1380	$34^o\ 56'$	$32^o\ 55'$

the lowest and the highest station ranges from 24% (dry year, 1989/90) to 62% (wet year, 2001/02) and it is independent of the catchment mean annual rainfall. The annual rainfall at the 16 stations for the period 1989/90 to 2008/09 is shown in Table 3.2. In order to calculate the mean daily rainfall of the catchment we have thus to take elevation into consideration.

We used a digital elevation model (DEM) of the catchment and we divided the catchment in N cells, attributing n_j cells to each station j, as was done in Croke et al. (2000). The catchment mean daily rainfall P_i on day i is the weighted arithmetic mean value of the daily rainfall values $P_{i,j}$ recorded at each station j via Eq. 3.1:

$$P_i = \frac{\sum_{j=1}^{ns} w_j P_{i,j}}{\sum_{j=1}^{ns} w_j} \tag{3.1}$$

where ns is the number of meteorological stations and w_j the adjusted weight of each station j, defined by Eq. 3.2:

$$w_j = \frac{n_j}{N}\left(1 + \frac{\Delta P_j}{P_j}\right) \tag{3.2}$$

with ΔP_j being the difference between annual rainfall at the average height of the area the station j is located within and P_j the annual rainfall at the station. ΔP_j is estimated from the regression line of the scatter diagram of annual rainfall against elevation. In Figures 3.1 - 3.5 are shown the scatter diagrams of the annual rainfall against elevation for the hydrological years 1989/90 to 2008/09. In this way we calculate the adjusted weights of the stations for a specific year. The long-term average adjusted weights for each one of the 16 stations range from 0.0333 to 0.1183 and the corresponding standard deviations range from 0.00003 to 0.0007. Thus, for every station, the variation of its adjusted weight with years is very small and the long-term average for the period 1989/90 to 2008/09 is taken as the adjusted weight of the station.

For the Kouris catchment the use of simple weights, defined by Eq. 3.3:

$$w_j = \frac{n_j}{N} \tag{3.3}$$

produced on average about less than 0.3% difference in the catchment annual rainfall and less than 1% difference in the computed annual discharge compared to when the adjusted weights were used. So, we used the adjusted weights, which have a more general formulation. The long-term average adjusted and simple weights of each station for the period 1989/90 to 2008/09 are shown in Table 3.3.

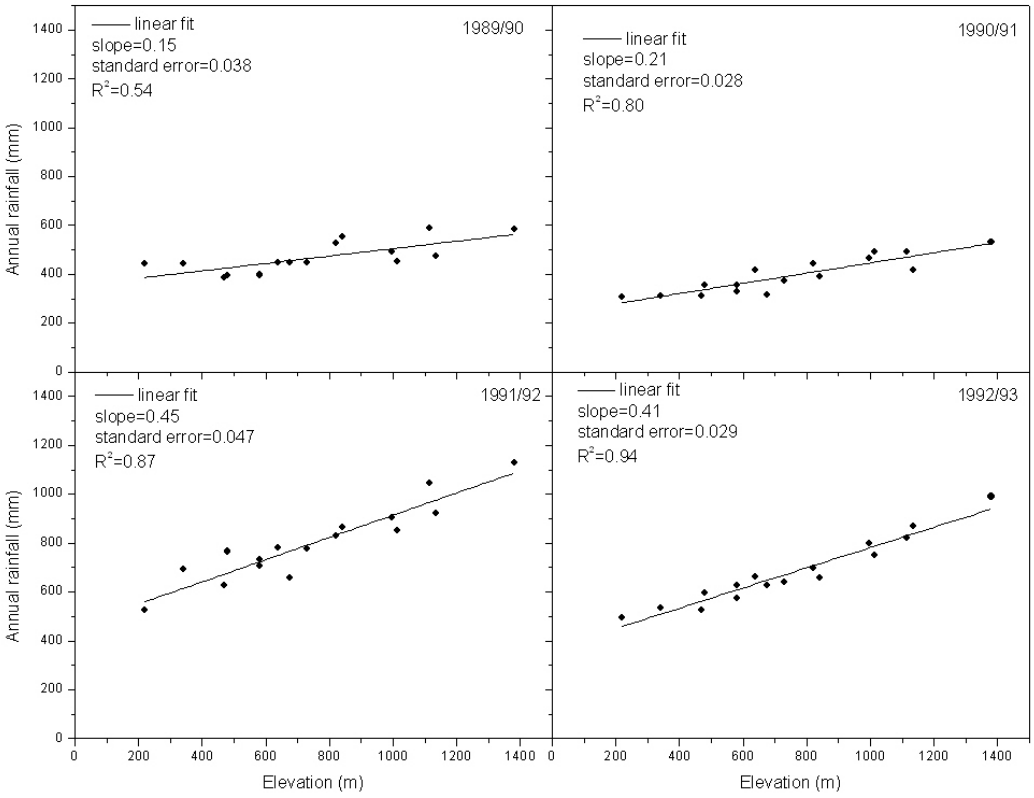

Figure 3.1: Annual rainfall of the 16 stations plotted against elevation for the hydrological years 1989/90 to 1992/93.

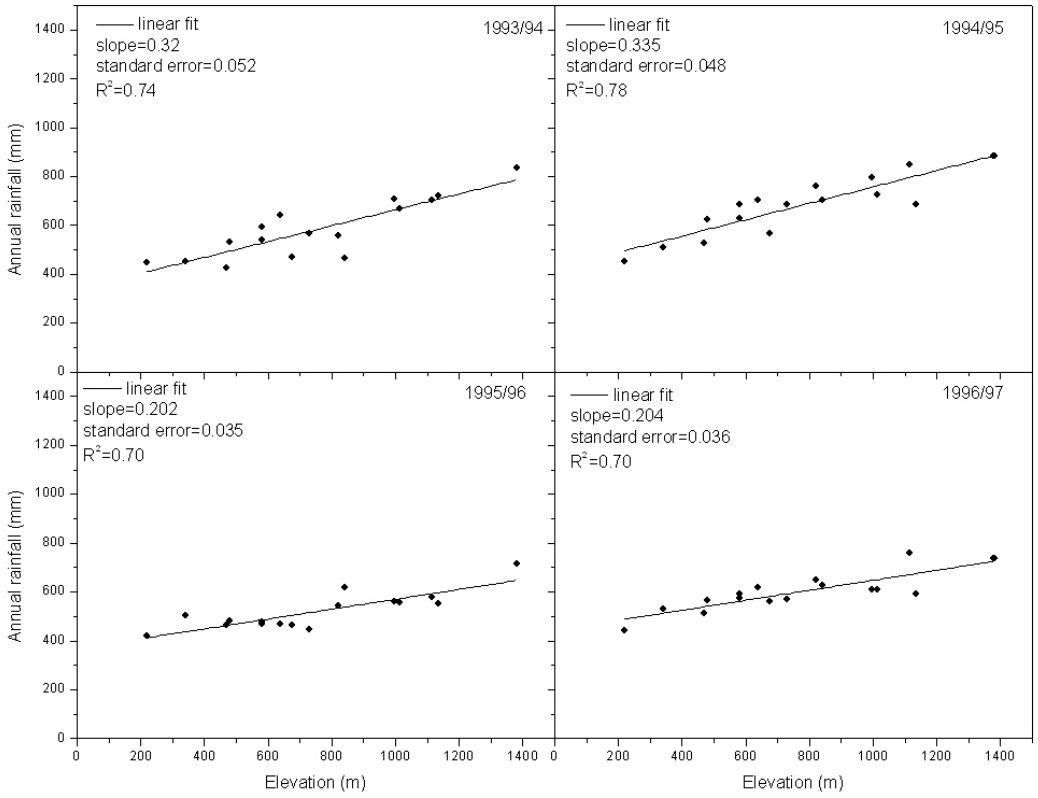

Figure 3.2: Annual rainfall of the 16 stations plotted against elevation for the hydrological years 1993/94 to 1996/97.

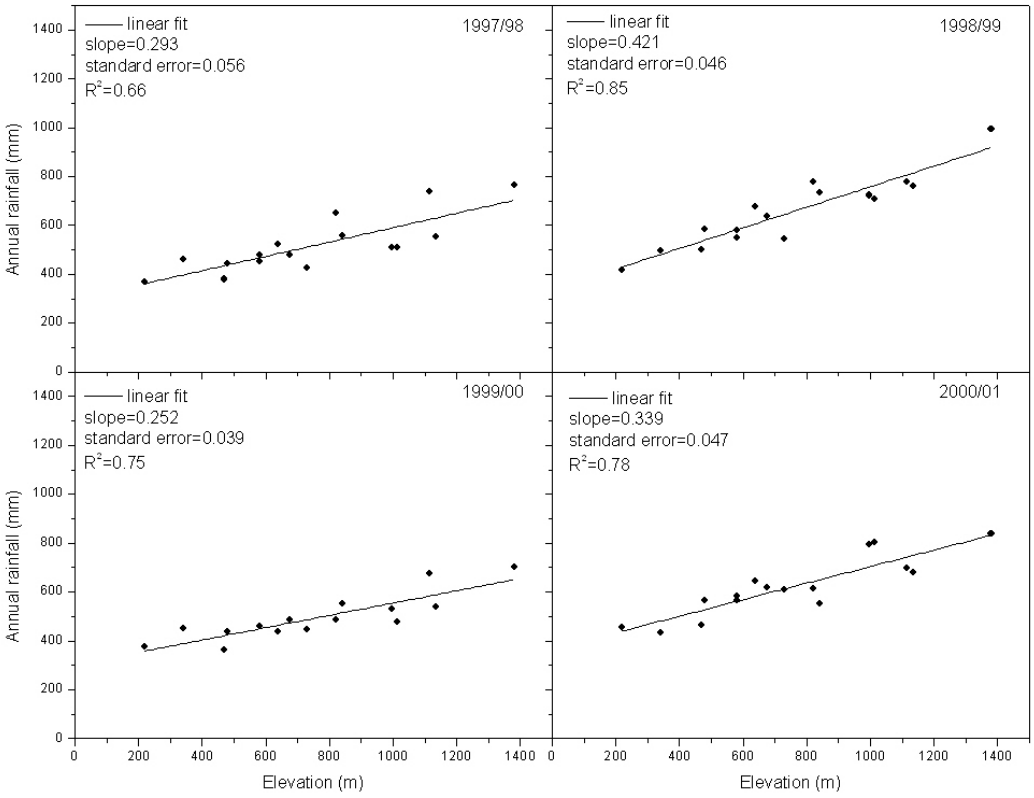

Figure 3.3: Annual rainfall of the 16 stations plotted against elevation for the hydrological years 1997/98 to 2000/01.

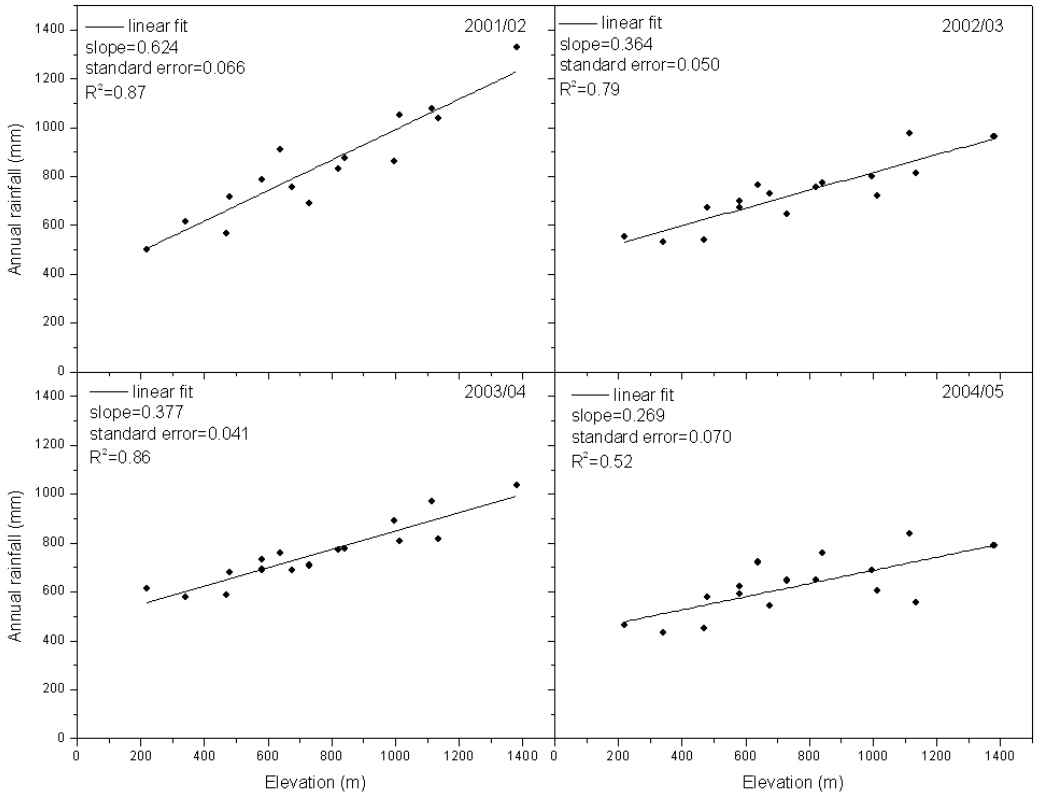

Figure 3.4: Annual rainfall of the 16 stations plotted against elevation for the hydrological years 2001/02 to 2004/05.

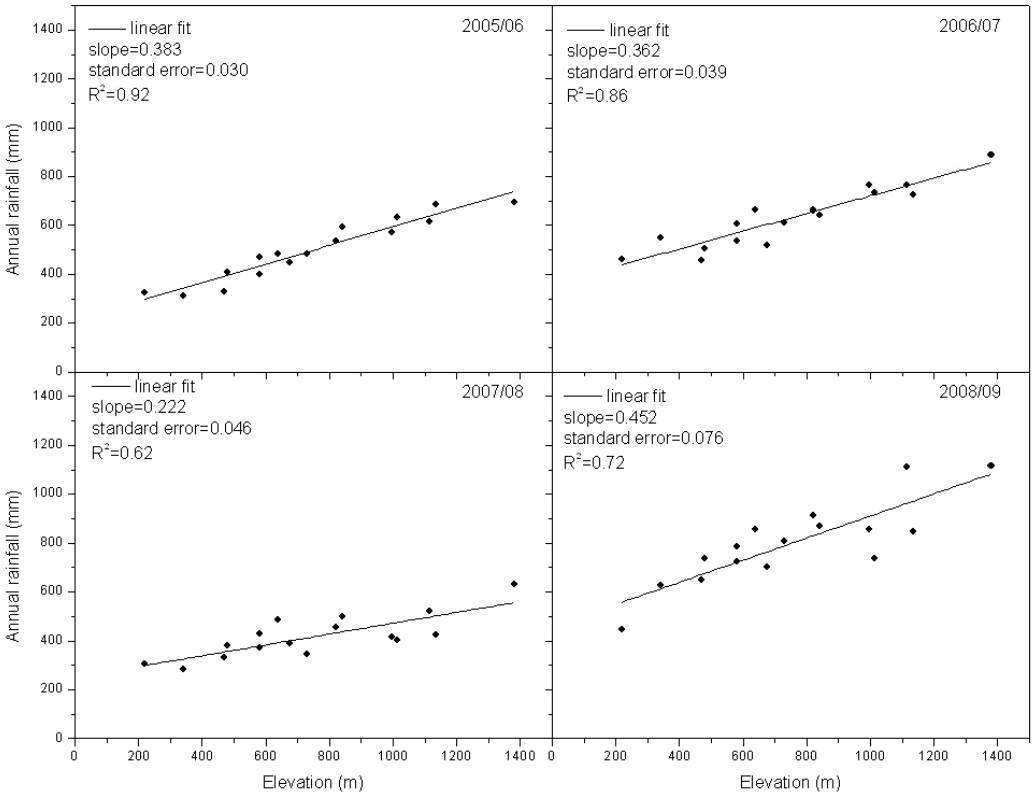

Figure 3.5: Annual rainfall of the 16 stations plotted against elevation for the hydrological years 2005/06 to 2008/09.

Table 3.2: Annual rainfall at the 16 stations

	Elevation of the stations															
	220 m	340 m	470 m	480 m	580 m	580 m	640 m	675 m	730 m	820 m	840 m	995 m	1015 m	1115 m	1135 m	1380 m
YEAR	Annual rainfall in mm															
1989	444.9	443.8	386.9	397.7	400.3	393.5	447.2	447.1	446.9	525.2	553.1	494.0	454.3	589.5	474.0	585.5
1990	307.6	310.5	312.0	356.5	331.2	355.5	418.9	316.1	374.9	443.5	390.3	465.1	493.4	492.2	419.1	531.1
1991	524.0	693.8	627.7	765.9	733.1	707.8	780.8	655.8	776.5	828.8	865.2	904.8	852.9	1045.0	923.7	1130.8
1992	496.7	535.3	525.4	596.7	573.4	627.5	662.7	626.2	641.9	695.9	656.4	797.0	748.0	819.0	867.4	990.7
1993	446.7	453.7	425.6	532.3	541.2	594.0	641.9	472.0	566.8	556.4	465.0	708.0	667.8	702.7	720.6	835.3
1994	454.0	509.4	526.5	624.4	626.9	686.0	705.3	566.5	687.6	760.9	701.5	798.5	724.6	847.8	684.4	885.9
1995	418.0	503.9	465.4	479.4	466.5	477.1	469.0	464.2	447.2	543.3	616.5	562.0	558.2	580.1	551.6	716.2
1996	443.2	531.9	511.5	566.0	575.3	591.2	619.5	562.5	567.5	647.4	625.9	610.5	607.5	760.0	594.0	739.4
1997	369.8	459.6	379.9	445.6	478.5	451.4	521.4	477.1	425.8	651.1	556.2	508.5	509.2	737.6	553.0	764.0
1998	418.8	497.2	500.9	582.6	580.0	548.5	675.5	638.6	544.3	778.7	734.7	723.5	706.7	778.2	759.1	995.9
1999	374.4	448.6	362.8	435.7	459.4	460.7	437.4	484.7	447.4	487.0	553.1	529.5	477.2	673.5	539.8	701.5
2000	455.0	434.9	464.5	566.8	565.8	581.2	644.3	616.9	609.4	611.6	551.3	793.0	804.8	698.5	679.4	836.2
2001	503.1	615.7	566.7	715.2	785.4	789.4	909.0	754.9	691.4	831.3	876.8	860.5	1052.8	1076.2	1038.1	1327.2
2002	555.8	533.4	539.6	673.3	699.4	672.6	766.0	730.6	647.1	755.3	773.7	802.0	721.3	977.6	812.6	964.0
2003	615.5	577.4	586.1	681.3	690.6	734.4	757.5	687.0	708.1	770.9	777.9	890.5	809.2	968.4	816.1	1038.4
2004	465.0	433.8	452.5	579.0	590.8	624.5	721.9	545.5	647.2	649.8	758.7	687.6	606.5	836.6	557.1	788.1
2005	323.5	311.3	328.5	409.6	401.0	472.4	481.3	448.7	483.8	535.4	594.4	573.1	635.0	615.5	686.6	696.2
2006	462.2	549.8	457.4	504.1	538.3	606.8	665.3	520.9	609.5	661.5	641.9	764.6	735.5	766.9	724.8	888.9
2007	303.6	284.1	331.0	379.8	372.7	428.9	488.1	387.4	345.5	455.1	500.1	415.5	403.6	521.8	422.8	631.8
2008	445.2	625.1	650.1	736.0	724.3	785.0	854.4	699.7	807.8	910.9	869.0	855.6	735.1	1112.7	845.9	1117.0

Table 3.3: Weights of rainfall stations

Station Name	Elevation (m)	Adjusted Weights	Simple Weights
KOURIS (DAM)	220	0.0362	0.0357
ALASSA (E.S.)	340	0.0676	0.0670
APESIA (E.S.)	470	0.0814	0.0826
DOROS	480	0.0545	0.0536
LANEIA	580	0.0638	0.0647
AGIOS MAMAS	580	0.0428	0.0424
SAITTAS (N.G.)	640	0.0556	0.0558
AGIOS THERAPON	675	0.0514	0.0513
KALO CHORIO (LEMESOU) (P.S.)	730	0.0786	0.0781
KOILANI (P.S.)	820	0.0464	0.0469
OMODOS (E.S.) (NEW)	840	0.1066	0.1049
AGIOS THEODOROS (LEMESOU)	995	0.0462	0.0469
AGROS	1015	0.0563	0.0558
PANO PLATRES (P.S.)	1115	0.0333	0.0335
KYPEROUNTA (E.S.)	1135	0.0683	0.0670
PANO AMIANTOS (MINES)	1380	0.1183	0.1138

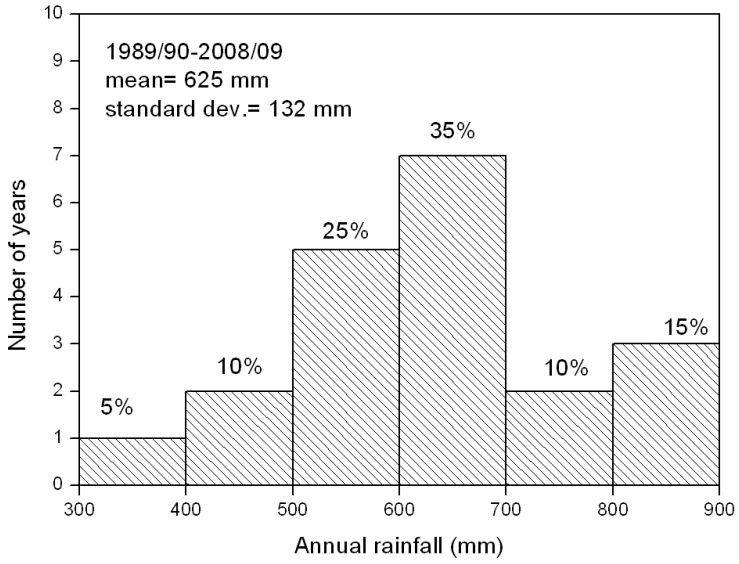

Figure 3.6: Annual rainfall distribution for the period 1989/90 to 2008/09.

3.1.2 Temporal variability

Rainfall also exhibits marked seasonal and inter-annual variability. On average 90 % of annual precipitation falls from October to April, with December and January being the rainiest months (Figure 3.8). Also 79 % of all days for the period 1989/90 to 2008/09 have no rain or rain less than 0.5 mm and only 3.6 % of all rainy days have daily values above 25.5 mm. There is also large variability in inter-annual rainfall with differences between years of over 500 mm. The catchment long-term mean annual rainfall for the above period is 625 mm and the standard deviation is 132 mm. For the period 1989/90 to 2008/09, 60% of the years have annual rainfall from 500 mm to 700 mm whilst 5% of the years have annual rainfall less than 400 mm and 15% have annual rainfall above 800 mm (Figure 3.6). The variation of rainfall with time is shown in Figure 3.13.

3.2 Discharge data

Three rivers drain the Kouris catchment: Kouris, Limnatis and Kryos. The total discharge is the sum of the recorded discharge at the three gauged rivers just upstream of Kouris dam. For each river, we have discharge data since 1965 but not from the same station and not continuously. The accuracy of the flow measurements is from 5% to 10%, and it is affected by the infrequency of flows, the steep gradient of riverbeds and the movement of bed loads

during floods. At the outlet of Kouris river there is the Kouris dam (the largest in Cyprus) having a 110 Mm^3 capacity. Kouris dam is located at 247 m above sea level and has a surface area of 3.6 Km^2. The construction of the reservoir commenced on the 1st of September 1984 and completed in the winter of 1987/88. When construction works commenced the existing gauge stations had to move upstream Kouris dam. Village Alassa was located on the site where the dam was going to be constructed so it was relocated on a site overlooking the reservoir between the valleys of Limnatis and Kouris. Since the hydrological year 1985/86 the outflow of each river is recorded continuously at the same station without any missing data. Characteristics of the stations are shown in Table 3.4. All the stations are upstream Kouris dam.

Table 3.4: Characteristics of discharge stations

Gauge	River	Elevation	Catch. area		DATA	
		(m)	Km^2	from	to	missing
r9-6-2-90	Kryos	250	67	1/10/1976	30/9/2009	No missing data
r9-6-4-90	Kouris	290	96	1/10/1985	30/9/2009	No missing data
r9-6-7-70	Limnatis	277	115	1/10/1985	30/9/2009	No missing data
r9-6-9-05	Kouris + Kryos	220	170	1/10/1965	30/9/1976	1/10/1966 to 30/9/1967
r9-6-4-95	Kouris	230	100	1/10/1965	30/9/1985	1/10/1968 to 30/9/1969
r9-6-7-75	Limnatis	228	120	1/10/1965	30/9/1985	No missing data

Since the winter of 1998/99 water is transferred via a tunnel from Arminou dam (lying outsite the catchment) to Kryos river (Figure 3.7). So, Kryos discharge is what is measured at the Kryos station, upstream of Kouris dam, minus the water transferred from Arminou dam, 5 km upstream of the Kryos gauge. The amount of water that is transferred from Arminou dam to Kryos river is known on a monthly basis. In order to convert it to a daily basis we divide it by the number of the days of the month with flow. This introduces an error in the measured discharge. The diversion of water from Arminou dam to Kouris dam began with a temporary diversion arrangement at the start of 1997/1998 hydrological year. Testing the tunnel, an unrecorded amount of water was transferred from Arminou tunnel to Kryos in the winter (January to March) of 1998. The diversion works were completed (WDD) by October 1998 and since then the amount of water that is transferred from the Arminou dam to Kryos river is known.

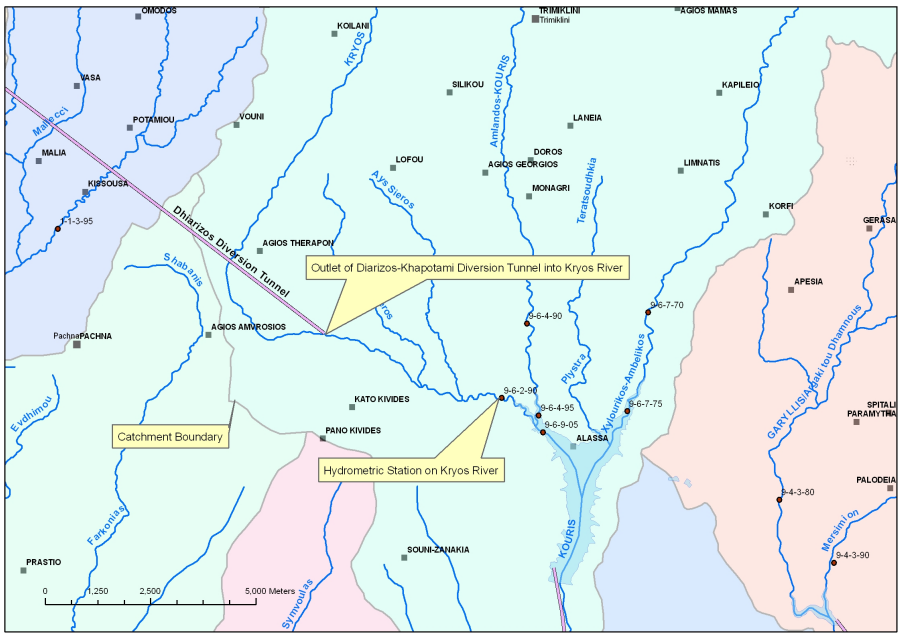

Figure 3.7: Diversion of Diarizos river via Arminou tunnel (from the WDD).

3.2.1 Temporal variability

On average 95.6 % of annual discharge appears at the catchment outlet in the period from November to May (Figure 3.8). Peak discharge occurs usually in the period from January to March (for the period 1989/90 to 2008/09, long-term mean monthly total values range from 14.1 mm to 16.7 mm) exhibiting, on average, a lag of one to two months compared to rainfall (Figure 3.9). This is expected because at the beginning of the rainy period the soil and groundwater stores are essentially empty and only towards the end of the rainy period the stores are filled and the surface runoff increases. Also the melting of snow in early spring contributes to surface runoff.

The annual discharge is very sensitive to the rainfall temporal variability. For the period 1989/90 to 2008/09, the long-term mean annual discharge is 78 mm but annual values range from 19 mm (2007/08) to 222 mm (2003/04), following the rainfall temporal variability. Most of the years have annual discharge less than 50 mm and only 10% of the years have annual discharge more than 100 mm (Figure 3.10). The coefficient of variation (CV), a measure of the variability of the data defined as the mean value over the standard deviation, for the above period, is 0.21 for the annual rainfall whilst the corresponding CV for the annual discharge is 0.68, i.e. three times higher, showing the large temporal variability of the annual discharge. The percentage of rainfall that goes to discharge is not constant but varies from 4.4% to 28.9% with lower values corresponding to the years with lower annual rainfall. For

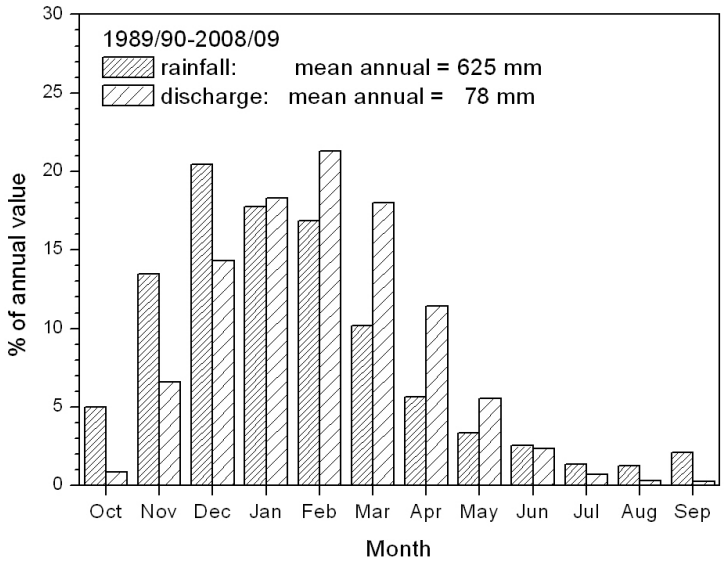

Figure 3.8: Seasonal variability of rainfall and discharge for the period 1989/90 to 2008/09.

the period 1989/90 to 2008/09, the long-term average percentage of rainfall that goes to discharge is 12.5%. The variabilty of discharge with years is shown in Figure 3.13.

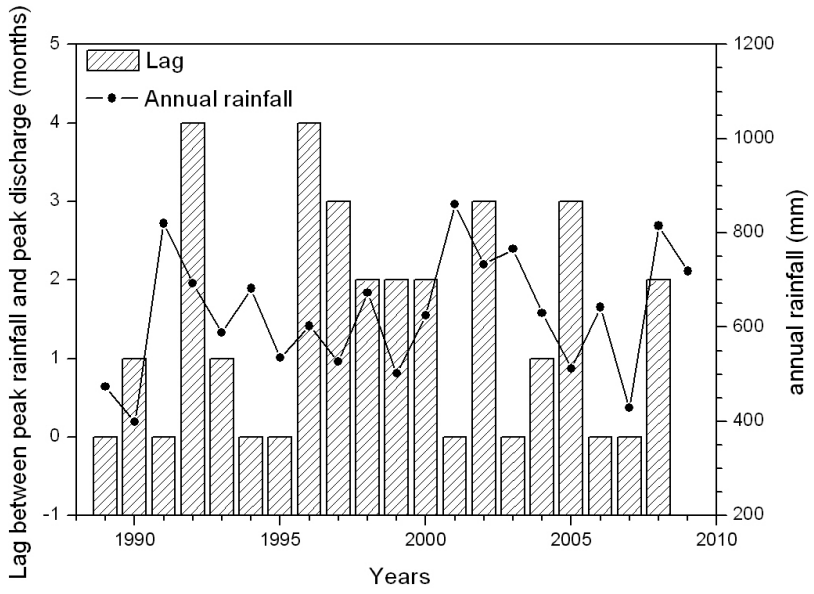

Figure 3.9: Lag in months between peak rainfall and peak discharge for the period 1989/90 to 2008/09. Annual rainfall is also shown.

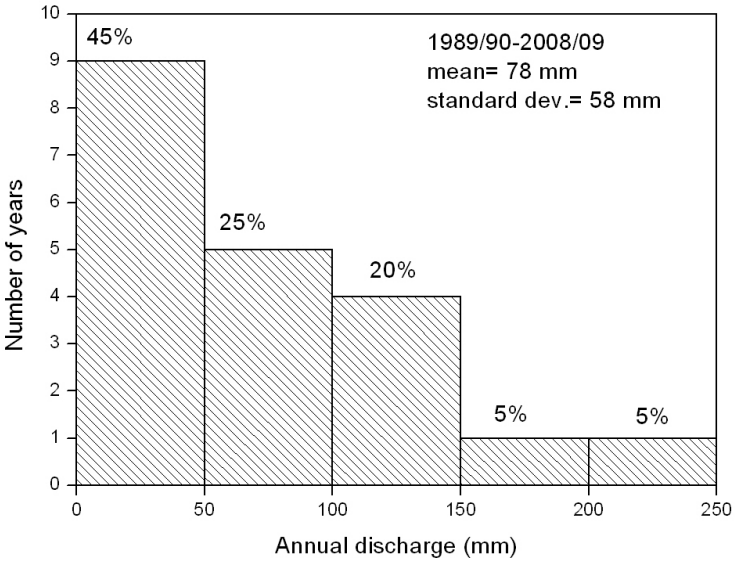

Figure 3.10: Distribution of annual discharge for the period 1989/90 to 2008/09.

3.3 Pan and potential evaporation

3.3.1 Pan evaporation

Class-A pan evaporation data are available from 3 stations at different elevations. The characteristics of the stations are shown in Table 3.5.

Table 3.5: Characteristics of pan evaporation stations

Station Number	Station Name	Elevation (m)	Lat. North	Long. East
313	KOURIS (DAM)	218	$34^o\ 43'$	$32^o\ 55'$
320	SAITTAS (N.G.)	640	$34^o\ 52'$	$32^o\ 55'$
377	AGROS	1015	$34^o\ 55'$	$33^o\ 01'$

Spatial variability of pan evaporation

The pan evaporation is very dependent on elevation (Figure 3.11) with long-term mean annual values, for the period 1989/90 to 2008/09, varying from 1689 mm at the highest station to 2281 mm at the lowest station. The mean of the three stations is considered as the pan evaporation of the catchment. For the above period, the mean annual catchment pan evaporation is 1884 mm.

Temporal variability of pan evaporation

Pan evaporation exhibits large seasonal variability with lowest values in winter and highest in summer. For the period 1989/90 to 2008/09 the long-term mean monthly pan evaporation varies from 1.8 mm/day in January (ranges from 1.3 mm/day to 2.1 mm/day) to 9.3 mm/day in July (ranges from 8.2 mm/day to 10.9 mm/day), (Figure 3.12). Inter-annual variability is fairly small. For the period 1989/90 to 2008/09 the annual pan evaporation ranges from 1747 mm to 2079 mm with an average value of 1884 mm and a standard deviation of 86.5 mm, (Figure 3.13). However, the monthly pan evaporation exhibits a rather larger inter-annual variability especially for the months from October to May. For the period 1989/90 to 2008/09, the coefficient of variation (CV) is 0.05 for the annual pan evaporation, around 0.08 for the monthly pan evaporation of the summer months and ranges from 0.11 to 0.18 for the months October to May.

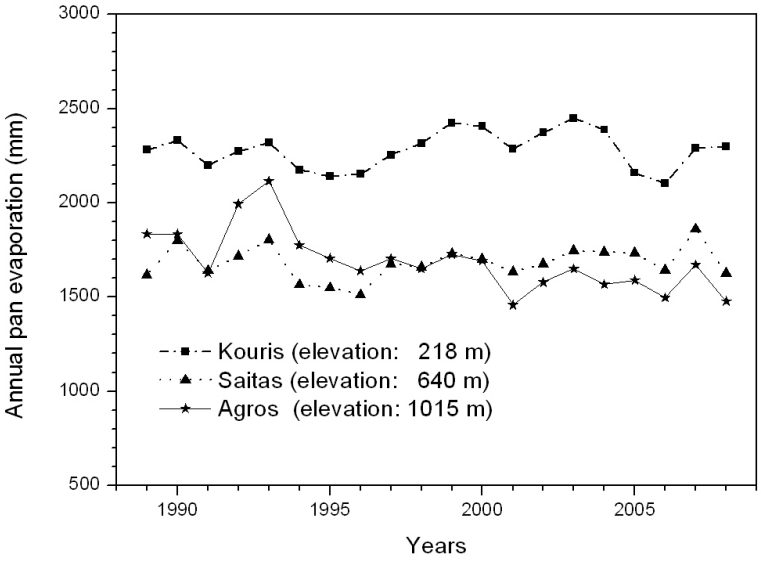

Figure 3.11: Annual pan evaporation for the Kouris, Saitas and Agros meteorological station for the period 1989/90 to 2008/09.

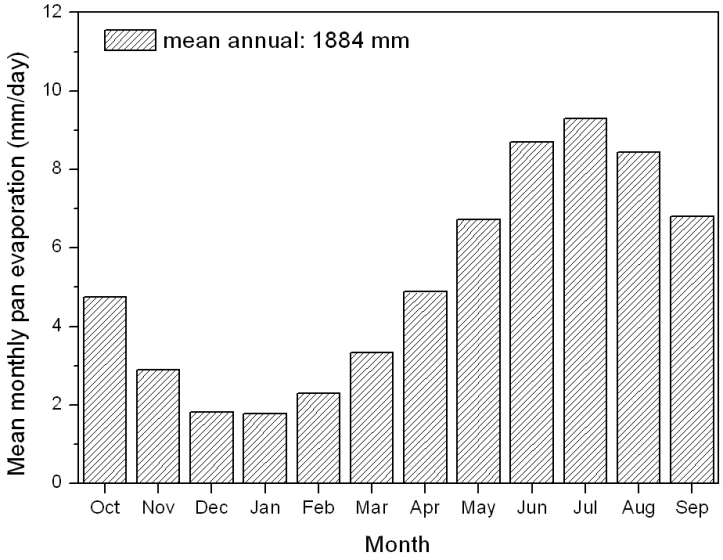

Figure 3.12: Long-term mean monthly pan evaporation for the period 1989/90 to 2008/09.

3.3.2 Potential evaporation

Estimation of the Penman Potential Evaporation over the catchment for the period 2002 to 2007

Potential evaporation is defined as the evaporation from a free water surface or from a surface where there is ambient water. It is an important component in the water budget of the catchment and an input to the rainfall-runoff model. The monthly potential evaporation rate over the catchment was computed for the period 1/1/2002 to 31/12/2007 using the Penman method from MODIS climatic data at a 10 × 10 km resolution (available from 2002 to today) and ground-based wind data from the Agros station were available up to 2007. Penman potential evaporation depends on the available energy for evaporation and on wind advection. The available energy for evaporation is computed using radiation transfer models (Hatzianastassiou and Vardavas 2001a,b; Pavlakis et al. 2007; Vardavas and Taylor 2011) and MODIS satellite atmospheric climatic data (Benas et al. 2011; Matsoukas et al. 2011) over the catchment. We note that MODIS gives also an evapotranspiration product (MODIS 16), which we do not use as this is based on radiation fluxes from reanalysis generated cloud cover and a variant of the Penmann-Monteith equation. We use instead actual climatic data over the catchment and surface measurements within the catchment together with substantially validated and tested radiation transfer models (Vardavas and Taylor 2011). Thus, the long-term mean monthly potential evaporation is computed. The annual potential evaporation rate for the catchment for the period 2002/03 to 2006/07, varies very little with years. It ranges from 1586 mm to 1614 mm with a mean of 1601 mm, standard deviation of 11 mm and a coefficient of variation CV of 0.007, almost ten times lower than the corresponding CV of the pan evaporation, for the same period. For the above period, mean monthly pan evaporation values for the winter months, are quite close to mean monthly potential evaporation (as computed from the radiation transfer models). However, there is a deviation in the summer months. Minimum values are in January and maximum in July for both pan and potential evaporation. The corresponding mean values are 1.79 mm/day and 9.29 mm/day for the pan evaporation and 1.80 mm/day and 7.57 mm/day for the the potential evaporation. Monthly total values range from less than 50 mm in January for both pan and potential evaporation to over 300 mm in July for pan evaporation and over 200 mm in July for potential evaporation (Figure 3.15).

The temporal variation of rainfall, discharge, pan and potential evaporation is shown in Figures 3.13 and 3.14.

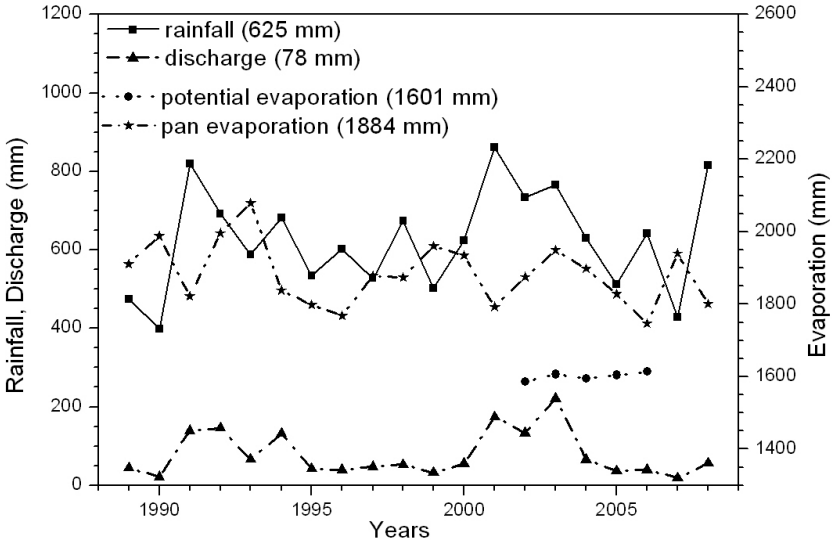

Figure 3.13: Annual variation of rainfall, discharge, pan and potential evaporation. Numbers in parentheses refer to long-term mean values for the period 1989/90 to 2008/09 for the rainfall, the discharge and the pan evaporation and for the period 2002/03 to 2006/07 for the potential evaporation.

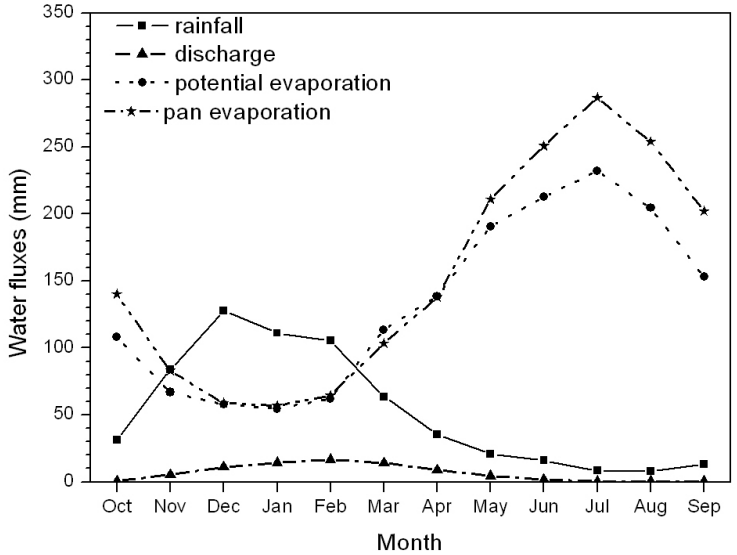

Figure 3.14: Seasonal variation of rainfall, discharge, pan and potential evaporation.

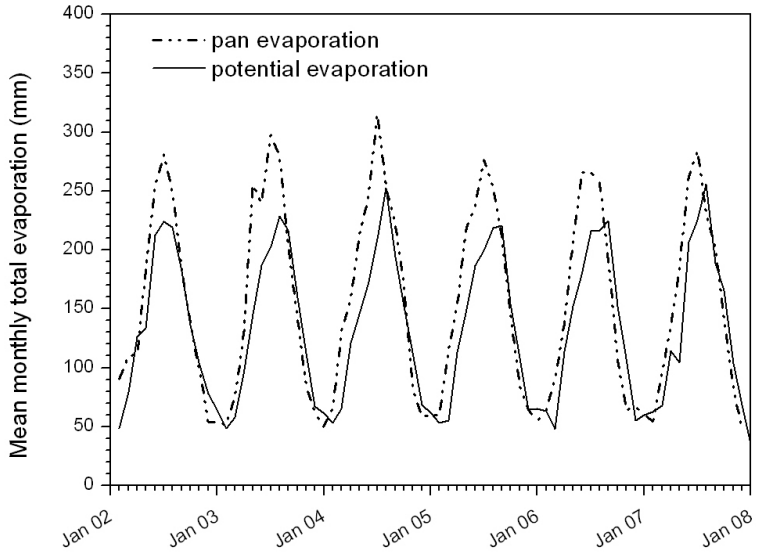

Figure 3.15: Monthly pan and potential evaporation for the period 1/1/2002 to 31/12/2007.

Estimation of the potential evaporation of the catchment for a specific year

Pan coefficient

The potential evaporation is directly related to the pan evaporation via Eq. 3.4:

$$E_p = p_c E_{pan} \tag{3.4}$$

where E_p is the monthly potential evaporation, E_{pan} the monthly pan evaporation and p_c the monthly pan coefficient. Monthly pan evaporation data and computed monthly potential evaporation data for the period 2002 to 2007 are used in Eq. 3.4 to derive monthly pan coefficients. The derived monthly pan coefficients are then used, for the entire modeling period 1989/90 to 2008/09, with the available pan evaporation data, to estimate the potential evaporation. The mean monthly value of the pan coefficient varies from 0.76 to 1.12 with highest values in the period from December to April and lowest values in September and October (Figure 3.16).

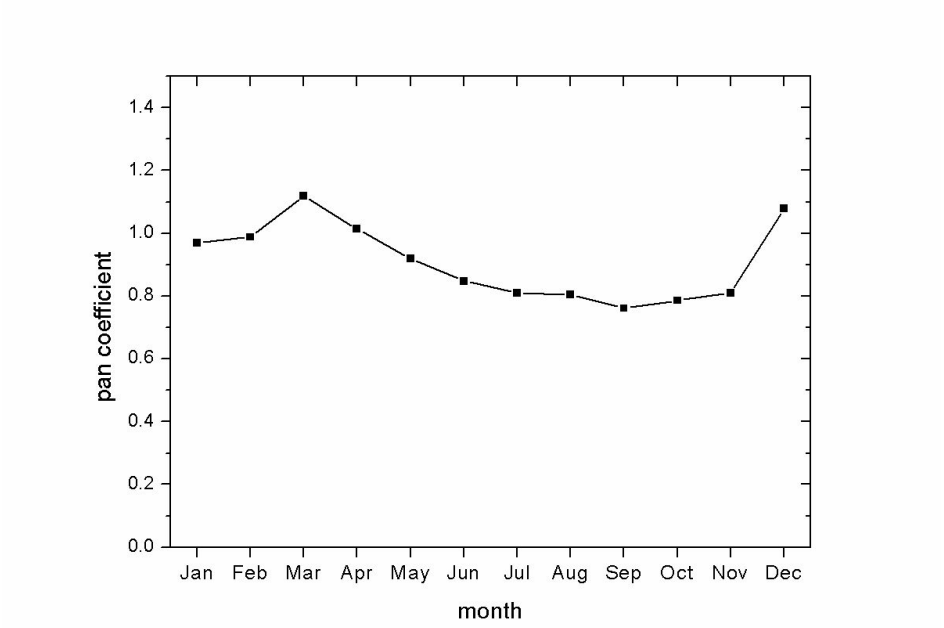

Figure 3.16: Pan coefficient long-term averages for the period 1/1/2002 to 31/12/2007.

Bibliography

Benas, N., Hatzianastassiou, N., Matsoukas, C., Fotiadi, a., Mihalopoulos, N., and Vardavas, I.: Aerosol shortwave direct radiative effect and forcing based on MODIS Level 2 data in the Eastern Mediterranean (Crete), Atmospheric Chemistry and Physics, 11, 12 647-12 662, doi:10.5194/acp-11-12647-2011, 2011.

Croke, B., Cleridou, N., Kolovos, A., Vardavas, I., and Papamastorakis, J.: Water resources in the desertification-threatened messara valley of Crete: estimation of the annual water budget using a rainfall-runoff model, Environmental Modelling and Software, 15, 387-402, 2000.

Hatzianastassiou, N. and Vardavas, I.: Shortwave radiation Budget of the Southern Hemisphere using ISCCP C2 and NCEP-NCAR climatological data, Journal of Climate, 14, 4319-4329, 2001a.

Hatzianastassiou, N. and Vardavas, I.: Longwave radiation Budget of the Southern Hemisphere using ISCCP C2 climatological data, Journal of Geophysical Research, 106, 17 785-17 798, 2001b.

Matsoukas, C., Benas, N., Hatzianastassiou, N., Pavlakis, K. G., Kanakidou, M., and Vardavas, I.: Potential evaporation trends over land between 1983–2008 driven by radiative fluxes or vapour-pressure deficit?, Atmospheric Chemistry and Physics, 11, 7601-7616, doi:10.5194/acp-11-7601-2011, 2011.

Pavlakis, K. G., Hatzidimitriou, D., Drakakis, E., Matsoukas, C., Fotiadi, A., Hatzianastassiou, N., and Vardavas, I.: ENSO surface longwave radiation forcing over the tropical Pacific, Atmospheric Chemistry and Physics, 7, 2013-2026, 2007.

Vardavas, I. and Taylor, F.: Radiation and Climate: Atmospheric Energy Budget from Satellite Remote Sensing, International Series of Monographs on Physics, OUP Oxford, 2011.

Chapter 4

The Daily Rainfall-Runoff Model

4.1 Model description

A conceptual daily rainfall-runoff model (CREEK, Vardavas 1988; Croke et al. 2000) is adapted to the Kouris catchment and used to estimate the water budget for a period of twenty years, using daily rainfall and discharge data. Our original conceptual model, developed based on the three hydrological phases of the earlier Boughton model (Boughton 1968), was used to model the runoff from the Magela Creek catchment in the wet/dry climate of the Northern Territory of Australia (Vardavas 1988). It was then adapted, calibrated and validated successfully for the wet/dry climate Messara Valley catchment of the Mediterranean island of Crete. In this work, the existing model, as described in Croke et al. (2000) is modified and adapted for the Kouris alpine catchment which has an extensive network of streams and is drained by three major rivers.

The conceptual rainfall-runoff model is based on conservation of mass so that on any given day precipitation P is partitioned between surface runoff Q, evapotranspiration E, and recharge R.

The catchment is considered as a homogeneous unit consisting of four stores: interception store, surface store, soil store and groundwater store. The interception store is the vegetative area, surface store is the thin topsoil layer, soil store is the underlying soil layers and groundwater store is the perched aquifer above the bedrock.

The model consists of three hydrological phases occurring sequentially daily: a) a quick wetting b) a slower infiltration-runoff phase and c) an even slower drying phase.

In the wetting phase, rainfall is intercepted by the vegetative cover and any excess water passes down through the interception store to the surface store. In the infiltration-runoff phase, the water infiltrates into the soil store and eventually either reaches the groundwater

Table 4.1: The set of model parameters

Parameter	Description
DEL_0	advective flow delay for fast runoff
DEL_1	delay coefficient for fast runoff delay store
DEL_2	delay coefficient for slow runoff delay store
L_m	interception store capacity
D_m	surface store capacity
S_m	soil store capacity
G_m	groundwater store capacity
α	fraction of S that goes to fast runoff
β	fraction of S that goes to slow runoff
δ	fraction of G that goes to runoff
F_0	maximum infiltration rate
p_0	maximum percolation rate
G_0	minimum G for contribution to the slow runoff
q	fraction of G lost via evaporation and sea leakage
γ	power law for contribution to flow from S

store through percolation or finds its way out of the catchment through runoff. In the drying phase, water is taken out of the system through evaporation and transpiration from the plant canopy and through evaporation from bare soil. The structure of the model is shown in Figure 4.1 and the associated model parameters are shown in Table 4.1. Below, we describe the model in more detail.

4.1.1 Wetting phase

If we assume that the capacities of interception, surface, soil and groundwater stores are L_{max}, D_{max}, S_{max}, G_{max} and the corresponding storages on day i are L_i, D_i, S_i, G_i, respectively, then: on day i the daily precipitation P_i is added to the interception store and the new storage is then:

$$L_i = L_{i-1} + P_i \tag{4.1}$$

If the interception storage L_i exceeds the interception capacity L_{max} the excess water U_i passes to the surface store:

$$\begin{aligned} U_i &= 0 && \text{if} \quad L_i \leq L_{max} \\ &= L_i - L_{max} && \text{if} \quad L_i > L_{max} \end{aligned} \tag{4.2}$$

The surface store storage is then:

Figure 4.1: A flow diagram of the conceptual rainfall-runoff model.

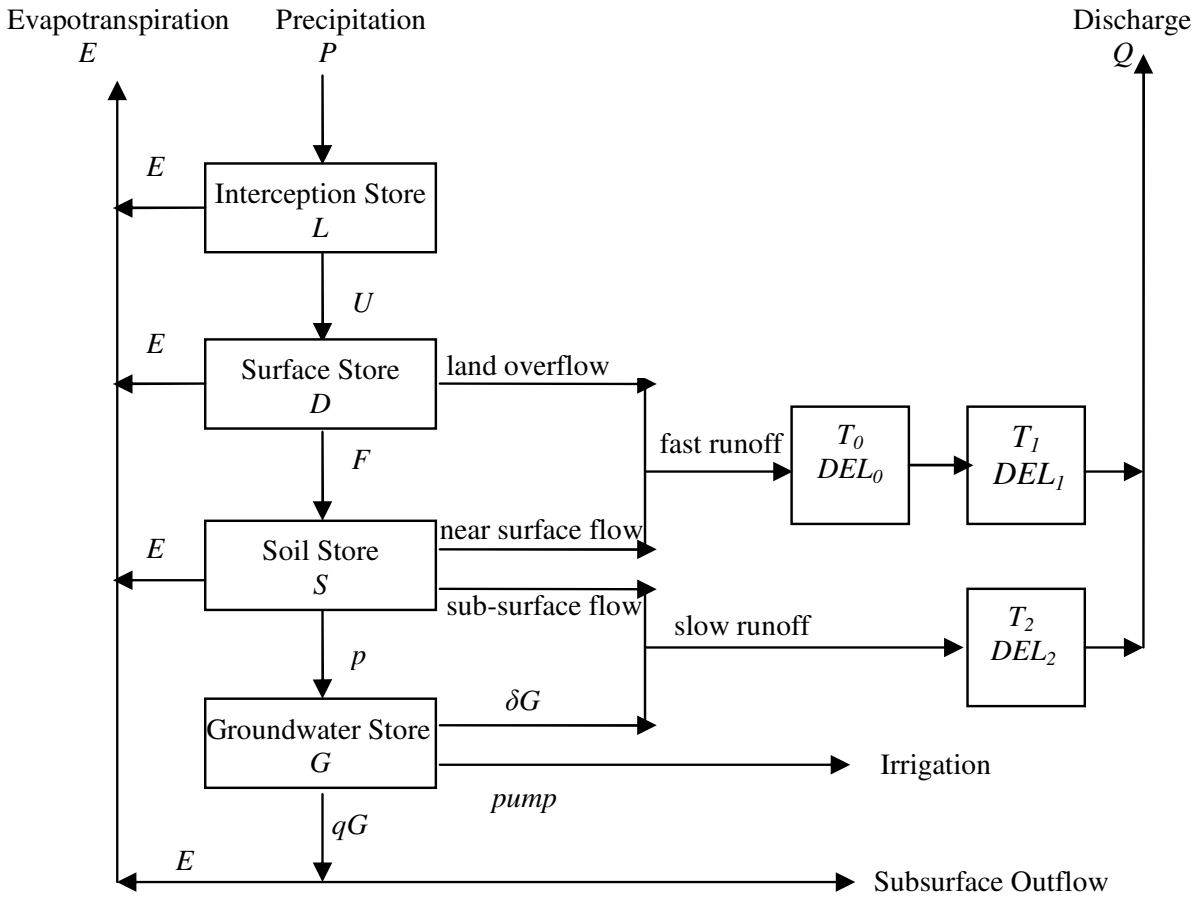

$$D_i = D_{i-1} + U_i \tag{4.3}$$

If V_i is the excess water of the surface store then:

$$\begin{aligned} V_i &= 0 && \text{if} \quad D_i \le D_{max} \\ &= D_i - D_{max} && \text{if} \quad D_i > D_{max} \end{aligned} \tag{4.4}$$

4.1.2 Infiltration-runoff phase

The excess of surface store V_i will either infiltrate into the soil store with rate F_i or appear as overland flow R_d, depending on the infiltration rate F_i, thus:

$$\begin{aligned} R_d &= V_i - F_i && \text{if} \quad V_i > F_i \\ &= 0 && \text{if} \quad V_i \le F_i \quad \text{and then} \quad F_i = V_i \end{aligned} \tag{4.5}$$

The infiltration rate F depends on the soil and the groundwater store moisture and is given by Eq. 4.6:

$$F = F_0 exp(-kS) \tag{4.6}$$

where S is the soil moisture and k is a parameter given by Eq. 4.7

$$k = -\frac{ln(F_c/F_0)}{S_{max}} \tag{4.7}$$

where F_0 is the maximum infiltration rate, given as a model parameter and F_c is the minimum infiltration rate, given by Eq. 4.18. The infiltration rate is maximum when the soil store is dry (S=0), whilst it is minimum when the soil store is saturated (S=S_{max}). The infiltrated water will either percolate into the groundwater store with a percolation rate p or discharge to the local rivers or will be added as moisture to the soil store.

The percolation rate p attains its maximum value p_0 when the soil store is saturated and the groundwater store is empty i.e. G=*0*. If the groundwater store is saturated (G=G_{max}), no percolation takes place. The maximum percolation rate p_0 is given as a model parameter and the percolation rate p is given by Eq. 4.8:

$$p = p_0 \left(1 - \frac{G}{G_{max}}\right) \cdot \frac{S}{S_{max}} \tag{4.8}$$

We consider the runoff to have two components: a fast component and a slow component. The two-component runoff allows for a delay between the local runoff and discharge at the outlet of the order of days for the fast component and of the order of weeks for the slow

component. Otherwise, the model cannot reproduce the peaks and the slow decrease of flow towards the end of the hydrological year, in the observed hydrograph. The peaks of the hydrograph correspond to the fast component of the runoff whilst the slow decay towards the end of the hydrological year, corresponds to the slow component of the runoff. The fast component R_s consists of the overland flow R_d and the near surface soil flow $subf_1$ whilst the slow component R_g consists of the deep surface soil flow $subf_2$ and the flow from the groundwater store $\delta(G-G_0)$. G_0 is the critical value of groundwater storage below which there is no flow from the groundwater store to surface runoff and δ is the fraction of groundwater that goes to runoff and it is also given as a model parameter.
Thus:

$$R_s = R_d + subf_1 \tag{4.9}$$

$$R_g = subf_2 + \delta\,(G - G_0) \tag{4.10}$$

The two components of the soil flow are given by Eq. 4.11 and Eq. 4.12:

$$subf_1 = \alpha F \left(\frac{S}{S_{max}} \right)^{\gamma} \tag{4.11}$$

and

$$subf_2 = \beta F \left(\frac{S}{S_{max}} \right)^{\gamma} \tag{4.12}$$

where α, β, γ are model parameters; γ determines the sensitivity of the sub-surface flow on the fractional soil storage S/S_{max} and α, β are the fractions of daily infiltration F that goes to the river (α is the fraction of F that contributes to the near-surface fast component and β is the fraction of F that contributes to the sub-surface slow component). The sum $\alpha + \beta$ is always less than unity since some of the infiltrated water will go to percolation or stored as moisture in the soil store and thus:

$$0 \le \alpha + \beta \le 1 \tag{4.13}$$

When the soil store is saturated $(S=S_{max})$, the infiltration rate is at its minimum value F_c and all infiltrated water either percolates or goes to the rivers as runoff thus:

$$F_c = subf_{1c} + subf_{2c} + p_c \tag{4.14}$$

with

$$subf_{1c} = \alpha F_c \tag{4.15}$$

$$subf_{2c} = \beta F_c \tag{4.16}$$

and

$$p_c = p_0 \left(1 - \frac{G}{G_{max}}\right) \tag{4.17}$$

So

$$F_c = \frac{p_c}{1 - (\alpha + \beta)} \tag{4.18}$$

The estimated F_c is used to calculate the parameter k in Eq. 4.6.
The rate of change of soil moisture with time is given by Eq. 4.19:

$$\frac{dS}{dt} = F - subf_1 - subf_2 - p = A \tag{4.19}$$

Using the Euler-trapezoidal integration method the above equation can be written as

$$S_i = S_{i-1} + \Delta t \left(A_i + A_{i-1}\right)/2 \tag{4.20}$$

with Δt=1 day. In the same way we find the rate of change B of groundwater store:

$$\frac{dG}{dt} = p - \delta \left(G - G_0\right) - qG - pump = B \tag{4.21}$$

where qG is the amount of water lost from groundwater store through evaporation and sub-surface flow out of the catchment, with q being a model parameter and *pump* is the abstracted groundwater. The high elevation of the catchment (up to 1905 m) and the small distance to the sea (about 30 Km) gives a significant gradient in the watertable, and thus, the sub-surface leakage is not negligible.
The groundwater storage on day i is then:

$$G_i = G_{i-1} + \Delta t \left(B_i + B_{i-1}\right)/2 \tag{4.22}$$

where Δt=1 day.
The above equations are solved using the Newton-Raphson method and the fast R_s and the slow R_g components of runoff are thus calculated.
R_s and R_g are then accumulated into three delay stores T_0 and T_1 for the R_s and T_2 for the R_g component, before reaching the catchment outlet. The delay of runoff in the stores is controlled by the corresponding model parameters DEL_0, DEL_1 and DEL_2. The greater their

value the quicker the runoff leaves each store.
On day i

$$T_{1,i} = (1 - DEL_1)T_{1,i-1} + T_{0,i-1} + DEL_0 R_s \tag{4.23}$$

$$T_{0,i} = (1 - DEL_0)R_s \tag{4.24}$$

$$T_{2,i} = (1 - DEL_2)T_{2,i-1} + R_g \tag{4.25}$$

The first two terms on the right hand side of Eq. 4.23 and the first term of Eq. 4.25 is the contribution to the delay stores from the previous day whilst the other term is the contribution from the current day. Finally, the discharge Q at the outlet is given by Eq. 4.26:

$$Q_i = Q_{1,i} + Q_{2,i} \tag{4.26}$$

where

$$Q_{1,i} = DEL_1 T_{1,i} \tag{4.27}$$

$$Q_{2,i} = DEL_2 T_{2,i} \tag{4.28}$$

The intoduction of T_0, a modification in this version of the model, was needed in order to capture the response of the catchment to the rainfall event. Without the introduction of T_0 the peak discharge would appear on the same day the rainfall event occurs. However, observed data shows that the peak appears one day after the rainfall event. This is expected, since the catchment has a dense river network and the discharge gauges are located in the lower part of each subcatchment river network (Fig. 2.1). This results in an advective delay of the fast runoff. This delay corresponds to the time it takes for the water from all the small streams to be accumulated in the main rivers. This advective flow delay is thus handled by the delay store T_0. The effect of DEL_0 and subsequently T_0 on runoff is shown in Figures 5.9 and 5.10 in section 5.5. There is then the extra delay due to the exponentially decaying stores for the fast and slow components of the main stream flow until they reach the outlet, represented by the stores T_1 and T_2, respectively.

4.1.3 Drying phase

During the drying phase water is lost by evaporation from bare soil and open water areas and by transpiration from roots and leaves of the vegetative area. The rate, at which water is lost from bare soil and vegetation, when there is sufficient water in the soil and air, is called potential evapotranspiration. In regions with arid or semi-arid climate like Cyprus, this condition does not always happen, especially in summer, and actual evapotranpiration takes place under water deficit conditions. The calculation of actual evapotranpiration is not an easy task and certain assumptions have to be made. According to our model the interception store is first depleted by evapotranspiration, followed by the surface store and finally the soil store. Evapotranspiration from the groundwater store is not significant and is not taken into account here but in the general losses of water from the groundwater store. Groundwater evapotranspiration is only significant in alluvial aquifers with a shallow water table. In our case, the area of alluvial aquifer is only a small portion of the total aquifer. Evapotranspiration rate from interception and surface store is set equal to potential evaporation (Vardavas 1988). The estimation of actual evapotranspiration rate from soil is a rather complicated process because it depends on the transport of water through the soil. The transport of water is affected by the atmospheric conditions, the soil water pressure, the amount of solute in the water etc. A simplification is to assume that soil evapotranspiration rate ET is proportional to the potential evaporation rate E and the soil moisture S, provided that the surface store is dry (Vardavas 1988) :

$$ET = E.S/S_{max} \tag{4.29}$$

If the soil store is saturated the soil evapotranspiration ET is equal to the potential evaporation E. As the water content of the soil store S decreases the soil drying rate ET decreases linearly with it.
If on day i :

L_i is the interception moisture
D_i is the surface moisture
S_i is the soil moisture
E_i is the potential evaporation

then after the daily evaporation the new value of the interception store $L_{i'}$ is:

$$L_{i'} = L_i - E_i \tag{4.30}$$

If L_i is greater than E_i then all water evaporates from the interception store and the actual evaporation ET_i is equal to the potential evaporation E_i thus:

$$\begin{aligned} &\text{if} \quad L_i' \geq 0 \quad \text{then} \quad D_{i'} = D_i \\ &\qquad\qquad\qquad\qquad\quad ET_i = E_i \end{aligned} \tag{4.31}$$

If L_i is less than E_i then the evaporation in excess of the interception moisture goes into drying the surface moisture store D_i and so:

$$\text{if} \quad L_i' < 0 \quad \text{then} \quad D_{i'} = D_i + L_{i'} \tag{4.32}$$

If there is excess water in the surface store ($D_{i'} \geq 0$) no evaporation takes place in the soil store and all evaporation occurs in the interception and surface stores, i.e.:

$$\begin{aligned} &\text{if} \quad D_i' \geq 0 \quad \text{then} \quad S_{i'} = S_i \\ &\qquad\qquad\qquad\qquad\quad ET_i = E_i \end{aligned} \tag{4.33}$$

If the surface store is depleted by evaporation ($D_{i'} < 0$) the soil store is in turn depleted by evaporation. The potential evaporation rate for the soil store equals $D_{i'}$, i.e. what is left from the evaporation rate after the depletion of the interception and the surface store. The change in soil moisture due to the drying process is equal to the evapotranspiration rate ET_i and is calculated by using Eq. 4.29 as follow:

$$dS = (D_{i'} S / S_{max})\, dt \tag{4.34}$$

$$\int_{S_i}^{S_{i'}} \frac{dS}{S} = \int_0^1 (D_{i'} / S_{max})\, dt \tag{4.35}$$

$$S_{i'} = S_i exp(D_{i'} / S_{max}) \tag{4.36}$$

Thus:

$$\text{if} \quad D_i' < 0 \quad \text{then} \quad S_{i'} = S_i exp(D_{i'} / S_{max}) \tag{4.37}$$

The amount of water that evaporates from the soil store is then equal to S_i-$S_{i'}$. Soil evaporation is a slow process and it is most important during the dry months when the interception and surface stores are empty. The total actual evaporation ET_i of day i is then the sum of the evaporation from the three stores.

4.2 Model calibration

We have used the sequential Fibonacci search technique (Vardavas 1989) for model parameter selection. Initial search ranges are selected based on the physical properties of the catchment components. The search technique includes an objective function sensitivity criterion to optimise model parameter selection within a specified search interval. The technique is ideally suited to complex and nonlinear system models for which many parameter sets may fit the observed data adequately, provided that the modeling aim is to predict the system response to external stimuli rather than to determine precisely the optimum values of the individual parameters.

The model uses fifteen parameters in order to simulate the discharge at the catchment outlet. The selection of the parameters is such that the difference between simulated and observed daily discharge at the outlet is minimized. In order to achieve this we use the chi-squared statistic per degree of freedom as the objective function defined by Eq. 4.38:

$$\chi^2 = \frac{1}{N - n_p - 1} \sum_{i=1}^{N} \frac{(Q_{oi} - Q_{mi})^2}{Q_{oi}} \tag{4.38}$$

where N-n_p-1 represents the number of degrees of freedom for an n_p- parameter model and N is the number of daily measurements, Q_{oi} is the observed discharge on day i at the catchment outlet and Q_{mi} is the simulated discharge (both in m^3/s). For those days when there is zero flow Q_{oi} is set equal to $Q_{oi} + \delta$ with $\delta << 1$. For the modeling period 1989/90 - 2008/09 eleven years out of twenty have from 20 to 132 days of zero flow (1990/91 has the highest number of zero flow days).

The calibration method was a combination of an automatic and manual one and it was made in three steps: 1) Initial estimates of parameter values and expected ranges were assessed based on catchment properties and on previous model applications; 2) sensitivity analysis performed to show the most sensitive parameters; 3) automatic calibration starting from the most sensitive parameter. The calibration procedure was repeated for three different calibration periods. As calibration periods we used: a) the dry year 1989/90, b) the wet year 1991/92 and c) the period 1989/90 to 1994/95 which includes wet and dry years. The model performance was better on the full record of data when the dry year 1989/90 was used as a calibration period so the optimized parameters set derived from this calibration was kept as model parameters. Furthermore, the model will be used to simulate discharge by the end of the 21st, when the climate is expected to be drier and thus model calibration based on a dry period is expected to be appropriate. The groundwater storage limit G_o, under which there is no flow from the groundwater store to surface runoff, is set to the groundwater storage at

the end of 1989/90, the first year with no summer flow. This enables the simulated discharge to become zero at the end of the hydrological year 1989/90, so as to be consistent with the observed data. Since 1985/86 from when we have a continuous discharge data series, the hydrological year 1989/90 was the first year to have some days of zero flow (92 days). As a consequence of the low flow, a drop in groundwater level was expected at the end of the 1989/90 hydrological year, which was confirmed from borehole tests (Fig. 6.13).

The capacity of the groundwater store G_m and the groundwater sub-catchment losses q are calculated by the model. The groundwater is assumed to have about 100 m depth and the water level is set at 15 m below the surface on the average, based on borehole pumping tests (Boronina 2003a; Udluft et al. 2003). The aquifer is assumed to have a mean porosity of 0.005 in all its depth (Ragab et al. 2010). It is a rather low value, but it is in accordance with values given by Boronina (2003a) and since there are no other reliable field data for this parameter we accept this value. The soil is thin with an average depth of 1 m and with the remaining 99 m depth at the above porosity gives a groundwater capacity of 495 mm. The fraction of groundwater storage q lost via sub-catchment leakage is determined from the drop in groundwater level in the early 1980s.

In the automatic calibration, the iterative sequential Fibonacci technique (Vardavas 1989), together with a sensitivity criterion is used to find the optimum value. The sensitivity s of the objective function for a Δp change in a parameter value p is defined by Eq. 4.39:

$$s = \frac{\Delta\chi^2/\chi^2}{\Delta p/p} \tag{4.39}$$

where $\Delta\chi^2$ is the change in the objective function. The optimized value of each parameter and the sensitivity of the objective function for a 10% change in a parameter value are given in Table 4.2.

Table 4.2: Values of model parameters, search range and sensitivity of the objective function to a 10% change in a parameter value.

Parameter	Range	Value	Sensitivity
DEL_0	0-1	0.5	4.48E-06
DEL_1	0-1	0.4443	0.00162
DEL_2	0-1	0.0306	2.53E-04
L_m	0-10	7	0.09728
D_m	0-10	3	0.04132
S_m	250-500	336.9	0.05383
G_m	0-5000	495	
α	0-1[a]	0.18	0.01893
β	0-1[a]	0.54	0.05583
δ	0-1	0.0328	0.00116
F_0	200-600	550.2	7.02E-04
p_0	1-5	4.78	0.41595
G_0		0.67	0.03333
q		0.1790	
γ	1-5	1.22	0.12419

a $0 \leq \alpha + \beta \leq 1$

Bibliography

Boronina, A.: Application of numerical modelling, isotope studies and streamflow observations for quantitative description of hydrogeology of the Kouris catchmen(Cyprus)., PhD thesis in Natural Sciences, Centre for Hydrogeology, Zurich, Swiss Federal Institute of Technology (ETH), 2003a.

Boughton, W.: A mathematical catchment model for estimating runoff, J. Hydrol. NZ, 7, 75-100, 1968.

Croke, B., Cleridou, N., Kolovos, A., Vardavas, I., and Papamastorakis, J.: Water resources in the desertification-threatened messara valley of Crete: estimation of the annual water budget using a rainfall-runoff model, Environmental Modelling and Software, 15, 387-402, 2000.

Ragab, R., Bromley, J., Dorflinger, G., and Katsikides, S.: IHMS—Integrated Hydrological Modelling System. Part 2. Application of linked unsaturated, DiCaSM and saturated zone, MODFLOW models on Kouris and Akrotiri catchments in Cyprus, Hydrological Processes, 24, 2681-2692, 2010.

Udluft, P., Dünkeloh, A., Mederer, J., Külls, C., and Schaller, J.: Water balances for catchments and for the whole island, Appendices 1+2, GRC Project Report T6/7, Cyprus Geological Survey Department, Nicosia, pp. 111-112, 2003.

Vardavas, I.: A simple water balance daily rainfall-runoff model with application to the tropical Magela Creek catchment, Ecological Modelling, 42, 245-264, 1988.

Vardavas, I.: A Fibonacci search technique for model parameter selection, Ecological Modelling, 48, 65-81, 1989.

Chapter 5

Model Validation

The performance of the rainfall-runoff model is assessed graphically and numerically through a number of tests, with a focus on monthly and annual discharge values.

5.1 Graphical analyses: time-series plots

The first validation of the model was performed by comparing the simulated and observed daily, monthly and annual discharge plots (Figures 5.1 - 5.4). Figures 5.1 and 5.2 show trends for low flow years and Figure 5.3 for high flow years. Figure 5.4 shows monthly and annual simulated and observed discharge, showing the better agreement on these time scales. For the 2008/09 hydrological year, which follows an extreme drought (4 years with considerably below average rainfall), the poor performance could be explained by the unmonitored excessive pumping, in the drought years, upstream of the gauge system, causing the lower observed than simulated discharge.

Another source of error is snow, which contributes to the precipitation but is not measured by rainfall gauges and thus not taken into account as water input. The amount of snow is generally small and the available snow data are limited. For the period 1989/90 to 2008/09, the only available snow data are the annual number of days with snow in Cyprus (average 33 days per year). Also known, but only for the period 1976/77 to 1991/92, is the mean annual value of total depth of new snow (251 cm) at the Troodos Square (elevation: 1725 m) and the corresponding average number of days with snow (38 days per year). There are some years (1991/92, 1992/93 and 2002/03) when the number of days with snow is above average (61, 53 and 43, respectively) implying that for those years the snow is not negligible and thus, an underestimation of the simulated discharge is expected.

A divergence between simulated and observed flow data was also found during the 1997/98

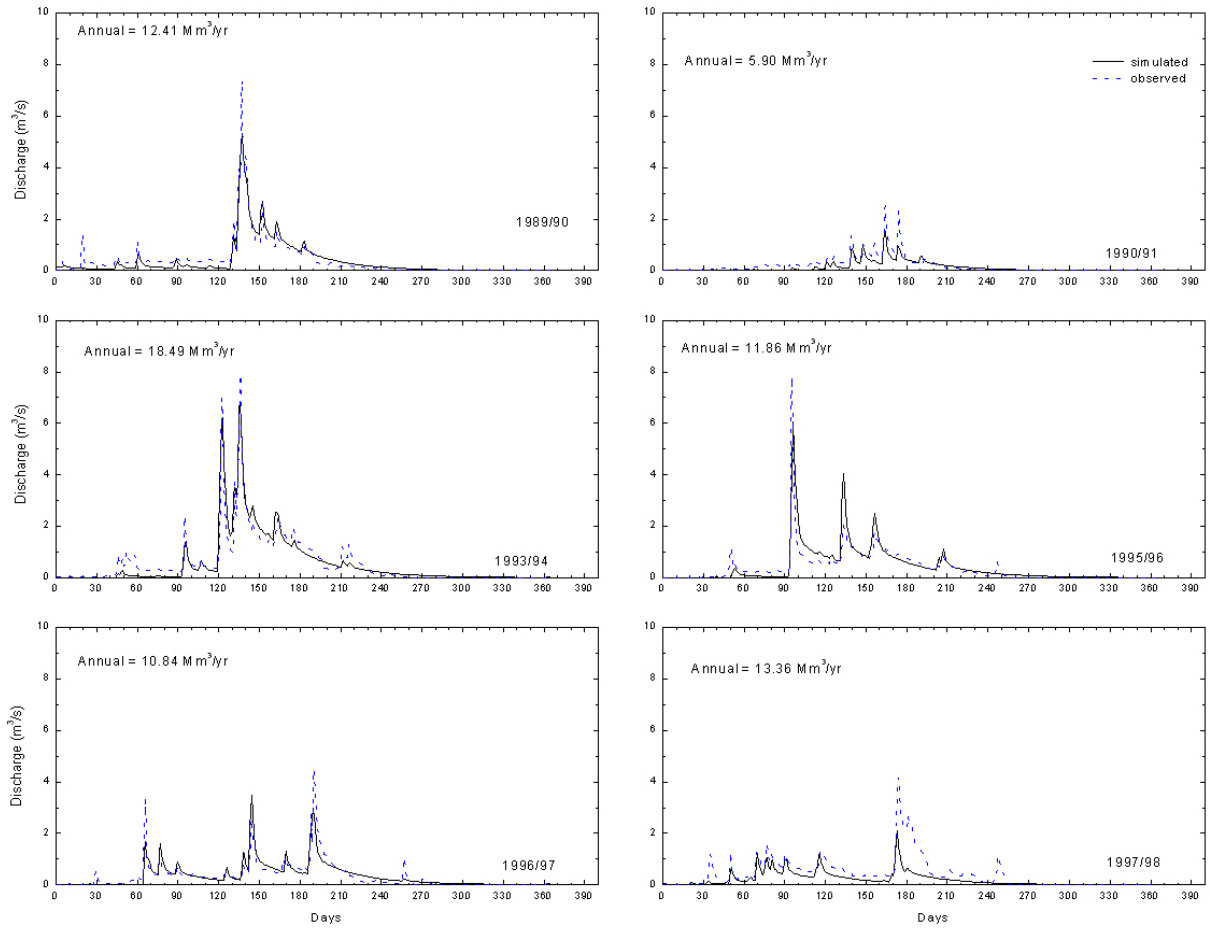

Figure 5.1: Daily simulated and observed discharge at the catchment outlet for low-flow hydrological years 1989/90, 1990/91, 1993/94, 1995/96, 1996/97, 1997/98. Hydrological year begins on 1st October and ends 30th September.

year that can be attributed to the unknown amount of water that was transferred from Arminou dam, situated outside the catchment, to the Kryos River via a tunnel, during the testing period of the tunnel in the winter of 1998. Since October 1998, the amount of water transferred from Arminou dam to the Kryos River is known and it is thus subtracted from the recorded discharge value at the Kryos gauge.

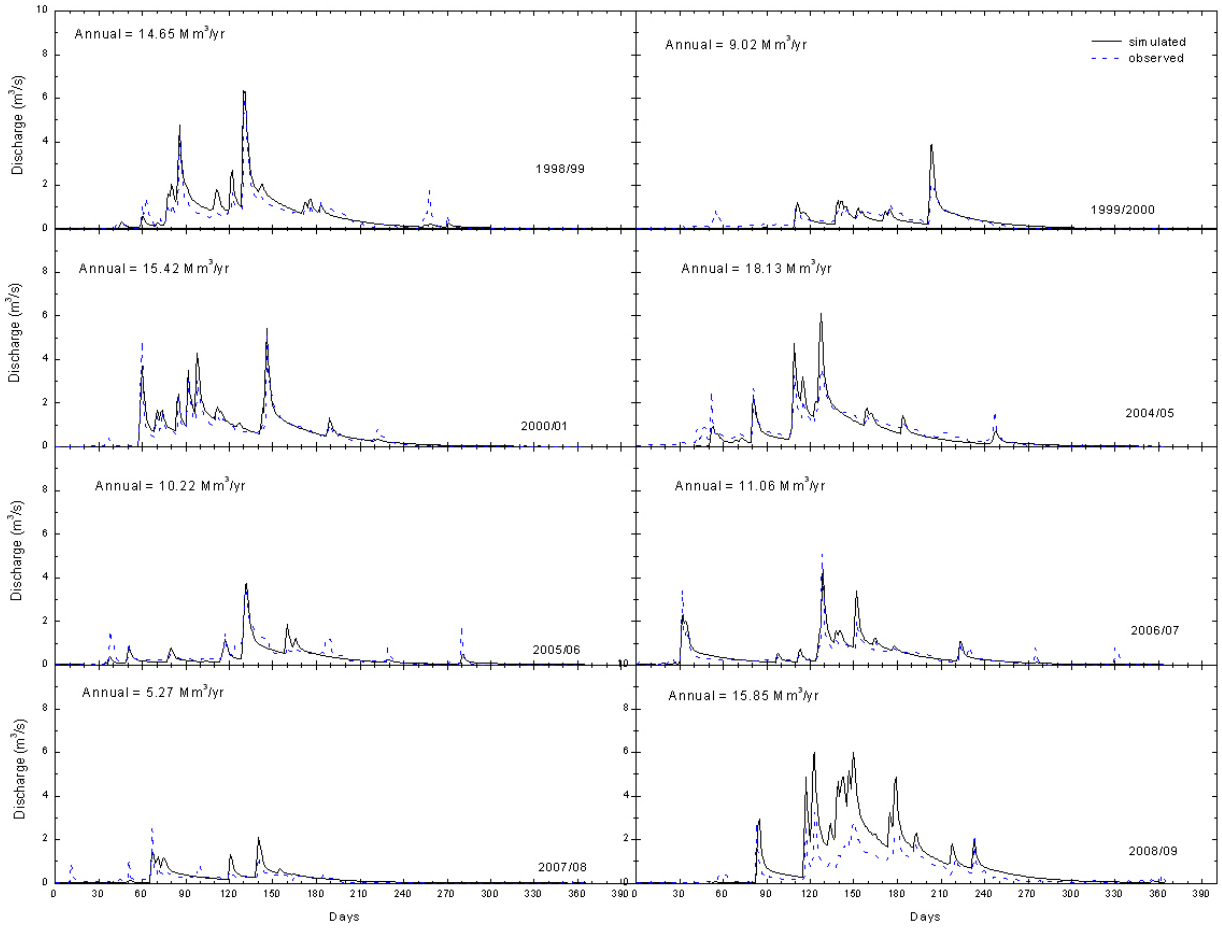

Figure 5.2: Daily simulated and observed discharge at the catchment outlet for low flow hydrological years 1998/99, 1999/00, 2000/01, 2004/05, 2005/06, 2006/07, 2007/08 and 2008/09.

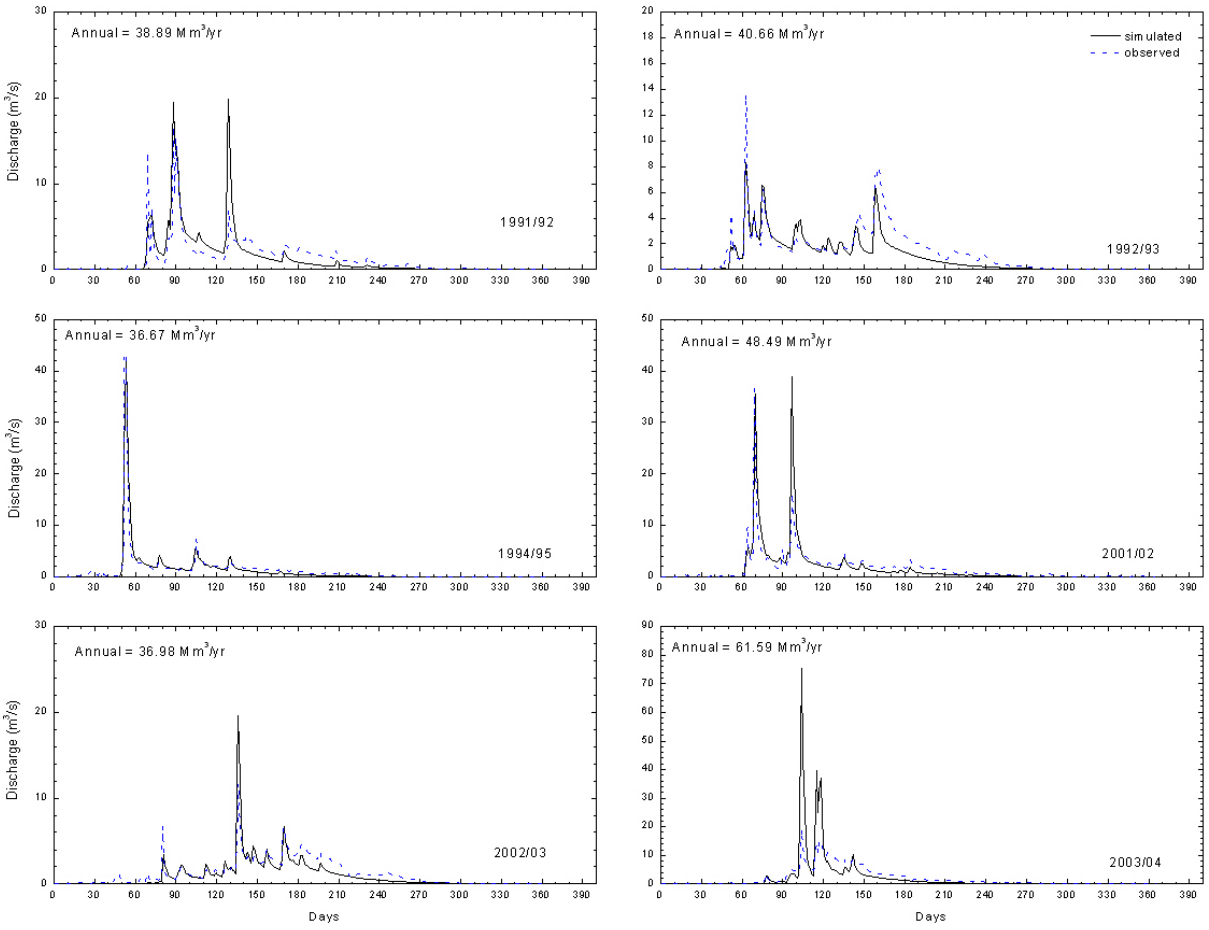

Figure 5.3: Daily simulated and observed discharge at the catchment outlet for high flow hydrological years 1991/92, 1992/93, 1994/95, 2001/02, 2002/03 and 2003/04.

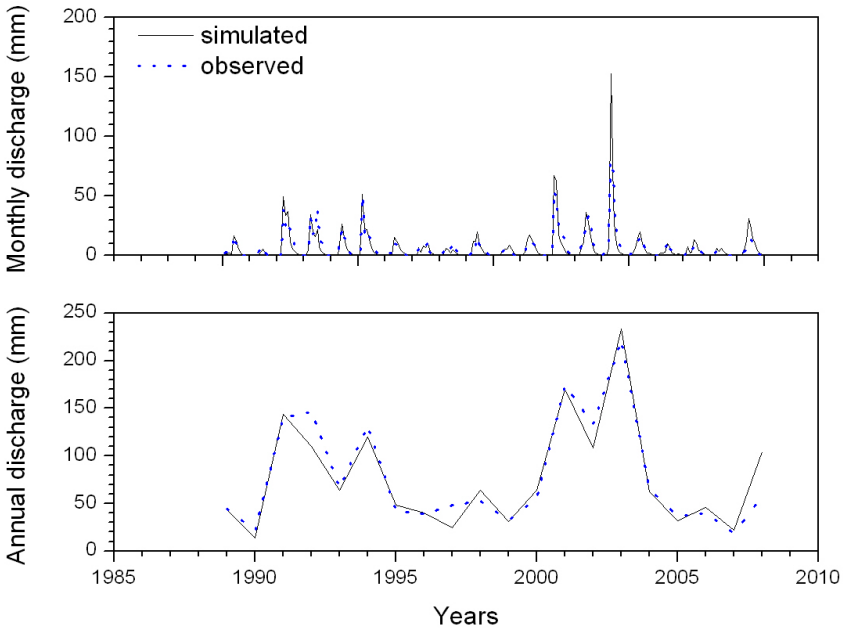

Figure 5.4: Annual and monthly simulated and observed discharge at the catchment outlet.

5.2 Graphical analyses: flow duration curves

We compare the flow duration curves of simulated and observed discharge, based on the mean daily flow rates for the period 1989/90 to 2008/09. Figure 5.5 shows the simulated and observed flow rate plotted against the percentage of days a flow is exceeded. The point at 100% corresponds to the percentage of days that have a flow rate other than zero and 0% corresponds to the percentage of days with a flow rate equal to or greater than 70 m^3/s and it is the same for both simulated and observed discharge. The shape of the curve can reveal some characteristics of the catchment and the very good match between simulated and observed discharge reveals that the model captures well the characteristics of the catchment. A steep curve in the high flow region indicates that the rare flood events are caused by intense rainfall and not by, for example, snow melting, which would last for a longer period. On the other hand, the flat curve at the low flow rate region indicates an intermittent stream with groundwater storage that cannot sustain summer flow. To check the performance of the model at low flow rates we use a log-transform on the flow rate axis (Bennett et al. 2013). We see a fairly good match between the simulated and the observed discharge down to 0.3 m^3/s.

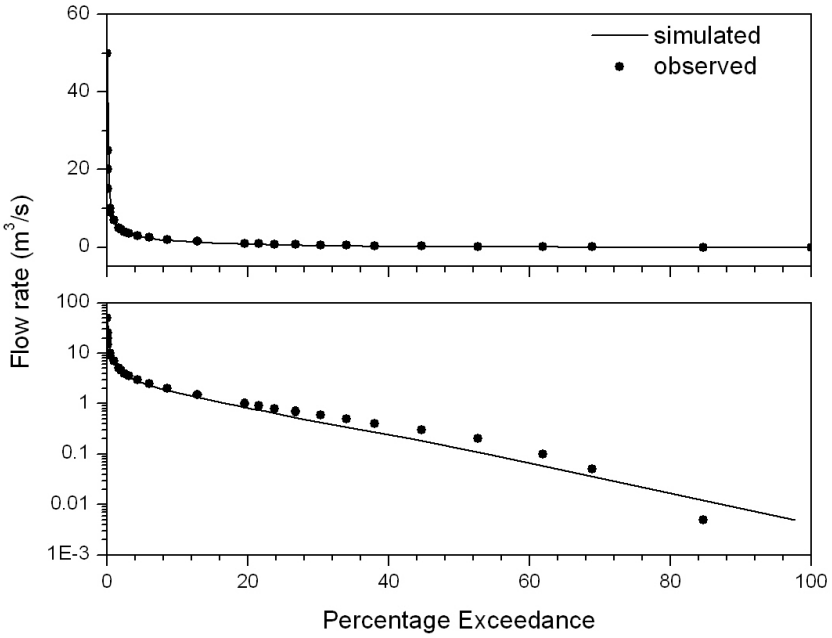

Figure 5.5: Normal and logarithmic transformation of simulated and observed flow (bin data) duration curves for the period 1989/90 to 2008/09.

5.3 Numerical analyses: objective function χ^2, relative error ε and Nash-Sutcliffe efficiency

To check simulated discharge against observed discharge data, the values of the objective function χ^2 and relative error ε are calculated, as well as the Nash-Sutcliffe efficiency *NSE*. The objective function χ^2 provides the square of the differences between observed and simulated data so it is expected to give higher values for years with high flows and lower values for years with low flow so it may be a little unreliable for low flow years overestimating the efficiency of the model. On the other hand model performance may be underestimated during high flow years. For this reason we calculate the relative error. The relative error gives higher values for years with low flow, underestimating model performance. Thus, a combination of objective function χ^2 and relative error ε can give a more reliable picture for model performance on the entire flow range.

The relative error is defined by Eq. 5.1:

$$\varepsilon = \frac{\sum_{i=1}^{N} |Q_{oi} - Q_{mi}|}{\sum_{i=1}^{N} Q_{oi}} \tag{5.1}$$

In Table 5.1 we give the χ^2 values and the relative errors for the period 1989/90-2008/09. The χ^2 per degree of freedom is less than 1 for all years indicating reliable matching of simulated and observed discharge (Taylor 1982) and for 15 out of 20 years its value is less than 0.1, a value indicating good model performance and difficult to attain otherwise. The relative error is smaller than about 0.5 for most years indicating adequate model performance on a daily basis.

As a further check we calculate the Nash-Sutcliffe efficiency *NSE* (Nash and Sutcliffe 1970). *NSE* is defined by Eq. 5.2:

$$NSE = 1 - \frac{\sum_{i=1}^{N} (Q_{oi} - Q_{mi})^2}{\sum_{i=1}^{N} (Q_{oi} - \bar{Q}_o)^2} \tag{5.2}$$

where $\bar{Q}_o$ is the mean value of the observed data and N the number of measurements. The closer to unity the value of *NSE* is the better the fit. The Nash-Sutcliffe efficiency factor *NSE* squares the differences between simulated and observed discharge, and it is thus very sensitive to high extreme values whereas it is insensitive to very low values (Croke 2009). However, the values of *NSE* by themselves should be interpreted with caution (Jain and Sudheer 2008; Gupta et al. 2009) since a high value of *NSE* does not always mean high model performance. On the other hand, a low value may also not reflect model performance, as can be seen for the hydrological year 2002, where the other two indices and Figure. 5.3 indicate good model performance.

Values for the three indices calculated on a daily basis are given for 20 years in Table 5.1. When all three indices of model performance are good then the model performance is reliable on a daily basis. For the hydrological year 2000, for example, all three indices are very good as also can be seen in Figure 5.2, this is true for about 11 years out of the 20 years simulated. However on a monthly and annual basis, on which our climatic impact assessment is based, the agreement between simulated and observed discharge is very adequate as can be seen in Figure 5.4 and by the monthly *NSE*.

The values of monthly *NSE* given in Table 5.1 clearly indicate, together with χ^2 and ε, that for the hydrological years 2003 and 2008, model performance is weak. The year 2003/2004 was marked with an extreme January rainfall of 403 mm compared to a mean long-term annual

value of 625 mm (Figure 5.3). The year 2008 is problematic, reflecting the uncertainty in the observed data due to excessive unmonitored pumping prior to that year, as discussed earlier. If we omit the 2008/09 year the mean monthly Nash- Sutcliffe efficiency *NSE* is 0.88. For 17 years out of 20 the monthly *NSE* is more than 0.75 and the model efficiency is characterized as being very good, and was found to be independent of annual rainfall, which ranges from about 400 to 900 mm.

Table 5.1: Values on a daily basis of the objective function χ^2 , relative error ε and Nash-Sutcliffe efficiency *NSE* for each hydrological year. Also shown are the *NSE* values on a monthly basis. The total number of days with no flow is also shown

Hyd. Year	Days of no flow	χ^2	ε	*NSE* monthly	*NSE* daily
1989	92	0.079	0.389	0.95	0.89
1990	132	0.069	0.523	0.82	0.71
1991	18	0.247	0.546	0.85	0.43
1992	0	0.079	0.362	0.88	0.75
1993	73	0.074	0.310	0.97	0.91
1994	34	0.077	0.334	0.98	0.88
1995	75	0.100	0.426	0.92	0.70
1996	82	0.085	0.402	0.95	0.77
1997	90	0.066	0.532	0.72	0.43
1998	29	0.051	0.402	0.89	0.77
1999	63	0.075	0.445	0.91	0.58
2000	57	0.048	0.268	0.94	0.83
2001	0	0.082	0.374	0.89	0.63
2003	0	0.619	0.705	0.50	-1.40
2004	0	0.036	0.327	0.95	0.70
2005	1	0.086	0.392	0.94	0.76
2006	16	0.052	0.371	0.92	0.74
2007	83	0.047	0.592	0.82	0.28
2008	1	0.238	0.938	-0.03	-0.94

5.4 Numerical analyses: correlation criteria

In Figures 5.6 - 5.8 we compare the annual and monthly simulated and observed discharge for the period 1/10/1989 to 30/9/2009. In Figure 5.6 the least squares best fit line has a slope 0.942 ± 0.142 (95% confidence level under the normality assumption of simple linear regression) and intercepts the y-axis at 3.37 ± 13.6 mm. The divergence from the 1:1 line is judged to be not statistically significant at the 95% confidence level, because the 95% confidence interval of the slope defined by 0.942 ± 0.142 = (0.800, 1.084) contains the value 1. The points which lie outside the confidence band (shown in Figure 5.6) correspond to

the hydrological years 1992/93, 1997/98, 2002/03 and 2008/09 with big uncertainties in the measured data as commented earlier in this section. In Figure 5.7 the slope of the best fit line is 1.157 ± 0.071 (95% confidence level) indicating a slight over-estimation of the observed flow, and intercepts the y-axis at -1.12 ± 0.90 mm. However, if we omit the two extreme points the new best fit line (Figure 5.8) has a slope 1.04 ± 0.05 (95% confidence level) and intercepts the y-axis at -0.52 ±0.57 mm and thus the 1:1 line is within the confidence band. The two extreme points correspond to January 2004 and February 2004, months with extremely high monthly rainfall, (403 mm and 92 mm, respectively).

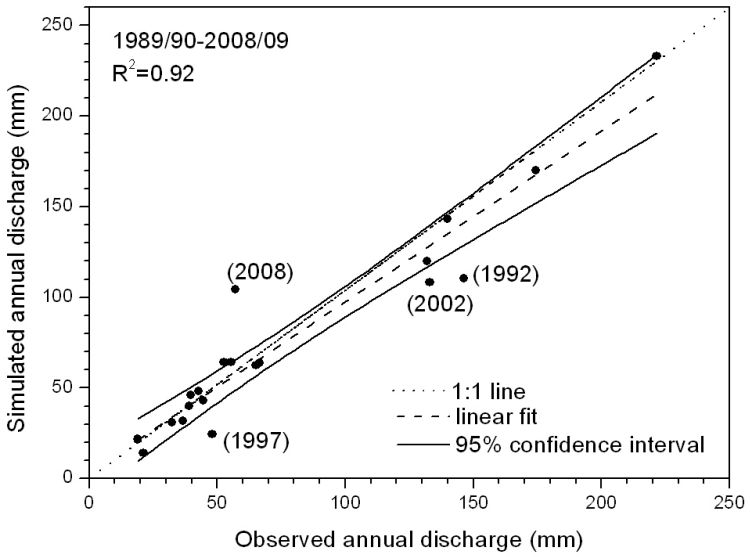

Figure 5.6: Scatter diagram with regression line and 95% confidence band of annual simulated and observed discharge. Numbers in parentheses represent the hydrological years with big divergences between model and observed flow.

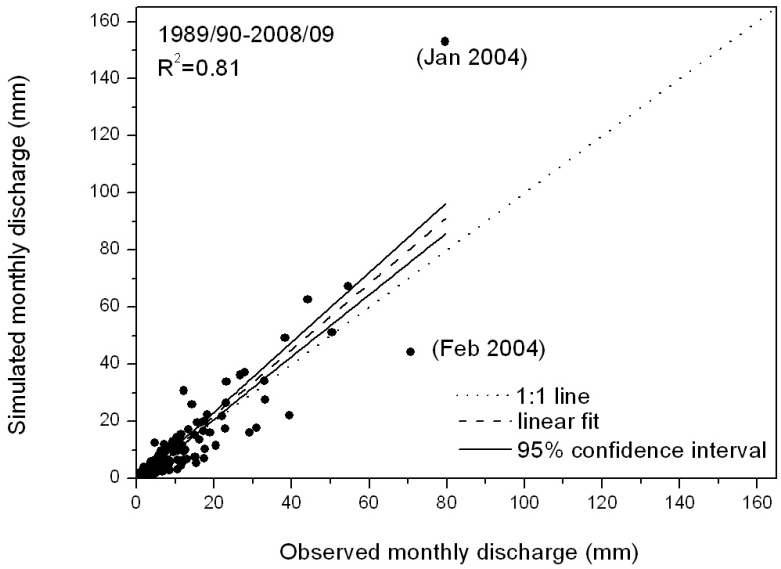

Figure 5.7: Scatter diagram with regression line and 95% confidence band of monthly simulated and observed discharge. Numbers in parentheses represent the months of a specific year with big divergences between model and observed flow.

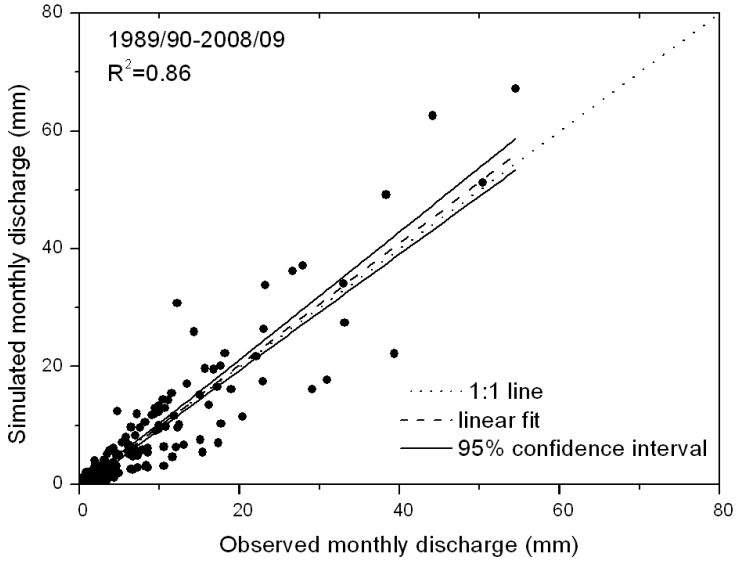

Figure 5.8: Scatter diagram with regression line and 95% confidence band of monthly simulated and observed discharge without the values of January and February 2004.

5.5 Fourier analysis of daily runoff coefficients

Fourier deconvolution can be used (with care) as a further test of model performance, such as the catchment response to rainfall, particularly when coupled with correlation analysis (Croke et al. 2011). Figure 5.9 shows the runoff coefficient (discharge/rainfall) as a function of days since last rainfall. The response of the catchment to rainfall is quick and flow appears at the discharge station within hours. The peak however appears one day after the rainfall event as measured by the gauge and this is well simulated by the present version of the model, which includes the advective delay (DEL_0=0.5) of fast runoff. Figure 5.10 demonstrates how the DEL_0 handles this delay. When DEL_0=1, no delay, (Figure 5.10) discharge arrives at the outlet the same day as the rainfall event.

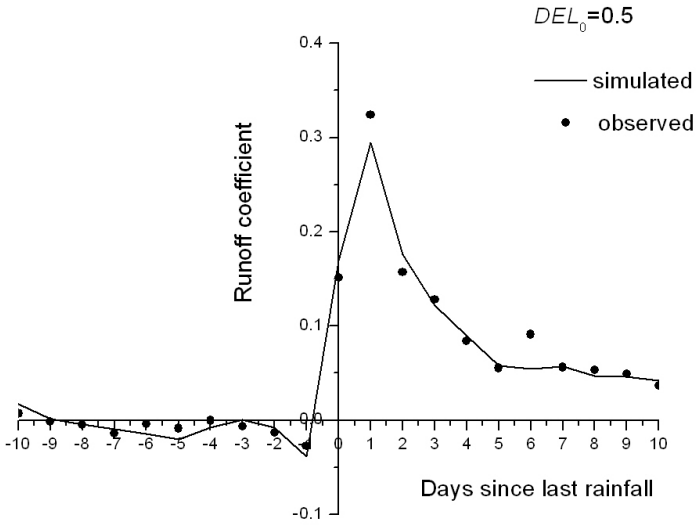

Figure 5.9: Runoff coefficient derived from Fourier analysis of rainfall and discharge data (simulated and observed), demonstrating the quick response of the catchment and the one day delay in the peak flow after the last rainfall, with DEL_0=0.5 obtained by model optimization.

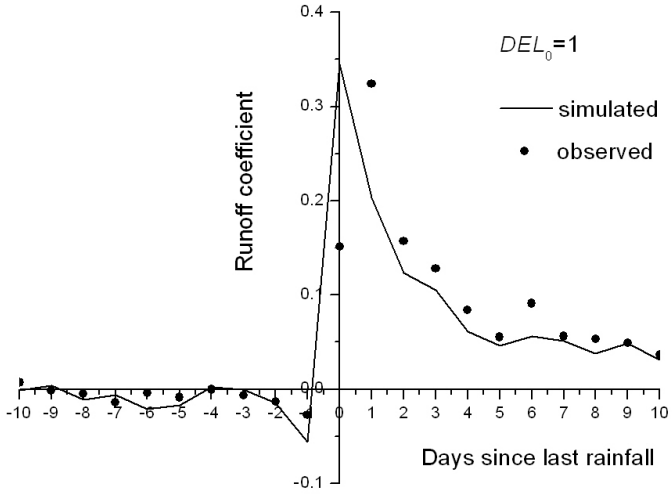

Figure 5.10: Runoff coefficient derived from Fourier analysis of rainfall and discharge data (simulated and observed), demonstrating the quick response of the model catchment to the rainfall event if DEL_0 parameter is set equal to 1, no delay.

Bibliography

Bennett, N., Croke, B., Guariso, G., Guillaume, J., Hamilton, S., Jakeman, A. J., Marsili-Libelli, S., Newham, L., Norton, J. P., Perrin, C., Pierce, S. A., Robson, B., Seppelt, R., Voinov, A., Fath, B., and Andreassian, V.: Characterising performance of environmental models, Environmental Modelling & Software, 40, 1-20, 2013.

Croke, B.: Representing uncertainty in objective functions: extension to include the influence of serial correlation., In Anderssen, R.S., R.D. Braddock and L.T.H. Newham (eds) 18th World IMACS Congress and MODSIM09 International Congress on Modelling and Simulation. Modelling and Simulation Society of Australia and New Zealand and International Association for Mathematics and Computers in Simulation, July 2009, pp. 3372-3378, 2009.

Croke, B., Islam, A., Ghosh, J., and Khan, M.: "Evaluation of approaches for estimation of rainfall and the Unit Hydrograph", Hydrology Research, 42(5), 372-385, 2011.

Gupta, H. V., Kling, H., Yilmaz, K. K., and Martinez, G. F.: Decomposition of the mean squared error and NSE performance criteria: Implications for improving hydrological modelling, Journal of Hydrology, 377, 80-91, 2009.

Jain, S. K. and Sudheer, K.: Fitting of hydrologic models: a close look at the Nash--Sutcliffe index, Journal of hydrologic engineering, 13, 981-986, 2008.

Nash, J. E. and Sutcliffe, J.: River flow forecasting through conceptual models, Part I - A discussion of principles, Journal of Hydrology, 10, 282-290, 1970.

Chapter 6

Model Application - Kouris Catchment Hydrology

The aim of this work is to assess the impact of climate change on the water resources of Cyprus. However, in order to describe the future water fluxes of the catchment, we firstly have to apply the hydrological model to the Kouris catchment and see if it adequately captures the behavior of the Kouris catchment for the period we have observed data. The model was applied to the Kouris catchment for the period 1989/90 to 2008/09 (hydrological year starts on the 1^{st} of October and ends on the 30^{th} of September of the next year). The hydrological model computes the water fluxes of the catchment, from the time the precipitated water enters the catchment, passing through the various stores until it leaves the system. We are mostly interested in monthly and annual values of the rainfall, discharge, actual evaporation and recharge. Yearly fluctuations in groundwater level can also be estimated.

6.1 Catchment evaporation

Most of the precipitated water returns to the atmosphere through evaporation and transpiration from the plant canopy and through evaporation from bare soil and water surfaces. In Cyprus, the evaporation rate is very high and it is estimated to be up to 80% of the precipitated water (Omorphos et al. 1996). As we shall see, for the period 1989/90 to 2008/09 the fraction was 74% based on our model calculations.

Potential evaporation is defined as the amount of water that would evaporate if sufficient water were available. On the other hand, actual evaporation depends on the water availabilty of the soil. In winter, when there is plenty of moisture, (Fig. 6.1) the actual evaporation rate can be set equal to the potential evaporation rate (Brutsaert 1984) whilst in the dry season,

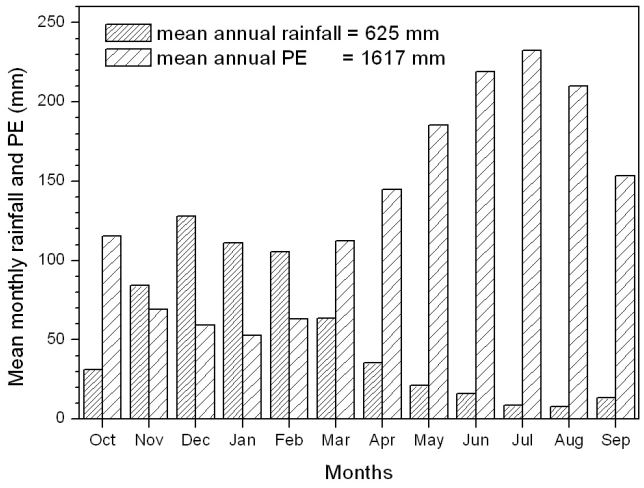

Figure 6.1: Long-term monthly rain and potential evaporation for the period 1989/90 to 2008/09.

actual evaporation rate is limited by soil water availability and it is thus less than the potential evaporation rate.

In the present work, the actual evaporation can be computed by the rainfall-runoff model as described in paragraph 4.1.3. Actual evaporation is considered as the sum of the evaporation from the three stores i.e. interception store, surface store and soil store. Evaporation from the groundwater store is not taken into account separately but it is included in the general losses of the groundwater store. Groundwater evaporation is more significant in alluvium aquifers where the water table is not very deep. For the Kouris catchment, the alluvium part, lying along the river bed, is about 2 km^2 i.e. 0.7% of the catchment's area (Boronina et al. 2005b), and it is thus only a small percentage of the catchment.

Simulated soil evaporation

At the beginning of the hydrological year most of the evaporation comes from the interception and surface store whilst the evaporation from the soil store is insignificant because the soil is dry. However, after the wet season, when the soil store has been wetted, the soil evaporation becomes more important (Fig. 6.2). The soil store moisture usually attains its maximum value in the period from January to March depending on the year. For the period 1989/90 to 2008/09, maximum values vary from 91 mm to 241 mm with a long-term average value of 163 mm (Fig. 6.3). Soil evaporation usually peaks in the period from March to April. For the period 1989/90 to 2008/09, maximum values vary from 1 mm/day to 2.1 mm/day with

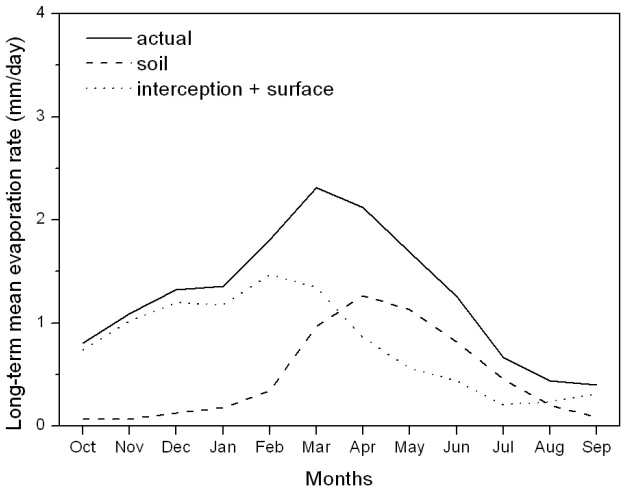

Figure 6.2: Long-term mean monthly simulated actual, soil and interception plus surface evaporation for the period 1989/90 to 2008/09.

an average of 1.5 mm/day (Fig. 6.4). For the same period, the long-term mean monthly soil evaporation varies from about 2 mm in September to 38 mm in April but maximum values can be as high as 66 mm (March 2004). Annual values vary from 99 mm to 216 mm with a mean of 174 mm.

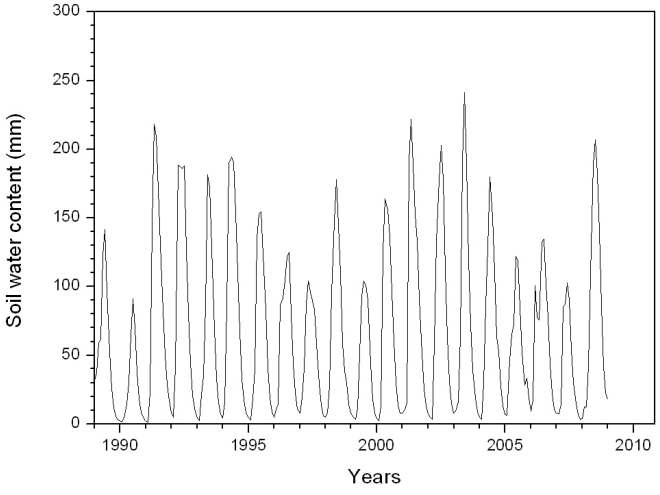

Figure 6.3: Simulated soil water content with years.

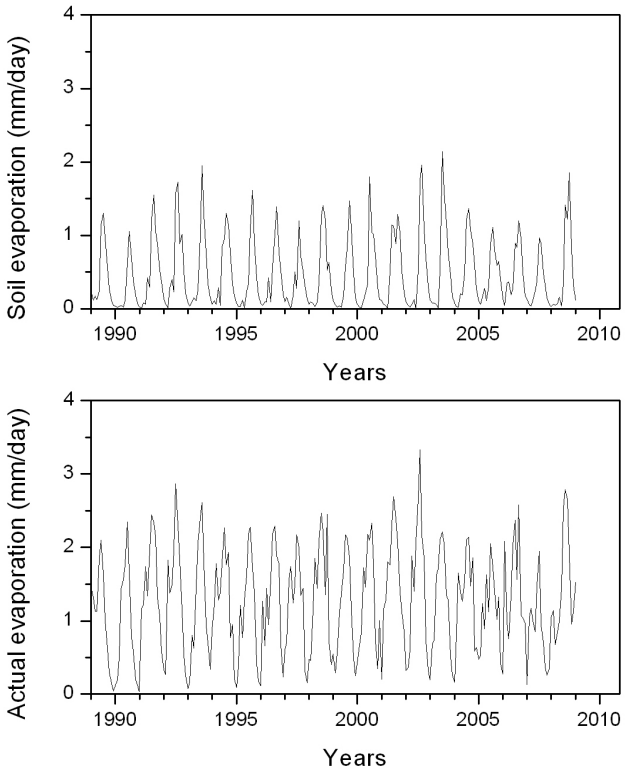

Figure 6.4: Mean monthly simulated soil and actual evaporation with years.

Simulated actual evaporation

Actual evaporation attains its maximum value in March or April. For the period 1989/90 to 2008/09, peak values range from 1.9 mm/day to 3.3 mm/day (April 2003) with an average of 2.4 mm/day (Figure 6.4). For the above period, monthly total values vary from 12 mm (September) to 72 mm (March) but the maximum value can be as high as 100 mm (April 2003). Annual values vary from 338 mm to 581 mm with a mean of 463 mm. On the other hand, for the same period, long-term mean monthly potential evaporation derived from pan coefficients and pan evaporation data (paragraph 3.3.2), ranges from 1.7 mm/day in January to 7.5 mm/day in July (Fig. 6.5). Long-term monthly total values are from 53 mm in January to 233 mm in July and mean annual values range from 1353 mm to 1807 mm with a mean value of 1617 mm (Fig. 6.6).

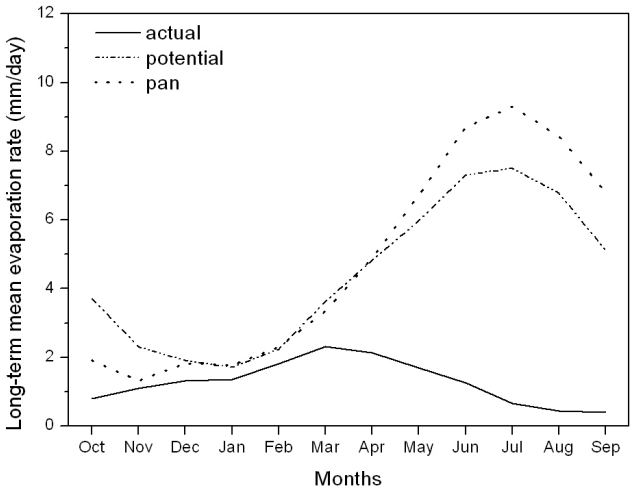

Figure 6.5: Long-term mean monthly potential, actual and pan evaporation for the period 1989/90 to 2008/09.

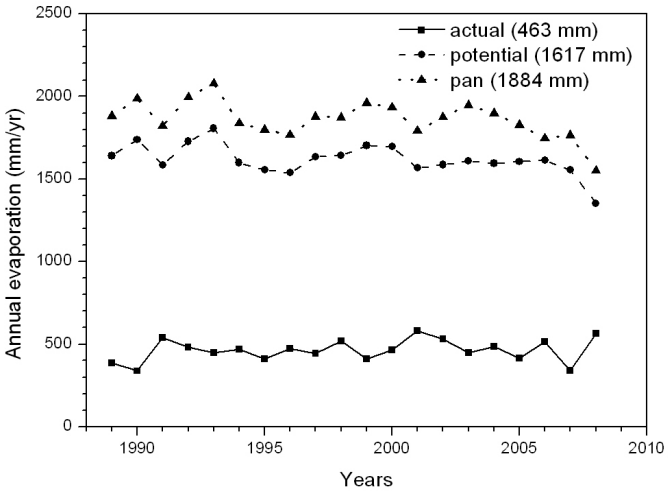

Figure 6.6: Variation of potential, actual and pan evaporation with years. Numbers in parentheses represent long-term mean annual values of the period 1989/90 to 2008/09. The actual evaporation is 463 mm or 74% of the mean annual rainfall of 623 mm for the same period.

6.2 Simulated discharge

The discharge is considered to have two components: the fast component consisting of the overland flow and the near surface soil flow and the slow component consisting of the deep surface soil flow and the flow from the groundwater. The slow component ranges from 39%

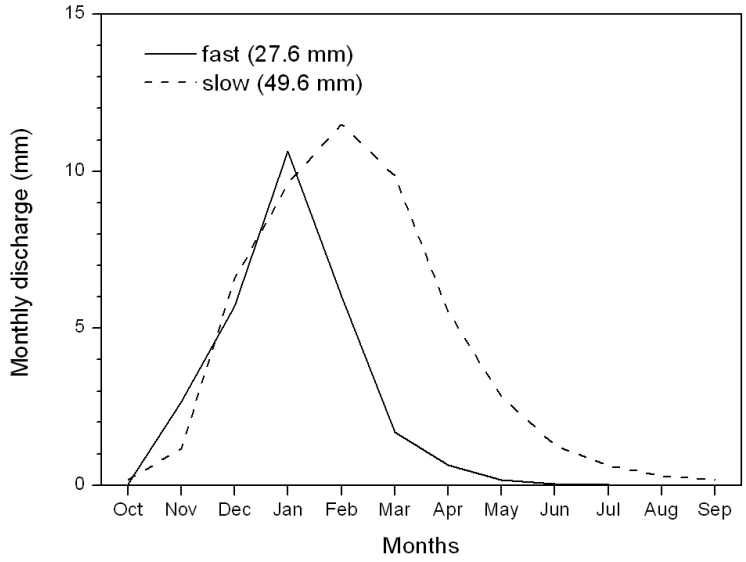

Figure 6.7: Long-term mean monthly fast and slow discharge. Numbers in parantheses represent mean annual values.

to 76% of total discharge but for 15 out of the 20 years the percentage is around 75% with an average at 70%, in agreement with Boronina et al. (2003b). The slow component has non-zero values all year round but it is more significant in the dry period, from May to September, when more than 95% of total discharge is deep flow (Fig. 6.7). Overland flow is only significant when the daily rainfall is very high. The relationship of simulated and observed discharge was presented in Chapter 5.

Dependence of discharge on rainfall

The relationship between annual discharge and annual rainfall is important, as it would help to estimate the discharge if the rainfall is known. At low annual rainfall values, the simulated discharge has a linear dependence with annual rainfall. At higher annual rainfall values the dependence seems to be quadratic (Figure 6.8). The same relationship exists between annual observed discharge and annual rainfall. Linear regression analysis on the scatter diagram of simulated discharge versus rainfall and on the scatter diagram of observed discharge versus rainfall, gives regression lines of almost the same slope, if the annual rainfall is low (below 600 mm) whilst the slopes are different if the annual rainfall is higher (Figures 6.9 and 6.10). Thus, the hydtological model seems to capture better the hydrology of the catchment for low rainfall values.

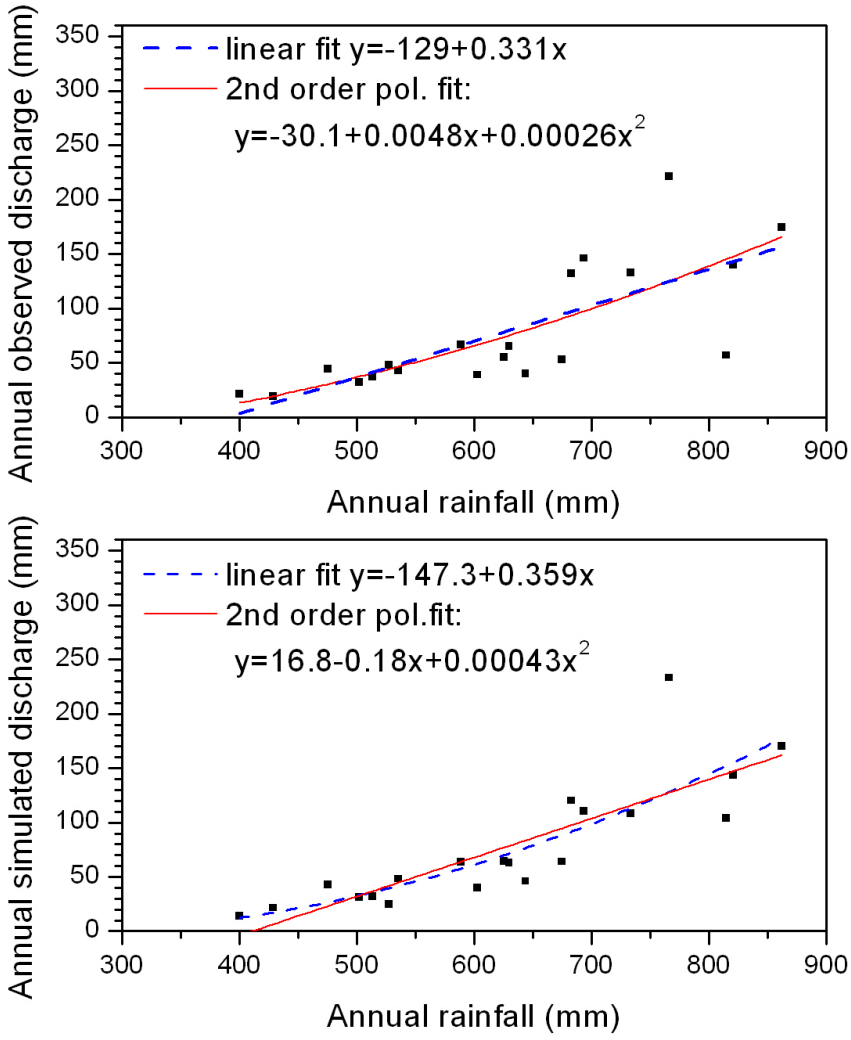

Figure 6.8: Scatter diagrams of observed and simulated annual discharge versus annual rainfall, for the period 1989/90 to 2008/09. Linear and quadratic fits valid only for the rainfall range 400-900 mm.

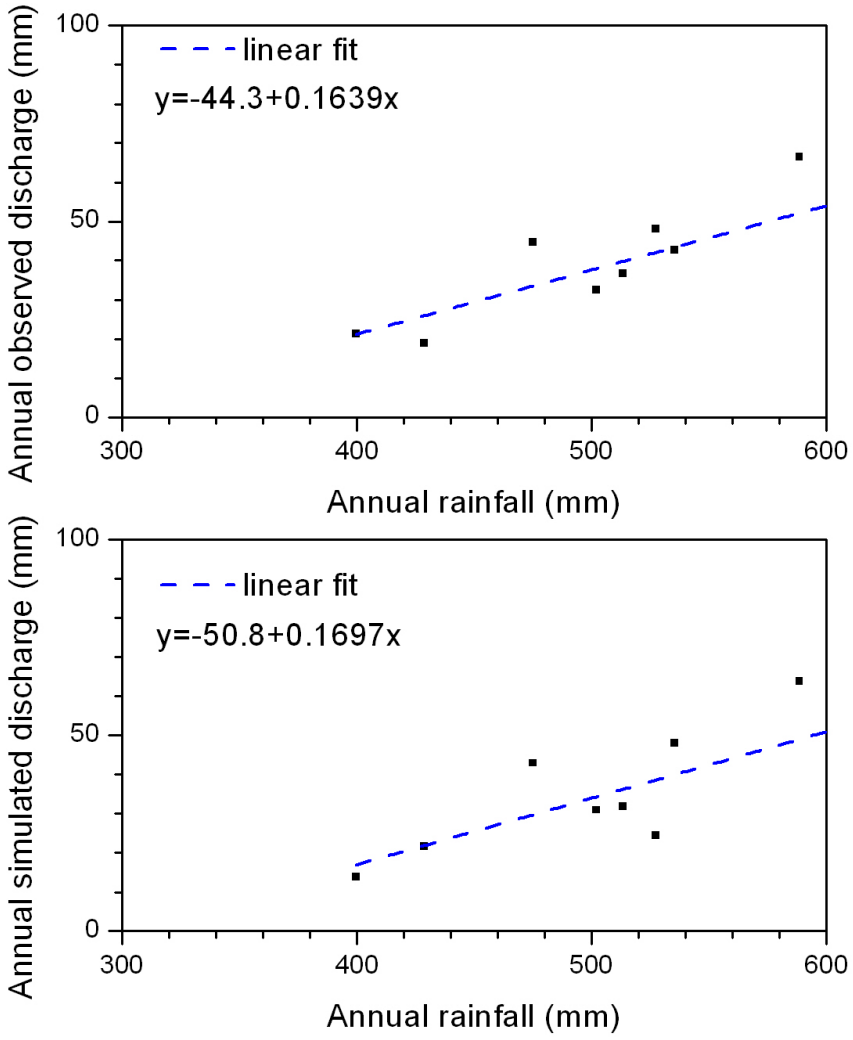

Figure 6.9: Scatter diagrams of observed and simulated annual discharge versus annual rainfall, for the 15 years, of period 1989/90 to 2008/09, with annual rainfall from 400 to 600 mm.

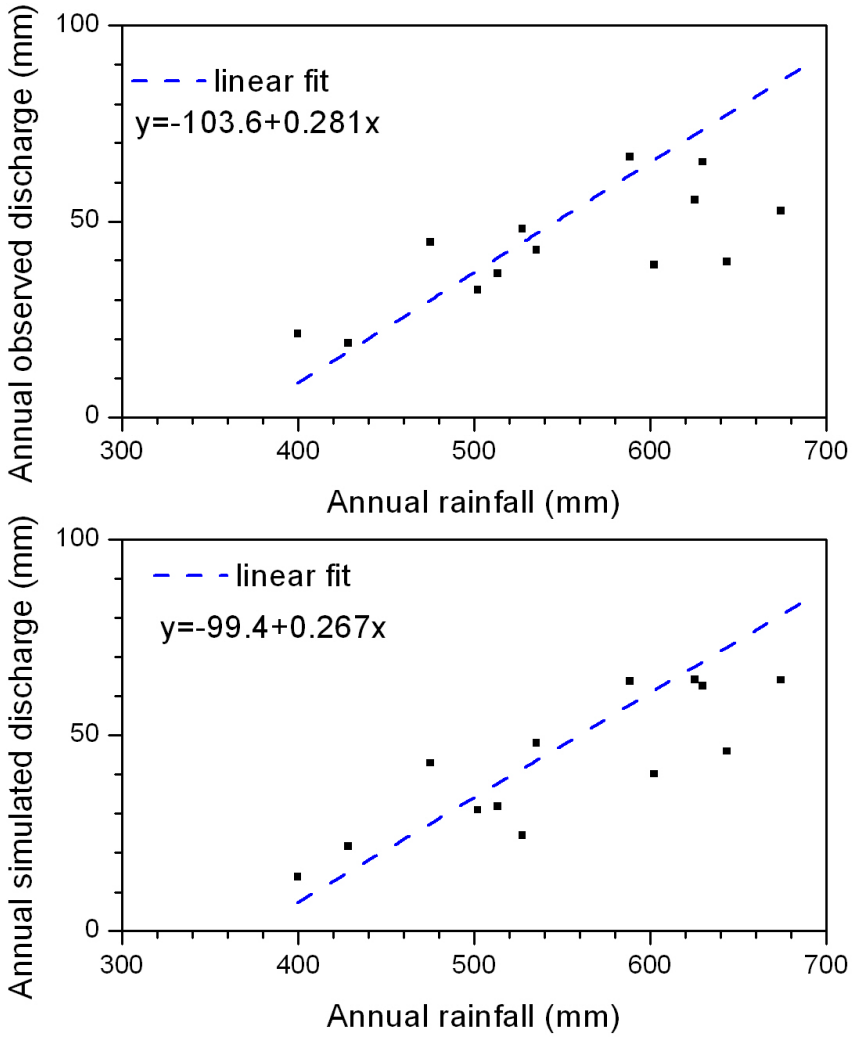

Figure 6.10: Scatter diagrams of observed and simulated annual discharge versus annual rainfall, for the 15 years, of period 1989/90 to 2008/09, with annual rainfall from 400 to 700 mm.

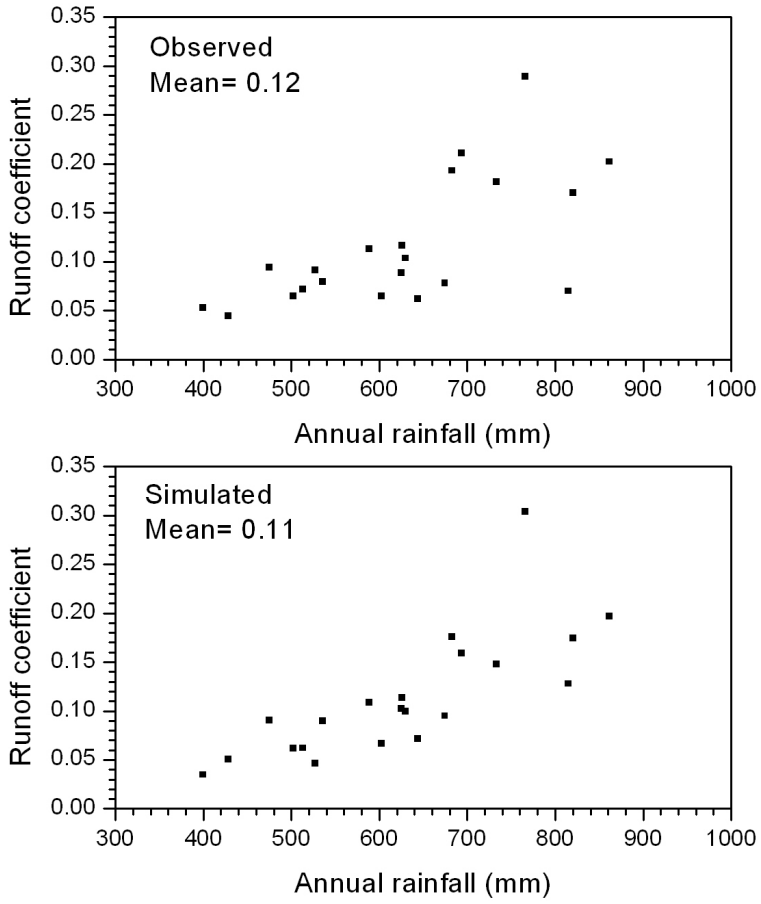

Figure 6.11: Scatter diagrams of runoff coefficient versus annual rainfall, for the observed and the simulated discharge data and for the period 1989/90 to 2008/09.

Runoff coefficient

The runoff coefficient is defined as the ratio of the discharge to the rainfall. For the simulated discharge, the runoff coefficient varies from 0.04 to 0.30 with a mean of 0.11, for the period 1989/90 to 2008/09. The corresponding value for the observed discharge is 0.12. The lower the rainfall the smaller is the runoff coefficient (Fig. 6.11). In most of the years the runoff coefficient is less than 0.2.

Pumping

The above analysis is based on an annual pumping of 8.9 Mm^3/yr, a value closed to the year 2000 water demand of the area (Savvides et al. 2001). By reducing the pumping to half this value, the long-term mean annual discharge increases by about 4.2% (from 21.5 Mm^3/yr or 77.2 mm to 22.4 Mm^3/yr or 80.5 mm, for the period 1989/90 to 2008/09) and the percentage of rainfall going to discharge increases from 12.3% to 12.9%. If there was no pumping, the long-term mean annual discharge, for the above period, would be 23.5 Mm^3/yr or 84.6 mm and the percentage of rainfall that goes to discharge would increase to 13.5%. Only an estimation of the pumping can be made since there are many unrecorded boreholes in the area upstream Kouris dam and the water demand is mostly satisfied from groundwater pumping and diversion of streams (Jacovides 1982).

6.3 Recharge

Recharge is defined in the model as the amount of rainfall stored as groundwater after evaporation and discharge. From this amount, a certain amount will be lost via groundwater losses and pumping. Groundwater losses are on average 7.8% of rainfall and they include groundwater evaporation and groundwater losses out of the catchment's boundaries. Its average value is 49 mm per year and it is almost constant with time. Annual recharge is from 46 mm to 145 mm with an average 86 mm or 24 Mm^3 per year. After groundwater losses and abstraction, the net recharge is from negative values to 97 mm per year with an average of about 37 mm or 10.2 Mm^3 per year. The recharge is very susceptible to rainfall and an increased amount of rainfall increases also the recharge. Maximum recharge occurs when the rainfall is high and the groundwater store is empty, as expected. For example, for the years 1991/92 and 2008/09, 17% and 17.8% of the annual rainfall, respectively, goes to recharge whilst the mean for the period 1989/90 to 2008/09 is 13.7%. 1991/92 and 2008/09 are high-rainfall years which follow an extreme drought period and the groundwater table is at a very low level; it is verified from borehole tests (Figure 6.13). As a consequence, the recharge rate for those years is high.

6.4 Groundwater

It is very difficult to estimate the groundwater resources. Borehole tests are not continuous in time and the groundwater level varies considerably from one borehole to the other due to the steep topography. However, by comparing the groundwater fluctuations at certain boreholes

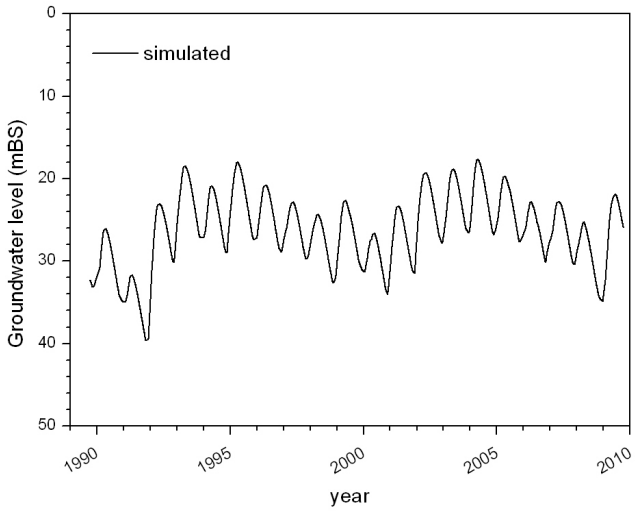

Figure 6.12: Simulated groundwater level for the period 1989/90 to 2008/09, expressed as meters below surface .

and those of the model we see that they follow the same pattern. For the period 1989/90 to 2008/09 we compare the groundwater level of five boreholes at various elevations with that of the model, for the month April when the groundwater store has its maximum storage. For the period 1989/90 to 2008/09, there are three years when the April groundwater level is at its minimum value and two years when it is at its maximum value. Low values recorded in April 1991 (hydrological year 1990/91), April 2000 (hydrological year 1999/00) and April 2008 (hydrological year 2007/08) and they are in agreement with the model. The biggest drop occured in April 2000 for all boreholes and it ranges from 1 m to 40 m, with higher values being occured in the areas of intensive cultivation where the groundwater is used for irrigation. However, the groundwater level recovers quite easily but not to its initial level at all boreholes (Figure 6.13). For the model the corresponding drop is about 8 m. Within a year the groundwater level drops by about 7 m to 12 m (Figure 6.12). Usually, in April the water level is at its maximum value and drops to its minimum in September before the start of the new rainy period.

6.5 Water balance

The rainfall-runoff model for the period 1989/90 to 2008/09 gives for the precipitated water the following partitioning: 74% returning to the atmosphere, 12.3% discharging to the catchment outlet (12.5% is the measured) and 13.7% going to recharge. After groundwa-

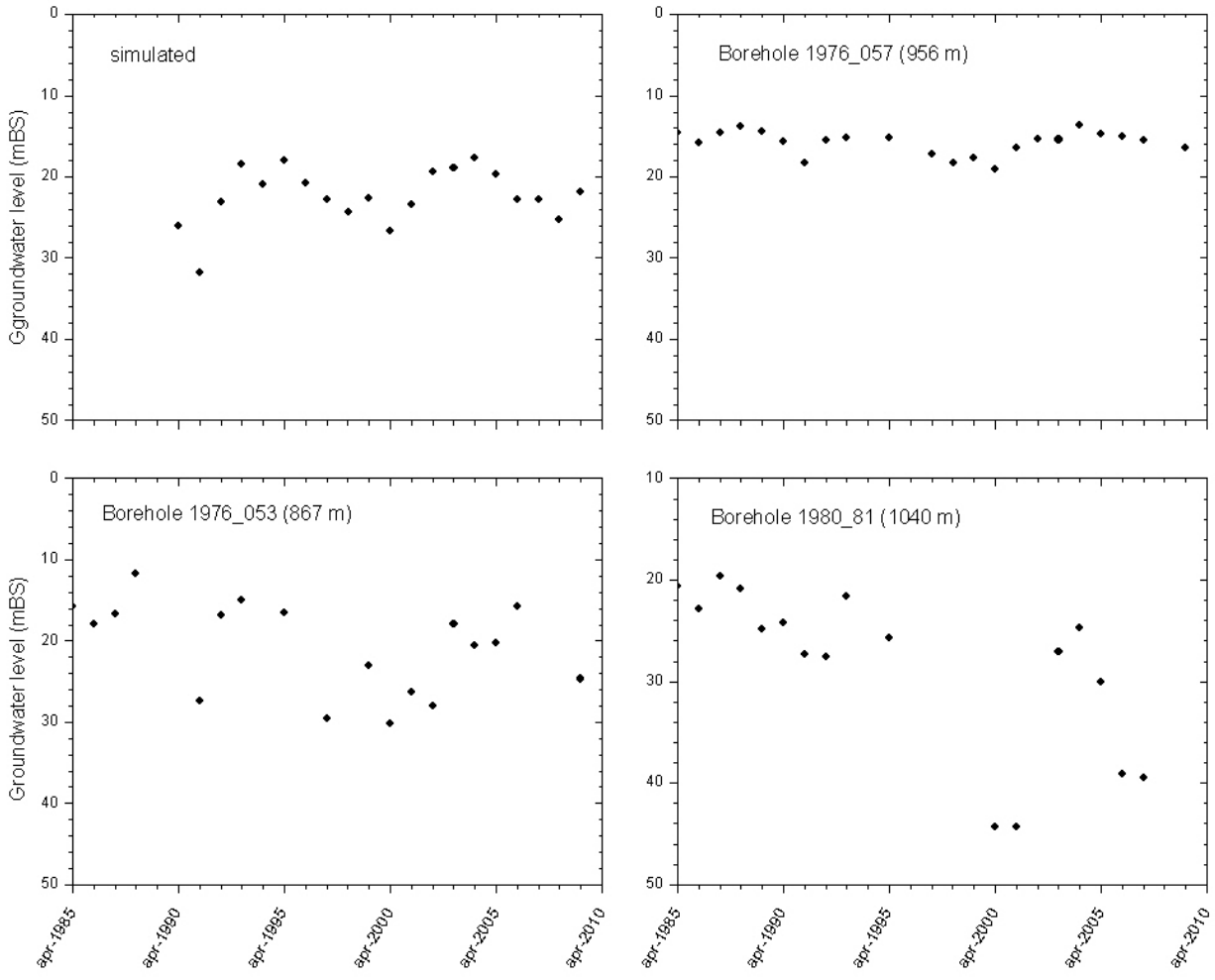

Figure 6.13: Simulated and observed (from boreholes tests) groundwater level, for the month April, expressed as meters below surface .

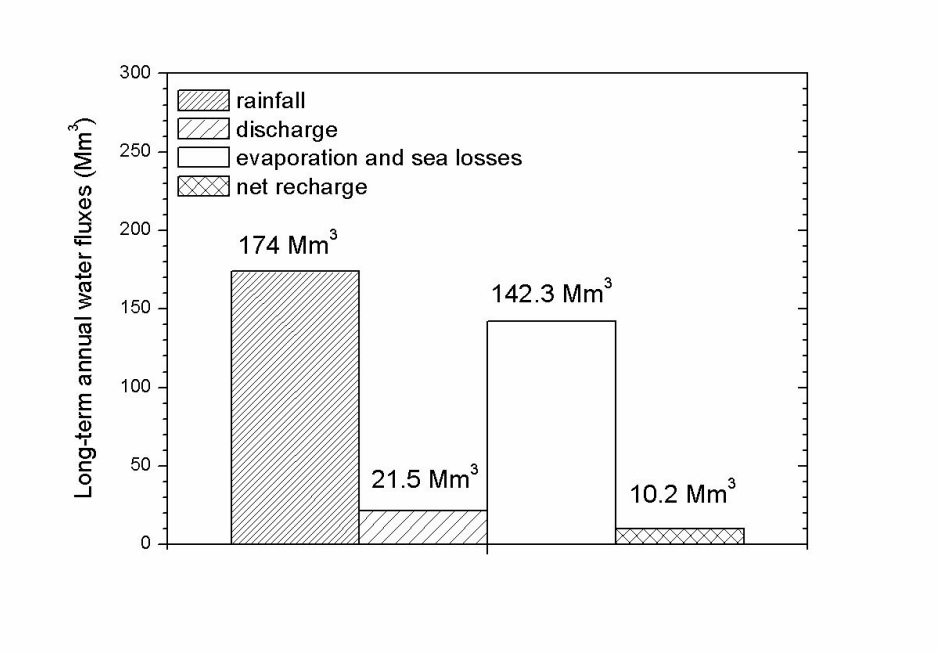

Figure 6.14: Long-term annual means of rainfall, discharge, actual evaporation and net recharge from the rainfall-runoff model for the period 1989/90 to 2008/09.

ter losses (excluding pumping) the net recharge is 5.9% of rainfall and the total water lost is 81.8%. Thus, only 18.2% of precipitation is available for surface and groundwater resources. In Figure 6.14 is shown the long-term (1989/90 to 2008/09) annual values of rainfall, total evaporation (total water lost), discharge and net recharge in Mm^3 per year. According to the Water Development Department of Cyprus the annual water demand for the Kouris catchment was more than 10 Mm^3 in 2000 with an increasing future trend (Savvides et al. 2001). Water demand is mostly satisfied from groundwater and surface water through pumping and river diversion reducing thus the available water for the Kouris dam even more. If we assume that all the water demand is satisfied via pumping then the net recharge including pumping falls to 0.2 Mm^3 per year whilst the available water for the dam is reduced to 12.5%. The above findings agree with the work of others. Boronina et al. (2003b) using the chloride method evaluated the direct recharge rate to be about 17% of total rainfall (period September 2000-November 2001) and for the same period our model gives 15.4% as a recharge rate. Udluft et al. (2003) used a distributed model and found for the period 1/10/1987 to 30/9/1997 that 73.3% of rainfall goes to evaporation including groundwater losses, 13.9% for surface runoff and 12.7% to recharge. For the same period we get respectively 79.7%, 14.7% and 13.2%. The percentage of rainfall that goes to surface runoff depends on the amount of rainfall. When annual rainfall is low the percentage going to runoff is very low (Table 6.1).

Table 6.1: The percentage of rainfall that goes to discharge, evaporation and recharge.

Hyd. Year	Annual rainfall mm	Observed discharge % of rainfall	Simulated discharge % of rainfall	Actual evaporation % of rainfall	Recharge % of rainfall
1989	475	9.4	9	81.2	9.8
1990	400	5.3	3.5	84.7	11.8
1991	820	17.1	17.5	65.5	17
1992	693	21.1	15.9	69.6	14.5
1993	588	11.3	10.9	75.9	13.2
1994	683	19.3	17.6	68.6	13.8
1995	535	7.9	8.9	76.8	14.2
1996	602	6.5	6.7	78.2	15.1
1997	527	9.1	4.7	84.2	11.2
1998	674	7.8	9.5	77	13.5
1999	502	6.5	6.2	81.8	12
2000	625	8.9	10.3	74.3	15.4
2001	862	20.2	19.7	67.5	12.8
2002	733	18.2	14.8	72.7	12.5
2003	766	28.9	30.4	58.3	11.2
2004	630	10.4	9.9	76.8	13.2
2005	513	7.2	6.2	80.8	13
2006	644	6.2	7.1	79.9	12.9
2007	429	4.4	5	79.1	15.8
2008	814	7.0	12.8	69.4	17.8

Bibliography

Boronina, A., Renard, P., Balderer, W., and A., C.: Groundwater resources in the Kouris catchment(Cyprus): data analysis and numerical modelling, Journal of Hydrology, 271(1-4), 130-149, 2003b.

Boronina, A., Golubev, S., and Balderer, W.: Estimation of actual evapotranspiration from an alluvial aquifer of the Kouris catchment (Cyprus) using continuous streamflow records, Hydrological Processes, 19(20), 4055-4068, 2005b.

Brutsaert, W.: Evaporation in the Atmosphere: Theory, History and Applications, D. Reidel, Dordrecht, The Netherlands, 299, 1984.

Jacovides, J.: Southern conveyor project, feasibility study Vol 2: Surface water resources, Technical Report. Ministry of Agriculture and Natural Resources, Water Development Department, Nicosia, Cyprus, p. 19, 1982.

Omorphos, C., Kambanellas, C., Hadjigeorgiou Savvidou, P., Selipa, S., Andreou, P., and Ioannou, E.: Water development in Cyprus, Ministry of Agriculture, Natural Resources and Environment, Water Development Department, Technical Report. Press and Information Office, Republic of Cyprus, p. 6, 1996.

Savvides, L., Dorflinger, G., and Alexandrou, K.: The assessment of water demand of Cyprus. Report, objective 1- output 1.5.1, Ministry of Agriculture, Natural Resources and Environment, Water Development Department and Food and Agriculture Organization of the United Nations (FAO) Land and Water Development Division. TCP/CYP/8921, FAO, Rome., p. 12, 2001.

Udluft, P., Dünkeloh, A., Mederer, J., Külls, C., and Schaller, J.: Water balances for catchments and for the whole island, Appendices 1+2, GRC Project Report T6/7, Cyprus Geological Survey Department, Nicosia, pp. 111-112, 2003.

Chapter 7

Historical Observed Climate Change

7.1 Representative station

For the Saitas station (elevation 640 m) we have rainfall data since 1916. Saitas can be considered as a representative station of the Kouris catchment because it is situated at a mid elevation (the catchment lies from 157 m to 1905 m) and the station mean annual rainfall is close to that of the catchment. For the period 1986/87 to 2009/10 the mean annual rainfall at Saitas station is 661 mm while catchment mean annual rainfall is 652 mm. Moreover, the rainfall pattern of Saitas station is similar to that of the catchment, as shown in Figure 7.1.

Linear regression analysis on the scatter diagram (Figure 7.2) of mean annual rainfall of Saitas versus catchment mean annual rainfall, for the period 1986/87 to 2009/10, gives a regression line of slope 1.033 ± 0.122 at a 95% confidence level and a coefficient of determination $R^2 = 0.93$ (with $p < 0.001$). We can thus analyze Saitas data and assume that the catchment follows a similar trend.

7.2 Historical trends

7.2.1 Rainfall

As we shall see, changes in rainfall will primarily determine future water resources so we need to analyse catchment rainfall trends. Further, we need to check the agreement between GCM historical rainfall data and the catchment observed average rainfall data (from the representative Saitas station) for the period 1916/17 to 2004/05, as this will engender more confidence in the GCM rainfall predictions for the catchment. The variation of the long-term annual rainfall at Saitas is shown in Figure 7.3, with a mean of 736 mm and standard deviation of 189

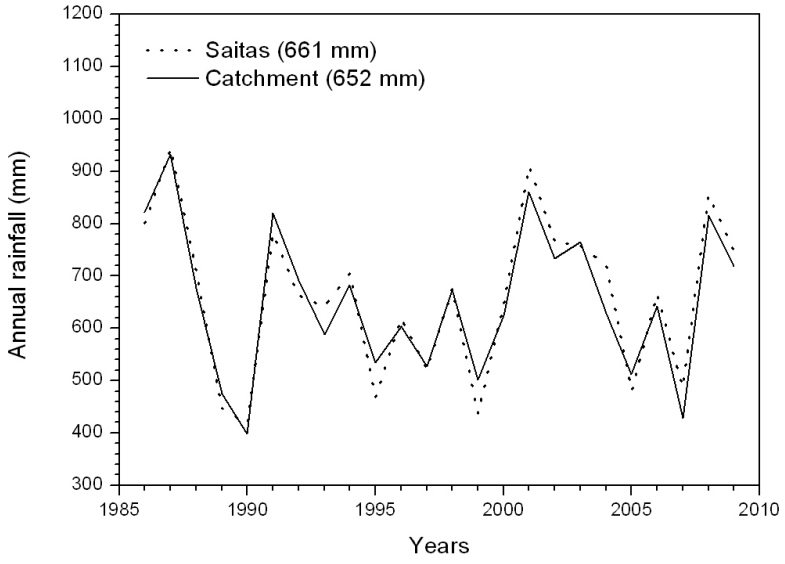

Figure 7.1: Catchment annual rainfall and Saitas annual rainfall with years, for the period 1986/87 to 2009/10. Numbers in parantheses are mean values for the above period.

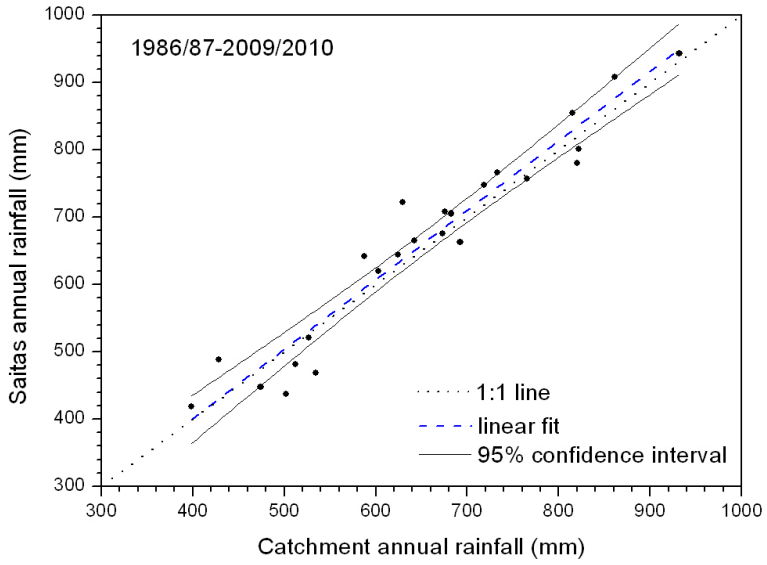

Figure 7.2: Scatter diagram of the Saitas annual rainfall versus catchment annual rainfall for the period 1986/87 to 2009/10.

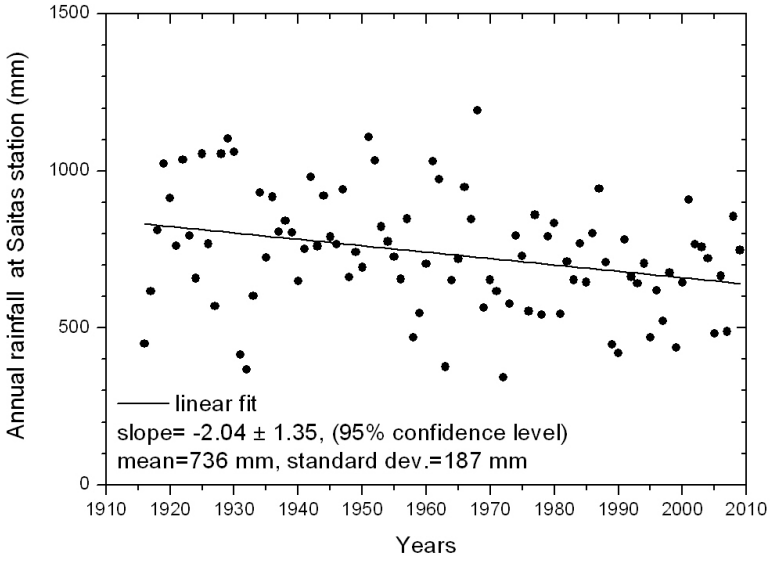

Figure 7.3: Scatter diagram of annual rainfall at Saitas station for the period 1916/17 to 2009/10.

mm. The slope of the least-squares line, on the scatter diagram of annual rainfall with time, was estimated at the 95% confidence level. We assign statistical significance to the estimated inter-annual trend if the 95% confidence interval of the slope does not contain the value zero. We estimate the 95% confidence interval to be between -2.04 - 1.35 = -1.39 mm/yr and -2.04 + 1.35 = -0.69 mm/yr, which contains only negative values and is therefore assigned to a negative trend, statistically significant at the 95% confidence level. The corresponding trend for all of Cyprus (see Figure 1.3) is a decrease of about 1 mm per year for the 20^{th} century and it is in accordance with other researchers who give higher decrease at higher elevations compared to the lowlands (Rossel 2001).

Long-term decadal rainfall exhibits also a decrease with time (Figure 7.4). Besides, by comparing a thirty-year average rainfall, in order to eliminate any fluctuations of rainfall, we arrive at the same conclusions. More specifically, for the period 1916/17 to 1945/46, the average rainfall is 798 mm whilst for the period 1980/81 to 2009/10 is 667 mm, implying a reduction of 16.4% on the long-term averages. In the study carried out by the Cyprus Water Development Department (WDD) in collaboration with FAO (Rossel 2001) for the reassessment of Cyprus water resources, they found that the mean annual precipitation for the period 1970/71 to 1999/00 is reduced by 15% to 25% compared to the mean annual precipitation for the period 1916/17 to 1969/70. The bigger reduction corresponds to higher elevations. Thus, there is a significant rainfall reduction since the beginning of the 20^{th} century.

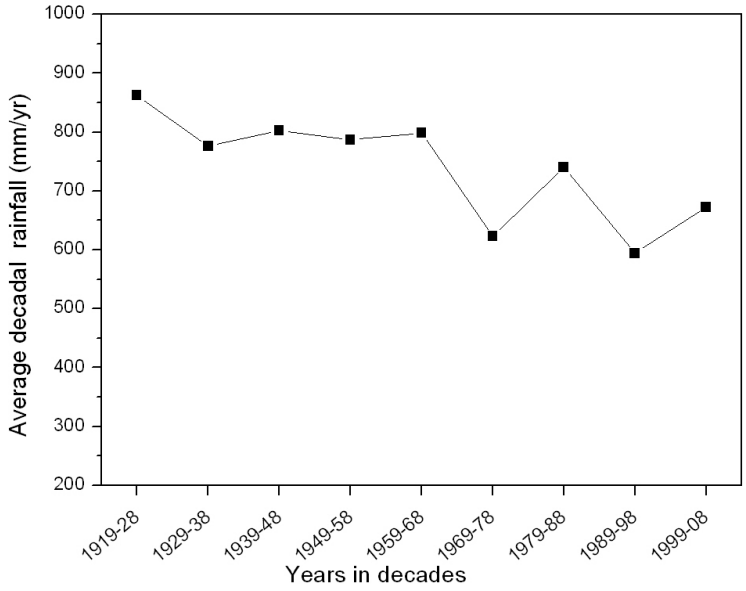

Figure 7.4: Long-term decadal rainfall of Saitas station for the period 1919/20 to 2008/09.

Moreover, the frequency of drought years, with mean annual rainfall less than normal rainfall minus the standard deviation, is increasing while the frequency of very wet years, with mean annual rainfall more than normal rainfall plus the standard deviation, is decreasing (Figure 7.5). Normal annual rainfall is considered by the Cyprus Meteorological Service the mean annual rainfall for the period 1961/62 to 1990/91 and its value for the Saitas station is 708 mm and the standard deviation is 198 mm. Thus, drought years are considered those with rainfall less than 510 mm and very wet years those with more than 906 mm.

The amount of rain per day is very important, so we would like to see if there is any change during the last century in the number of winter days; a) with no rain and b) with large amount of rain per day. Figure 7.6 shows the number of winter days (December, January and February) in every decade, with no rain (less than 0.5 mm/day) and with rain exceeding 40 mm/day. No pattern can be seen in the frequency of dry days (rain less than 0.5 mm/day) whilst there is a slight reduction in the frequency of very wet days (more than 20 mm/day). We then examined if the overall decrease in rainfall was due to a reduction in certain months. We looked for trends in the rainy period from November to March. There is a decreasing trend for the rainfall of these months but only for the months January and February it is statistically significant at the 95% confidence level giving a reduction from 10 mm to 130 mm in January rainfall in a period of a hundred years. The corresponding reduction for February rainfall is from 20 mm to 110 mm (Figures 7.7 and 7.8). The long-term average monthly rainfall

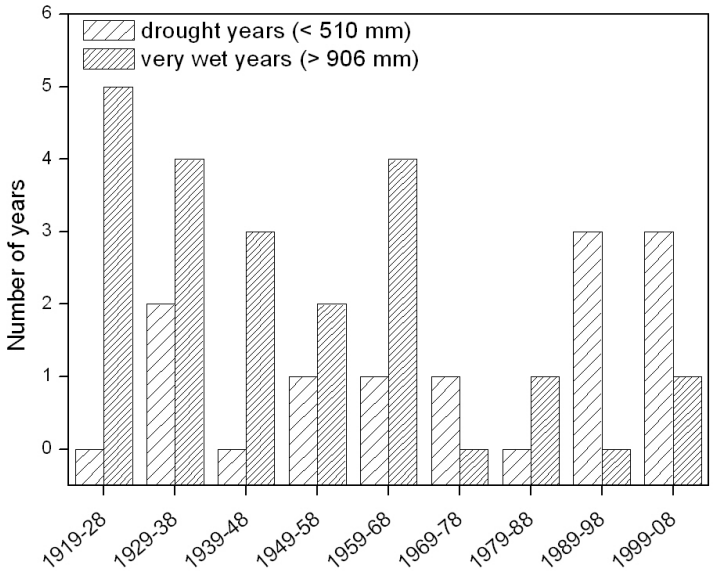

Figure 7.5: Frequency of dry and wet years in every decade.

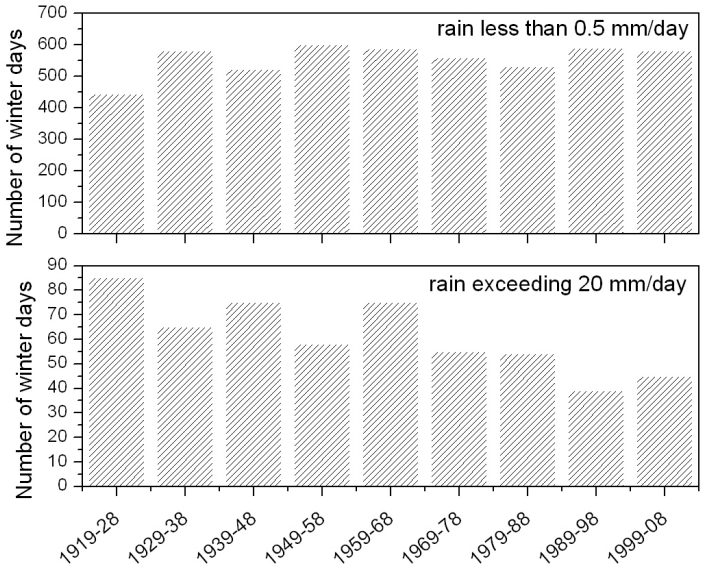

Figure 7.6: Frequency of winter days per decade, with no rain and with rain exceeding 20 mm/day.

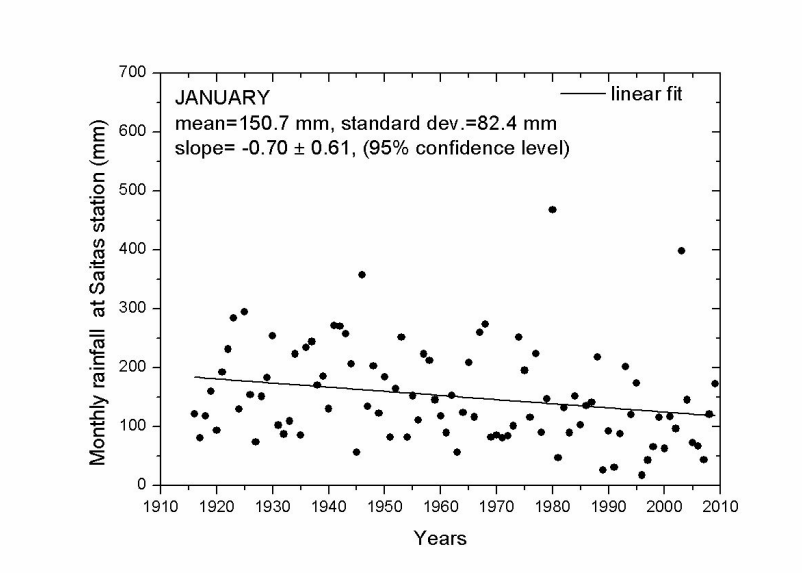

Figure 7.7: Scatter diagram of January rainfall at Saitas station.

of a thirty-year period is then examined by comparing the monthly rainfall of the periods 1916/17 to 1945/46 and 1980/81 to 2009/10 (Figure 7.9). There is a greater reduction in average monthly rainfall in the winter months. More specifically, the reduction is 22%, 27% and 29% for the months December, January and February, respectively. On average, more than 60% of the annual rainfall falls within the period December to February.

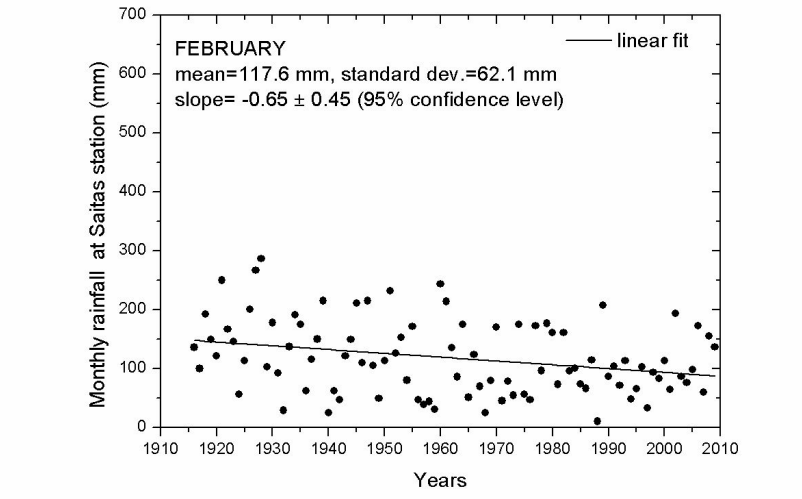

Figure 7.8: Scatter diagram of February rainfall at Saitas station.

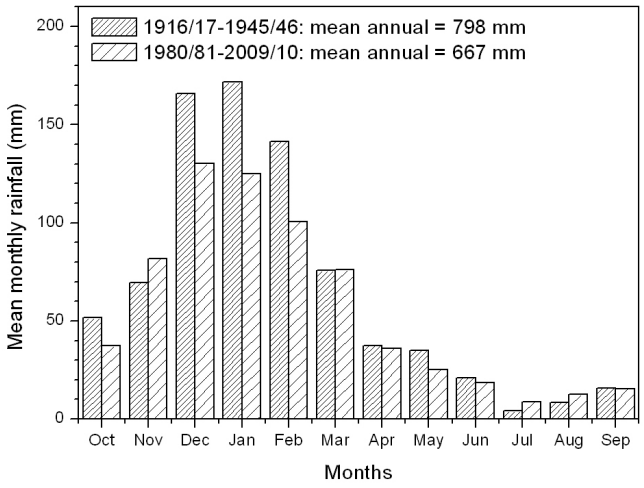

Figure 7.9: Long-term monthly rainfall at Saitas station for the periods 1916/17 to 1945/46 and 1980/81 to 2009/10.

7.2.2 Temperature

Long record mean annual temperature data exist only for two stations which are located outside the catchment. We have data for one of them, located in Lefkosia. Lefkosia is in the centre of the island at an elevation of 160 m. Figure 7.10 shows the scatter plot of the mean annual temperature with years for the period 1901 to 2004. There is an increasing trend of about 1.3 ^{o}C per 100 years, statistically significant at the 95% confidence level. We expect that the mean annual temperature of the catchment would follow an analogous increasing trend.

7.2.3 Discharge

For discharge we do not have enough data to deduce trends. However, we may look at the average discharge for the period 1969/70 to 2008/09. For the 20-year period 1969/70 to 1988/89 the long-term average annual discharge was 35.2 Mm^3/yr whilst for the period 1989/90 to 2008/09 it was 21.8 Mm^3/yr, implying a 38.1% reduction. The corresponding reduction for the annual rainfall was 7%, thus about five times more reduction in discharge than in rainfall. Moreover, for the period 1969/70 to 1988/89, there are only three years with annual discharge less than 20 Mm^3/yr, whilst for the period 1989/90 to 2008/09 the corresponding number is fourteen years (Figure 7.11), demonstrating thus the dramatic reduction in discharge since the 1970s.

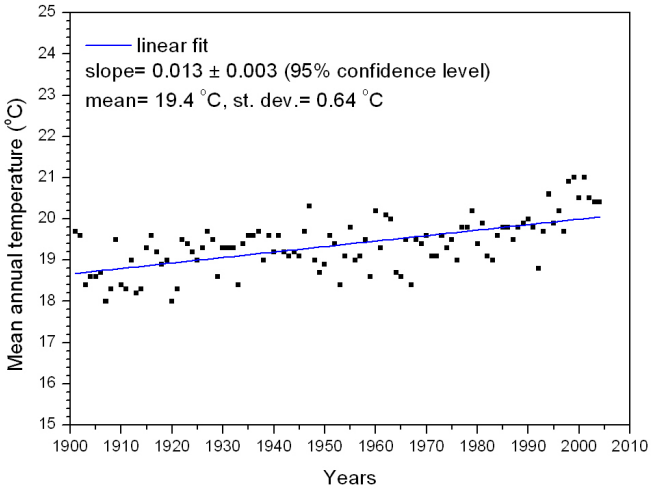

Figure 7.10: Scatter diagram of mean annual temperature with years at Lefkosia station, for the period 1901 to 2004.

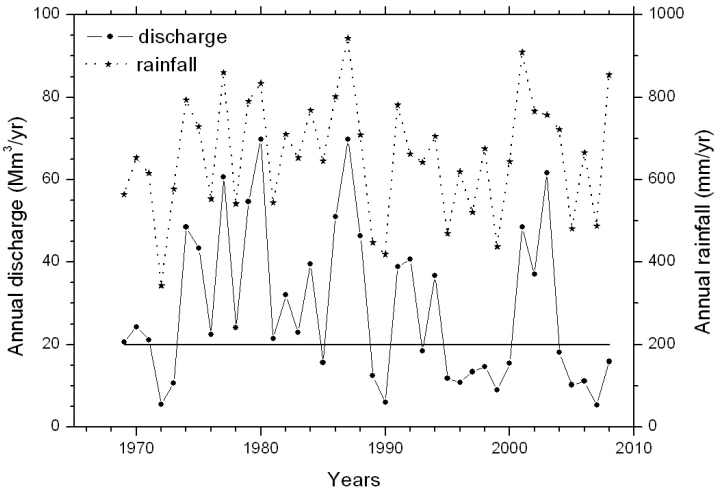

Figure 7.11: Catchment annual discharge and Saitas annual rainfall for the period 1969/70 to 2008/09.

Bibliography

Rossel, F.: Reassessment of the island's water resources and demand, Objective 1 - Output 1.2, Hydrometeorological study examining changes in recorded precipitation, Ministry of Agriculture, Natural Resources and Environment of the Republic of Cyprus, 2001.

Chapter 8

GCM Climate Projections

The Earth's climate is primarily controlled by solar radiation. Through the centuries there was a balance between incoming solar radiation and outgoing radiation and the Earth's mean temperature was fairly constant. However, during the last two centuries an increase in mean global temperature has been observed owing to the imbalance between incoming and outgoing radiation. The change in the Earth's energy balance and thus the Earth's climate, is expressed in terms of the radiative forcing. According to IPCC (2007) radiative forcing is defined as the change in the energy balance (incoming energy minus outgoing energy measured in watts per square meter) of the Earth-atmosphere system relative to the pre-industrial (1750) conditions when the radiative forcing was set equal to zero. A positive radiative forcing induces a warming effect whilst a negative one has a cooling effect.

The increased levels of aerosols and greenhouse gases since the pre-industrial era induce a change in the Earth's radiation budget which in turn drives a global change in climate. General Circulation Models (GCMs) predict a warmer and drier climate for Cyprus in the future. In this work the climatic change conditions are predicted using ECHAM6, a sixth-generation atmospheric general circulation model (AGCM) developed at the Max Planck Institute.

ECHAM6 forms the atmospheric component of the MPI-Earth System Model, a coupled climate model that includes dynamic vegetation, interactive carbon cycle and advanced representations of atmosphere and ocean processes. Its predictions for climatic change are within the middle range of estimates compared to other GCMs (Vaze and Teng 2011a; Vaze et al. 2011c). Vaze et al. (2011b) ranked MPI-ECHAM5 (the ancestor of MPI-ECHAM6) among the best GCMs based on its ability to reproduce the observed historical mean annual rainfall and daily rainfall distribution. ECHAM6 is well described in the literature (Giorgetta et al. 2011; Stevens et al. 2013). The GCM data we used are monthly values on a 1.9-degree grid resolution and they cover the period from 2006 up to 2100. The historical GCM data we used

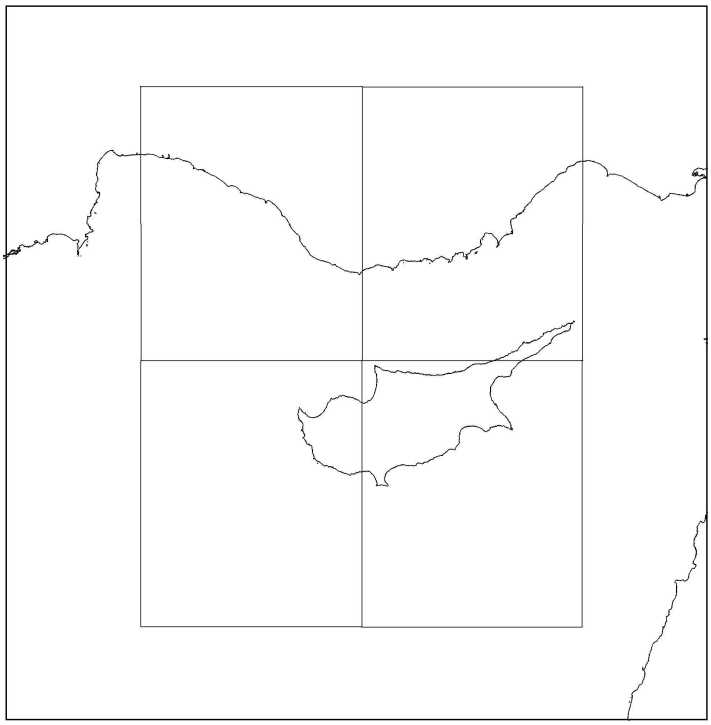

Figure 8.1: The ECHAM6 grid cells of 1.9-degree grid resolution that cover Cyprus.

cover the period from 1850 to 2005. The mean values of GCM data from the four grid cells, covering all of Cyprus (Figure 8.1), are used as the representative values of the climatic parameters such as temperature, rainfall etc. Two scenarios were used: the RCP8.5 and RCP2.6 which represent the two extremes in RCP (Representative Concentration Pathways) scenarios. The RCP8.5 scenario (no mitigation in fossil-fuel burning) assumes that greenhouse gas emissions and concentrations increase considerably with time leading to a radiative forcing of more than 8.5 W/m^2 and CO_2 (carbon dioxide) concentration of 936 ppm by 2100. The RCP2.6 scenario (strong mitigation) assumes a peak in radiative forcing of 3.1 W/m^2 by 2050 and a decline to 2.6 W/m^2 and CO_2 concentration at 420 ppm by 2100 (Brovkin et al. 2013). The CO_2 concentration in 2005 was 379 ppm and the radiative forcing was 2.63 W/m^2 (IPCC 2007).

8.1 Historical GCM trends

We compare GCM historical rainfall data and the catchment observed average rainfall data (from the representative Saitas station) for the period 1916/17 to 2004/05. The catchment annual rainfall is found to be about 11% higher than the GCM historical rainfall data. The range is from a -50% underestimation to an over 125% overestimation. Figure 8.2 shows the long-term decadal GCM historical rainfall and catchment rainfall data (Saitas station). A good correlation is however shown for the last five decades reflecting the fact that precise measurements of CO_2 and other WMGHGs (well-mixed greenhouse gases) were started in the late 1950s (Hartmann et al. 2013). For the period 1955/56 to 1974/75 the long-term GCM historical rainfall differs from the corresponding catchment observed rainfall by -2.3% whilst for the period 1985/86 to 2004/05 the difference is -0.6%. The change in the long-term annual rainfall between the above two periods is - 6.7% for the catchment observed rainfall and -5.1% for the GCM historical rainfall.
In general, climate models do not reproduce very well the precipitation, especially at the regional scale (Flato et al. 2013) and the correlation between observed and GCM data is poor. Having this in mind, the GCM historical data over Cyprus can be considered to represent satisfactorily the catchment long-term rainfall. On the other hand, the transition from GCM historical times into GCM future times is smooth, due to the harmonization that was done between historical GCM data and future GCM data (Figure 8.3), so we may argue that any change in a climate parameter value from GCM historical times to GCM future times can be analogous on the catchment scale.

Linear regression analysis on the diagram of GCM historical annual rainfall with time, for the period 1850/51 to 2004/05, (Figure 8.4), gives a regression line of slope -0.39 ± 0.29, at the 95% confidence level, implying a reduction of about 0.4 mm per year.
For the rainy months, December, January, February, which account for more than 60% of the annual rainfall, there is a decreasing trend, but only for January it is significant at the 95% confidence level. Regression analysis on the diagram of January rainfall with time gives a line of slope -0.16 ± 0.12 at the 95% confidence level, implying a reduction of about 0.16 mm in monthly rainfall per year (Figure 8.4). The twenty-year long-term GCM historical rainfall for the period 1850/51 to 1869/80 is 727.1 mm, whilst for the period 1985/76 to 2004/05 it is 659.8 mm, implying a reduction of 67.3 mm or 9.3% in 155 years.
There is a reduction in the monthly rainfall for all months except November when there is a slight increase. For the months December, January, February, the reduction is about 5% to 10% (Figure 8.5).

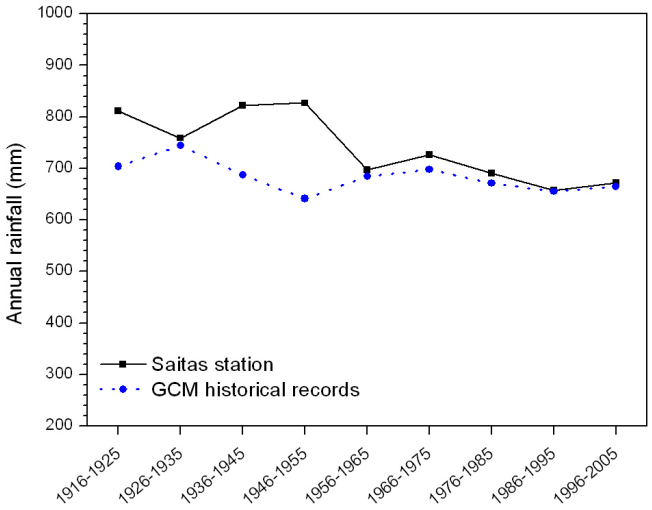

Figure 8.2: Comparison of the long-term decadal observed rainfall (Saitas station) and GCM historical rainfall for the period 1916/17 to 2004/05, showing the good agreement from the decade starting in 1956.

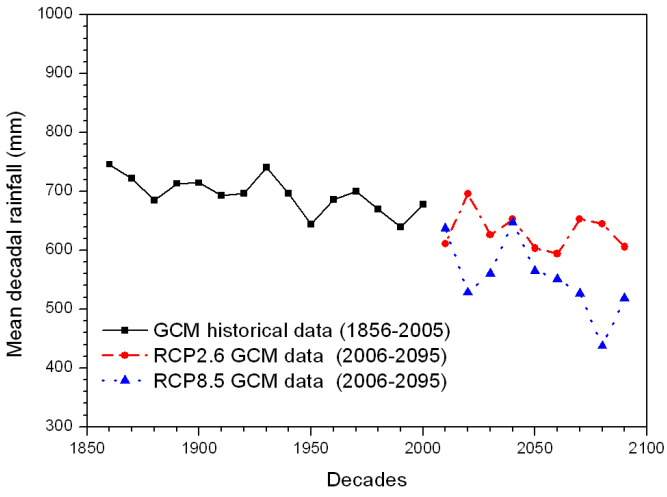

Figure 8.3: Long-term decadal rainfall for Cyprus from GCM data for the period 1856 to 2095.

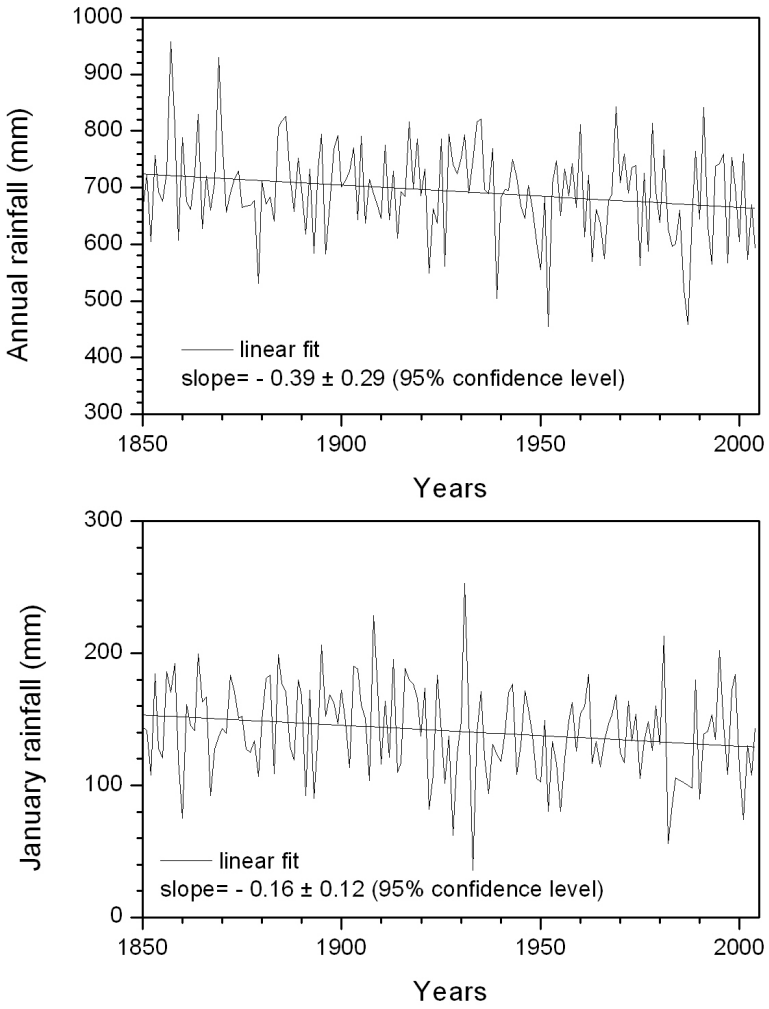

Figure 8.4: GCM historical mean annual rainfall and January mean rainfall, over Cyprus, for the period 1850/51 to 2004/05. Linear regression lines are also shown.

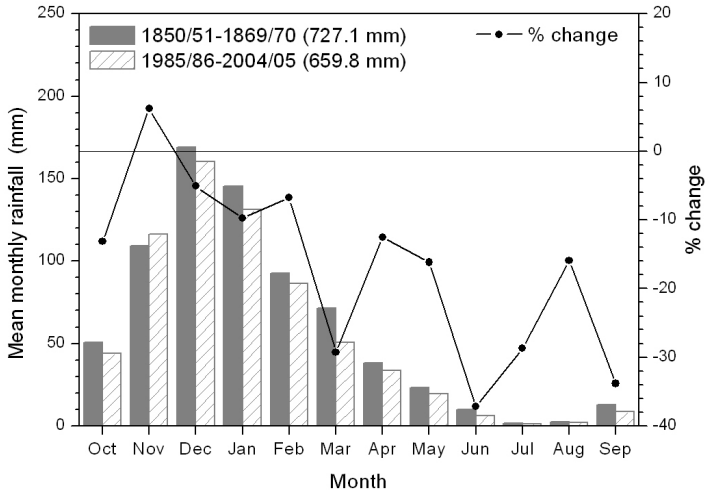

Figure 8.5: Twenty-year long-term monthly rainfall from GCM historical data. Numbers in parantheses represent mean annual values.

8.2 Future GCM projections

8.2.1 Rainfall

For the period 2006/07 to 2099/00, the slope of the least-squares best fit line, on the diagram of annual rainfall with time, was estimated at the 95% confidence level, giving a negative trend for the annual rainfall for both scenarios but only for the RCP8.5 the trend (-1.73 ± 1.09 mm reduction per year for the period 2006/07 to 2099/00), (Figure 8.6), is statistically significant at the 95% confidence level. This reduction is by 4.4 times per year more, than the corresponding reduction in the historical years (1850/51 to 2004/05). Greater reduction is expected in January with the slope of the least-squares best fit line on the diagram of January rainfall with time, (for the period 2006/07 to 2099/00) to be -0.49 ± 0.47 mm/month, at the 95% confidence level (Figure 8.6). The long-term annual rainfall for the RCP2.6 scenario, for the period 2006/07 to 2015/16, is 640.5 mm whilst for the period 2080/81 to 2099/00 it is 607.8 mm, implying a reduction of 5.1% between the first and the second period, with respect to the first period. The corresponding values for the RCP8.5 scenario are 651.6 mm and 487.1 mm, respectively, implying a reduction of 25.3%. For the RCP8.5 scenario the reduction in the long-term mean annual rainfall is expected to be apparent by the middle of the 21st century. More specifically, the long-term mean annual rainfall for the period 2030/31 to 2049/50 is expected to be 584.8 mm, implying a reduction of 10.3% compared to the period 2006/07 to 2015/16. However, for the RCP2.6 scenario the corresponding long-term mean

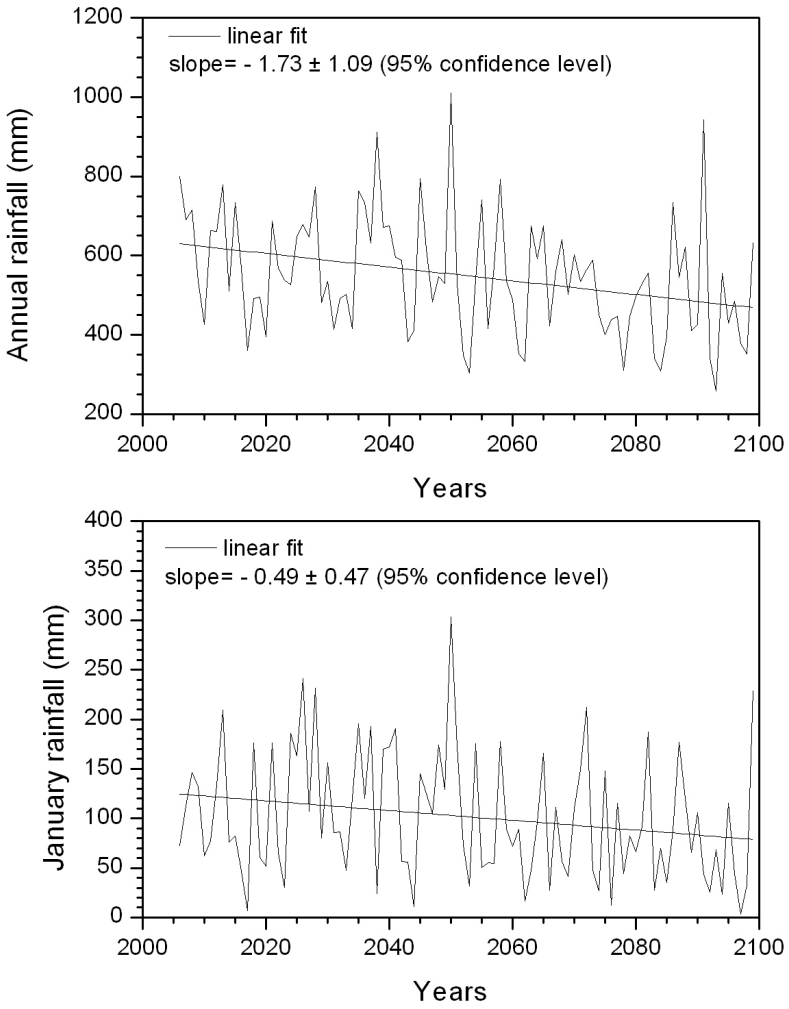

Figure 8.6: Mean annual rainfall and January mean rainfall, over Cyprus for the GCM RCP8.5 scenario, for the period 2006/07 to 2099/00. Linear regression lines are also shown.

annual rainfall is expected to be 643.9 mm, implying a slight increase with respect to the period 2006/07 to 2015/16. For the RCP8.5 scenario, the long-term monthly rainfall, for the period 2080/81 to 2099/00, is expected to decrease for all months from October to May (these months account for the 97% of the annual rainfall). For the most rainy months, December, January and February, the reduction is 24%, 27% and 11%, respectively, compared to the period 2006/07 - 2015/16. For the RCP2.6 scenario, the corresponding reduction for the months November and January is 25% and 37% respectively, but an increase is expected for the other months (Figure 8.7).

8.2.2 Temperature

The two scenarios (RCP2.6 and RCP8.5) give an increasing trend for the mean annual temperature which is statistically significant at the 95% confidence level. The slope of the least-squares line, on the diagram of mean annual temperature with time (available data for the period 2006/07 to 2099/2100), was estimated to be 0.0031 ± 0.0027 °C /yr (95% confidence level) for the RCP2.6 scenario and 0.0402 ± 0.0035 °C/yr (95% confidence level) for the RCP8.5 scenario, implying an increase of about 0.3 °C and 3.8 °C (Figure 8.8), respectively, for the two scenarios, by the end of the 21st century compared to the 2006/07 values. The RCP8.5 scenario gives an increasing trend for all months which is statistically significant at the 95% confidence level. The increase in monthly temperature by the end of 21st century is from 2.7 °C (January) to 4.9 °C (August) compared to the 2006 values. For RCP2.6 the increase is up to 0.95 °C (May) but there is no significant trend for the other months of the year. Long-term decadal annual temperature (Figure 8.12) shows an increase of about 1.2 °C or 5.8% by the middle of the 21st century (2046/47-2055/56) and up to 3.2 °C or 15.9% by the end of the century (2090/91-2099/00) compared to the decade 2006/07-2015/16 for the RCP8.5 scenario. For the RCP2.6 scenario there is an increase of about 0.5 °C or 1.7% by the middle of the century and an increase of about 1 °C or 6.9% by the end of the 21st century, compared to the values of the period 2006/07 to 2015/16 (Figure 8.12). By the end of the 21st century, the increase, is greater in the period from January to May for both scenarios, compared to the period 2006/07 to 2015/16. More specifically, the RCP8.5 scenario predicts an increase in the long-term mean monthly temperature of up to 22.5% (April) for all months whilst the RCP2.6 scenario predicts an increase from January to August, up to 6.9% (March) and a decrease for the rest of the months (Figure 8.9).

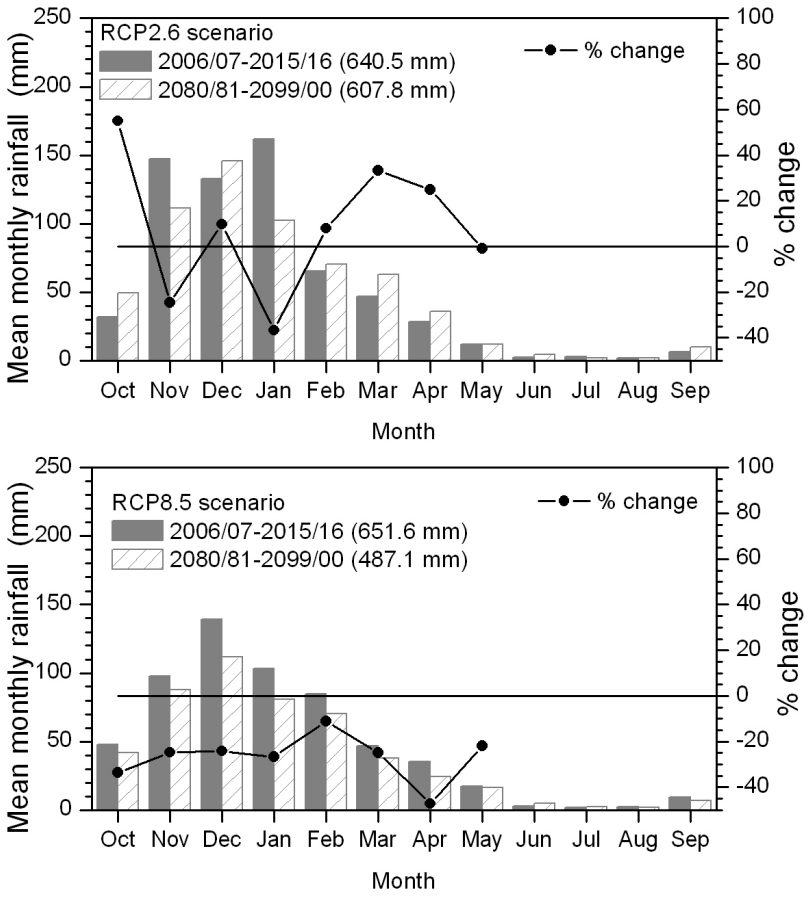

Figure 8.7: Long-term mean monthly rainfall over Cyprus, for the RCP2.6 and the RCP8.5 scenarios, for the periods 2006/07 to 20015/16 and 2080/81 to 2099/00. Numbers in parentheses represent mean annual values.

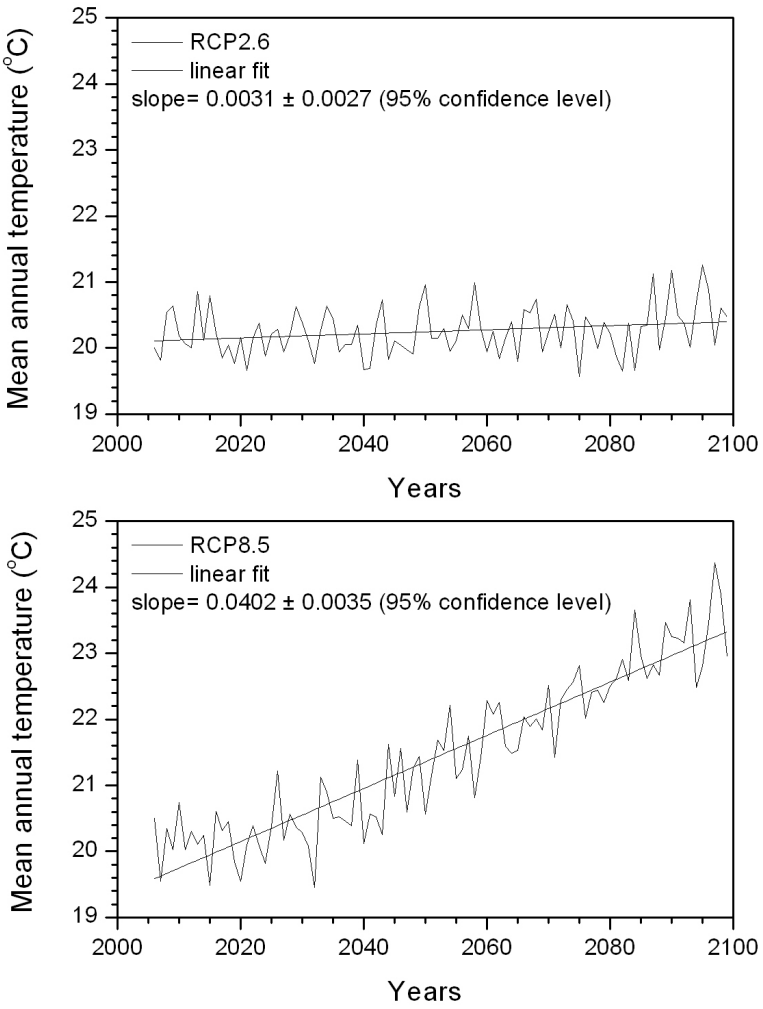

Figure 8.8: Mean annual temperatures over Cyprus for the RCP2.6 and the RCP8.5 scenarios, for the period 2006/07 to 2099/00. Regression lines are also shown.

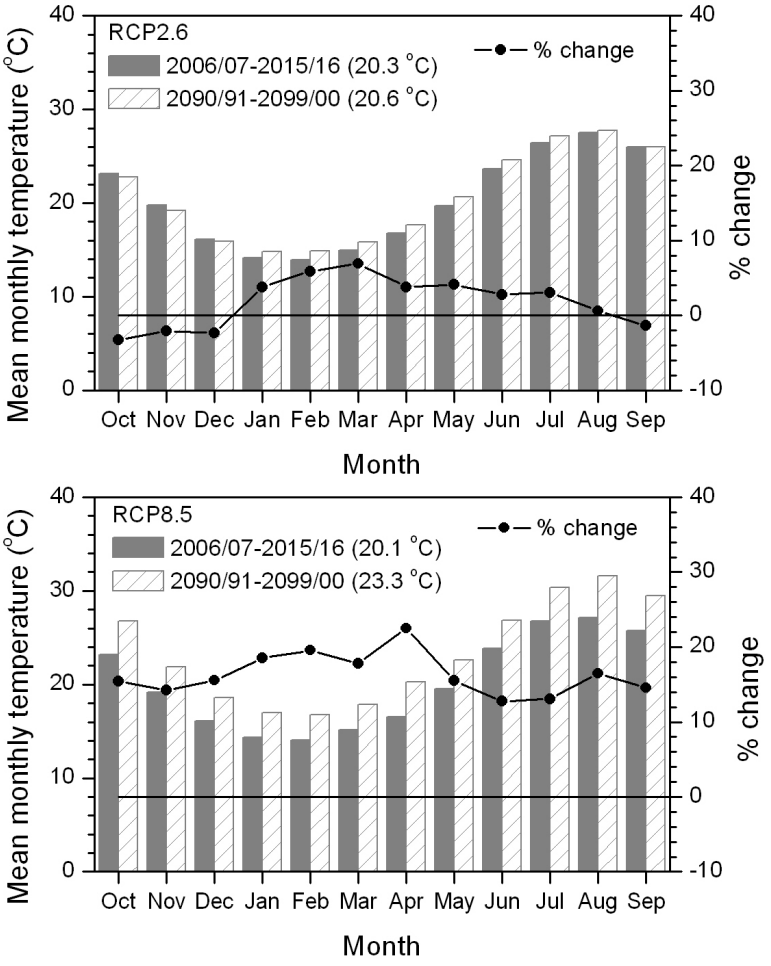

Figure 8.9: Decadal mean monthly temperatures over Cyprus for the RCP2.6 and the RCP8.5 scenarios for the periods 2006/07 to 2015/16 and 2090/91 to 2099/00. Number in parentheses represent long-term mean annual values.

8.2.3 Potential evaporation

The change in Earth's radiation energy budget drives a change in potential evaporation. Potential evaporation for the period 2006/07 to 2099/00 is estimated by using radiation fluxes and other physical quantities from the two GCM scenarios. The two scenarios (RCP2.6 and RCP8.5) give an increasing trend for the mean annual potential evaporation but only for the RCP8.5 scenario it is statistically significant at the 95% confidence level. For the RCP8.5 scenario,the slope of the least-squares line, on the diagram of mean annual potential evaporation with time (period 2006/07 to 2099/2100), was estimated to be 1.40 ± 0.24 mm/yr, statistically significant at the 95% confidence level (Figure 8.10), implying an increase of 131 mm/yr by the end of the 21st century compared to the 2006/07 values. The greater increase is in April with the slope of the best-fitting line to be 0.26 ± 0.06 mm/month at the 95% confidence level (Figure 8.10).

Long-term decadal annual potential evaporation shows an increase of about 3% by the middle of the 21st century (2046/47-2055/56) and up to 6.4% by the end of the century (2090/91-2099/00) compared to the decade 2006/07 to 2015/16 for the RCP8.5 scenario (Figure 8.12). For the RCP2.6 scenario there is even a decrease of about 1% by the middle of the century and only a slight increase of about 1% by the end of the 21st century, compared to the values of the period 2006/07 to 2015/16 (Figure 8.11). The increase is greater in the period from January to April for both scenarios. More specifically, the RCP8.5 scenario predicts an increase in the long-term mean monthly potential evaporation of up to 16.6% (April) for all months except December when there is a slight decrease whilst the RCP2.6 scenario predicts an increase from January to July, up to 11% (January) and a decrease for the rest of the months (Figure 8.13).

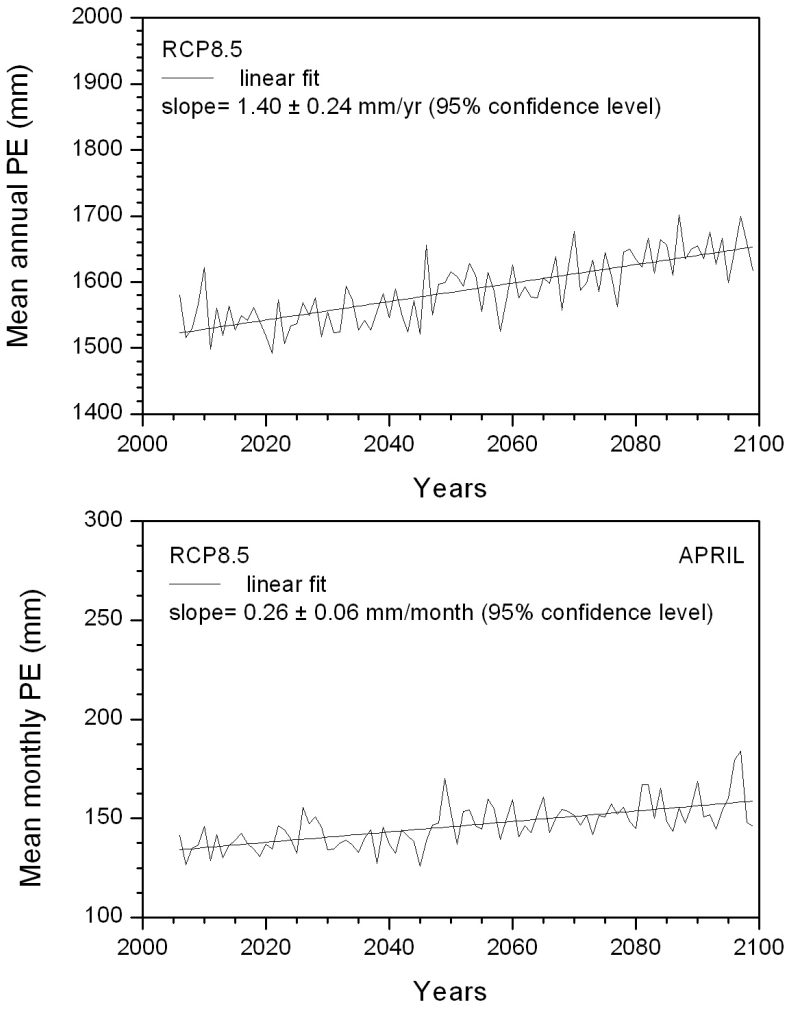

Figure 8.10: Mean annual and mean monthly for the month April, potential evaporation over Cyprus, for the period 2006/07 to 2099/00, for the RCP8.5 scenario.

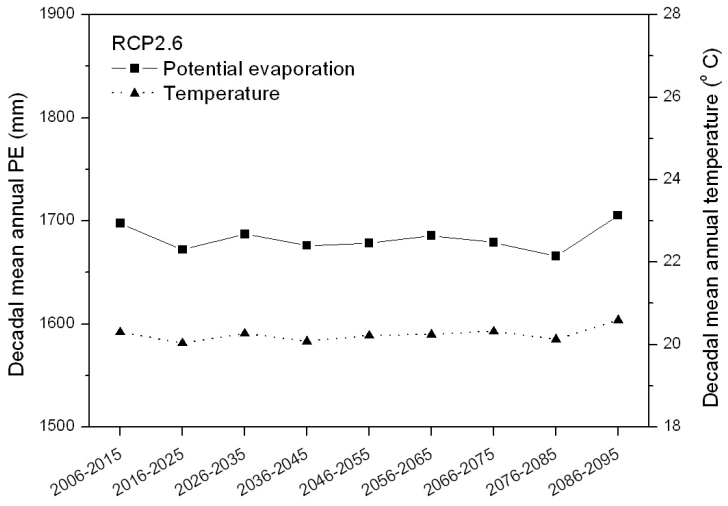

Figure 8.11: Long-term decadal annual potential evaporation and temperature over Cyprus, for the period 2006/07 to 2095/96, for the RCP2.6 scenario.

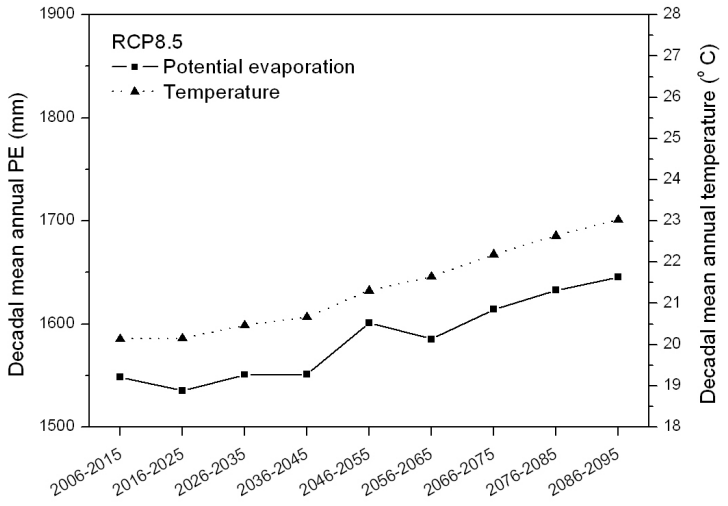

Figure 8.12: Long-term decadal annual potential evaporation and temperature over Cyprus, for the period 2006/07 to 2095/96, for the RCP8.5 scenario.

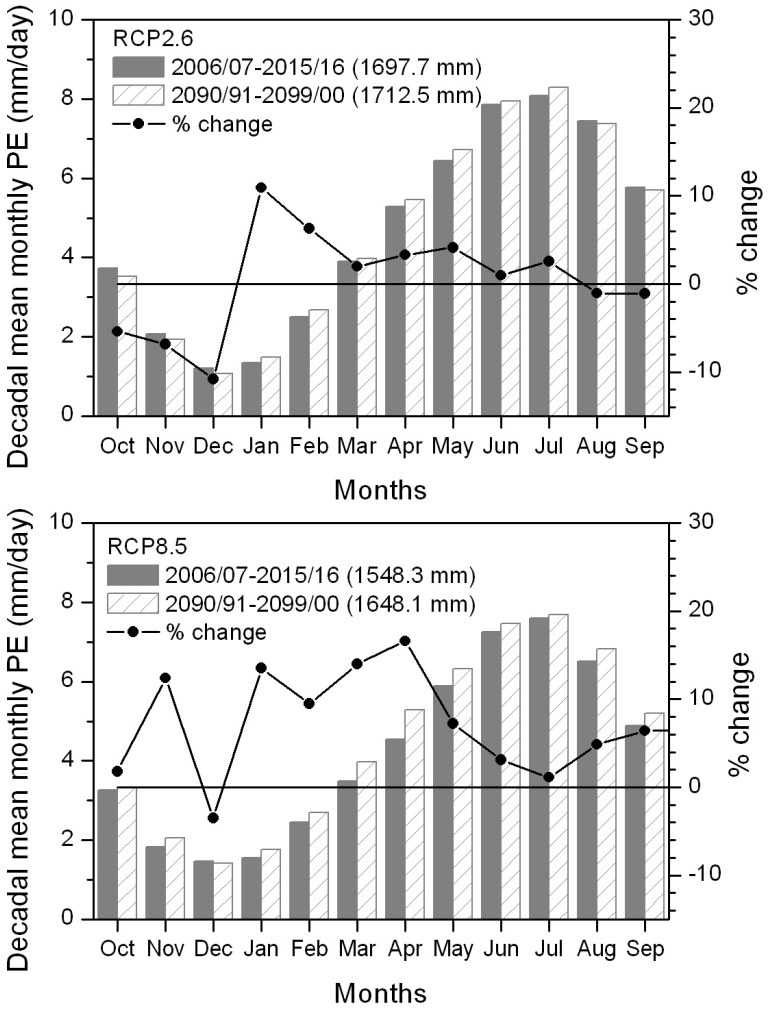

Figure 8.13: Long-term mean monthly potential evaporation over Cyprus for the RCP2.6 and RCP8.5 scenarios. Numbers in parentheses represent mean annual values.

Bibliography

Brovkin, V., Boysen, L., Arora, V. K., Boisier, J., Cadule, P., Chini, L., Claussen, M., Friedlingstein, P., Gayler, V., van den Hurk, B., Hurtt, G., Jones, C., Kato, E., de Noblet-Ducoudré, N., Pacifico, F., Pongratz, J., and Weiss, M.: Effect of anthropogenic land-use and land-cover changes on climate and land carbon storage in CMIP5 projections for the 21st century, in press, Journal of Climate, 26, 6859-6881, doi:http://dx.doi.org/10.1175/JCLI-D-12-00623.1, 2013.

Flato, G., Marotzke, J., Abiodun, B., Braconnot, P., Chou, S., Collins, W., Cox, P., Driouech, F., Emori, S., Eyring, V., Forest, C., Gleckler, P., Guilyardi, E., Jakob, C., Kattsov, V., C., R., and M., R.: Evaluation of Climate Models. In: Climate Change 2013: The Physical Science Basis. Contribution of Working Group I to the Fifth Assessment Report of the Intergovernmental Panel on Climate Change [Stocker, T. F., D. Qin, G.-K. Plattner, M. Tignor, S. K. Allen, J. Boschung, A. Nauels, Y. Xia, V. Bex and P. M. Midgley (eds.)], Cambridge University Press, Cambridge, United Kingdom and New York, NY, USA, 2013.

Giorgetta, M., Roeckner, E., Mauritsen, T., Stevens, B., Crueger, T., Esch, M., Kornblueh, L., Schmidt, H., Reick, C., Raddatz, T., and Gayler, V.: The atmospheric general circulation model ECHAM6 Model description, Max Planck Institute for Meteorology, Hamburg, Germany, 2011.

Hartmann, D. L., Klein Tank, A. M. G., Rusticucci, M., Alexander, L. V., Brönnimann, S., Charabi, Y., Dentener, F. J., Dlugokencky, E. J., Easterling, D. R., Kaplan, A., Soden, B. J., Thorne, P. W., Wild, M., , and Zha, P. M.: Observations: Atmosphere and Surface. In: Climate Change 2013: The Physical Science Basis. Contribution of Working Group I to the Fifth Assessment Report of the Intergovernmental Panel on Climate Change [Stocker, T. F., D. Qin, G.-K. Plattner, M. Tignor, S. K. Allen, J. Boschung, A. Nauels, Y. Xia, V. Bex and P. M. Midgley (eds.)], Cambridge University Press, Cambridge, United Kingdom and New York, NY, USA, 2013.

IPCC: Climate Change 2007 - The Physical Science Basis: Working Group I Contribution to the Fourth Assessment Report of the IPCC, Cambridge University Press, 2007.

Stevens, B., Giorgetta, M., Esch, M., Mauritsen, T., Crueger, T., Rast, S., Salzmann, M., Schmidt, H., Bader, J., Block, K., Brokopf, R., Fast, I., Kinne, S., Kornblueh, L., Lohmann, U., Pincus, R., Reichler, T., and Roeckner, E.: The Atmospheric Component of the MPI-M Earth System Model: ECHAM6, Journal of Advances in Modelling Earth Systems, 5, 146-172, doi:10.1002/jame.20015, 2013.

Vaze, J. and Teng, J.: Future climate and runoff projections across New South Wales, Australia: results and practical applications, Hydrological Processes, 25, 18-35, 2011a.

Vaze, J., Teng, J., and Chiew, F.: Assessment of GCM simulations of annual and seasonal rainfall and daily rainfall distribution across south-east Australia, Hydrological Processes, 25, 1486-1497, 2011b.

Vaze, J., Davidson, A., Teng, J., and Podger, G.: Impact of climate change on water availability in the Macquarie-Castlereagh River Basin in Australia, Hydrological Processes, 25, 2597-2612, 2011c.

Chapter 9

Climate Change Impact on the Water Resources

9.1 Downscaling the rainfall

The impact of climate change on the water resources of Cyprus is estimated by comparing water fluxes simulated by the rainfall-runoff model driven by: i) observed historical data and ii) future data predicted by GCM scenarios. GCM data are monthly values on a 1.9-degree grid resolution and cover all of Cyprus. In order to apply them to the daily rainfall-runoff model over the catchment we have to downscale them: i) to the catchment local spatial scale and ii) convert them from monthly to daily values. To achieve this we use the constant scaling method of Mpelasoka and Chiew (2009). We estimate the scaling factor which is the ratio of the GCM mean monthly rainfall in the future (2030/31 to 2049/50 or 2080/81 to 2099/00) to the historical GCM mean monthly rainfall in the 20^{th} century (historical reference period). The scaling factor is then multiplied by the catchment observed data (1989/90 to 2008/09) in order to get a scenario for catchment future rainfall data. In this way every day of a certain month of every year is scaled by the same factor. The scaling factor is different for every month. In this way we keep the same rainfall pattern. The disadvantage of this method is that it does not take into consideration possible rapid diurnal changes in rainfall intensity, which can increase runoff after a quick wetting phase.

In order to check the effect of the reference period to the scaling factor we used four different historical reference periods for the GCM historical rainfall data: a) 1985/86-2004/05, b) 1975/76-2004/05, c) 1965/66-2004/05 and d) 1970/71- 1999/00. For the RCP8.5 scenario the four different scaling factors (Table 9.1) give by the end of the 21^{st} century (2080/81 to 2099/00) a reduction in long-term annual rainfall of 24%, 24.5%, 25.9% and 24.6%, respec-

Table 9.1: The scaling factors for the RCP8.5 GCM scenario period 2080/81 to 2099/00 and for the four different historical reference periods.

Month	Reference historical period			
	1985/86-2004/05	1975/76-2004/05	1965/66-2004/05	1970/71-1999/00
Oct	0.95	1.06	1.06	1.26
Nov	0.76	0.77	0.76	0.73
Dec	0.70	0.70	0.69	0.71
Jan	0.62	0.62	0.61	0.65
Feb	0.81	0.79	0.78	0.77
Mar	0.75	0.68	0.65	0.64
Apr	0.74	0.72	0.70	0.69
May	0.82	0.76	0.78	0.76
Jun	0.79	0.81	0.74	0.75
Jul	1.96	1.94	1.85	1.72
Aug	0.83	0.94	0.96	0.96
Sep	0.82	0.83	0.77	0.83

tively, compared to the present (1989/90 to 2008/09) long-term catchment annual rainfall. The impact on the long-term annual rainfall is not so significant, so we used as reference historical period the most recent one, i.e. the period 1985/85-2004/05, which overlaps the period 1989/90 to 2008/09 for which we have catchment observed data. The scaling factors used for the present period (2006/06 to 2015/16) and the two future periods of time (mid and end of 21st century), for the two GCM scenarios, using the GCM historical period 1985/85 to 2004/05 as a reference period, are presented in Table 9.2.

Table 9.2: The rainfall scaling factor used for the two GCM scenarios and for the periods 2006/07-2015/15, 2030/31-2049/50 and 2080/81-2099/00. The reference GCM historical period is the period 1985/86-2004/05.

Month	2006/07-2015/16		2030/31-2049/50		2080/81-2099/00	
	RCP2.6	RCP8.5	RCP2.6	RCP8.5	RCP2.6	RCP8.5
Oct	0.72	1.43	1.05	0.91	1.12	0.95
Nov	1.27	1.00	0.89	1.12	0.96	0.76
Dec	0.83	0.92	0.86	0.79	0.91	0.70
Jan	1.23	0.84	0.96	0.90	0.78	0.62
Feb	0.75	0.92	1.11	0.66	0.81	0.81
Mar	0.93	1.00	1.00	0.92	1.24	0.75
Apr	0.86	1.40	1.38	1.10	1.07	0.74
May	0.62	1.05	1.04	0.71	0.62	0.82
Jun	0.39	0.43	0.78	1.06	0.71	0.79
Jul	2.43	0.40	1.70	1.34	1.61	1.96
Aug	0.86	0.74	0.96	1.04	0.95	0.83
Sep	0.74	1.49	1.01	0.59	1.15	0.82

9.2 Downscaling the potential evaporation (PE)

The same scaling method is applied to estimate the future PE. Analytically, the scaling factor for the potential evaporation is the ratio of the mean monthly PE computed from the available observed climatological data over the catchment (1/1/2002/ to 31/12/2007) to the mean monthly PE computed from the GCM (1/1/2006 to 31/12//2011) data . We thus get the scaling factor of each month. This factor is then multiplied by the long-term mean monthly PE computed from the future GCM data (2006/07-2015/16, 2030/31-2049/50 or 2080/81-2099/00). We used two different scaling factors, SF1 and SF2:

1) The scaling factor SF1 is the average of the scaling factors of calendar years 2006 and 2007 (the only years when the available observed climatological data and the GCM data overlap). Analytically, the scaling factor of each year is the ratio of the mean monthly PE computed from the observed MODIS satellite climatological data of the year to the mean monthly PE computed from the GCM climatic data of the same year.

2) The scaling factor SF2 is the ratio of the five-year mean monthly PE (period 1/1/2002 to 31/12/2007) computed from the observed climatological data to the five-year mean monthly PE (1/1/2006 to 31/12/2011) computed from the GCM data.

Linear regression analysis on the scatter diagrams of mean monthly potential evaporation computed from GCM data (RCP2.6, RCP8.5) versus mean monthly potential evaporation computed from MODIS data over the catchment, for the years 2006 and 2007, shows a correlation (Figure 9.1) that is significant. More specifically, for both scenarios scenarios R^2=0.97

and p<0.0001 for the calendar year 2006 whilst for the 2007 year, R^2=0.93 and p<0.0001 for both scenarios.

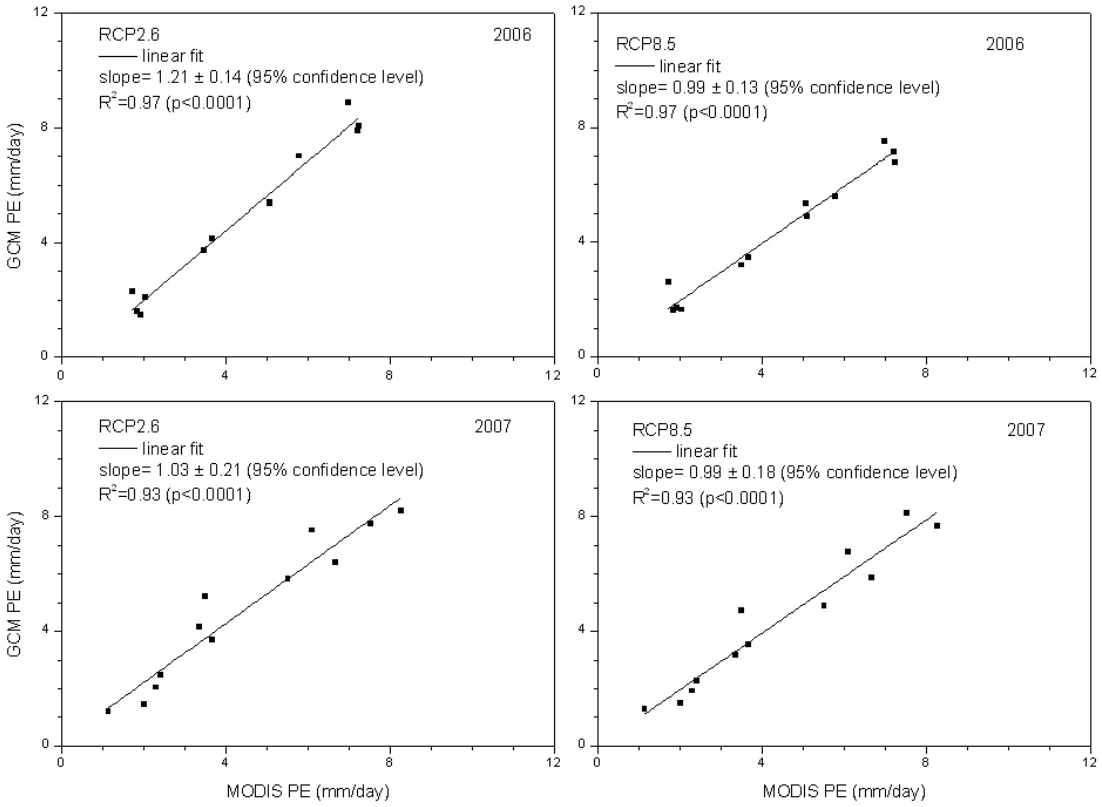

Figure 9.1: Scatter diagrams of mean monthly PE computed from the RCP2.6 and the RCP8.5 scenarios with mean monthly PE computed from MODIS data over the catchment, for the years 2006 and 2007. Regression lines are also shown.

There is though better correlation between the five-year mean monthly PE (1/1/2006 to 31/12/2011) computed from the GCM data and the five-year mean monthly PE (1/1/2002 to 31/12/2007) computed from the observed climatological data. Linear regression analysis on the scatter diagrams shows a correlation (Figure 9.2) that is significant (R^2=0.99, p<0.0001 for both scenarios). The agreement between PE computed from observed data and PE computed from GCM data gives more confidence in the estimation of the catchment future PE, when the GCM scenarios are applied.

For the RCP8.5 scenario, the per cent difference between the five-year mean monthly PE (1/1/2006 to 31/12/2011) computed from the GCM data and the five-year mean monthly PE

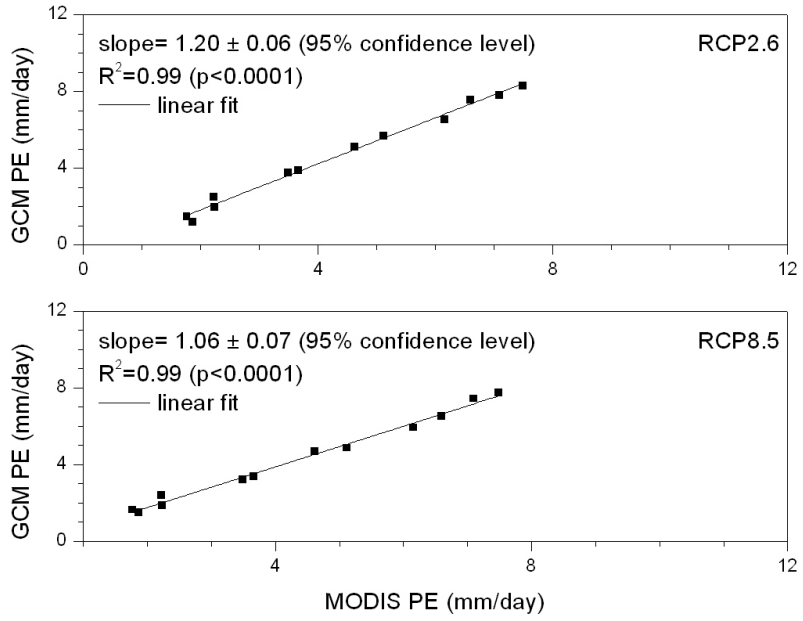

Figure 9.2: Scatter diagrams of the five-year mean monthly PE (1/1/2006 to 31/12/2011) computed from the GCM data and the five-year mean monthly PE (period 1/1/2002 to 31/12/2007) computed from the observed climatological data. Regression lines are also shown.

(1/1/2002 to 31/12/2007) computed from the observed climatological data (Figure 9.4) with respect to the PE (1/1/2002 to 31/12/2007) computed from the observed climatological data, is less than 10% for most of the months and only for November and December is above 10% (16% and 19% respectively). For the RCP2.6 the corresponding difference is below 15% for most of the months and only for December is 35.7%. We have to mention though that the December PE from MODIS data has not been estimated, due to the lack of data, but it was taken as the average of the PE of the previous and following month. So, there is a big uncertainty in its value.

The per cent difference between mean monthly PE of the calendar year 2006, computed from GCM data and that computed from MODIS data of the same year with respect to PE computed from MODIS data, is up to 33% for the RCP2.6 scenario and up to 20% (except February when the difference is 52%) for the RCP8.5 scenario. The corresponding difference for the 2007 is up to 30% (except April when the difference is 49%) for the RCP2.6 scenario and up to 35% for the RCP8.5 scenario. The plots of the PE derived from GCM data versus the PE derived from MODIS data, for the years 2006 and 2007 are shown in Figure 9.3. The mean PE of period 2002 to 2007 estimated from the observed MODIS satellite data and the mean scaled PE for the two scenarios and for the periods 2006/07 to 2015/16, 2030/31 to 3049/50

and 2080/81 to 2099/00, using the scaling factors SF1 and SF2, are shown in the Tables 9.3 and 9.4. The per cent difference between the mean PE computed from SF1 with respect to that computed from SF2 is less that 6% for most of the months (excluding December) for both scenarios. Only in April the difference is bigger for both scenarios (-10.7% for the RCP2.6 and -14.1% for the RCP8.5) and in January the difference is bigger for the RCP8.5 scenario (20.5%).

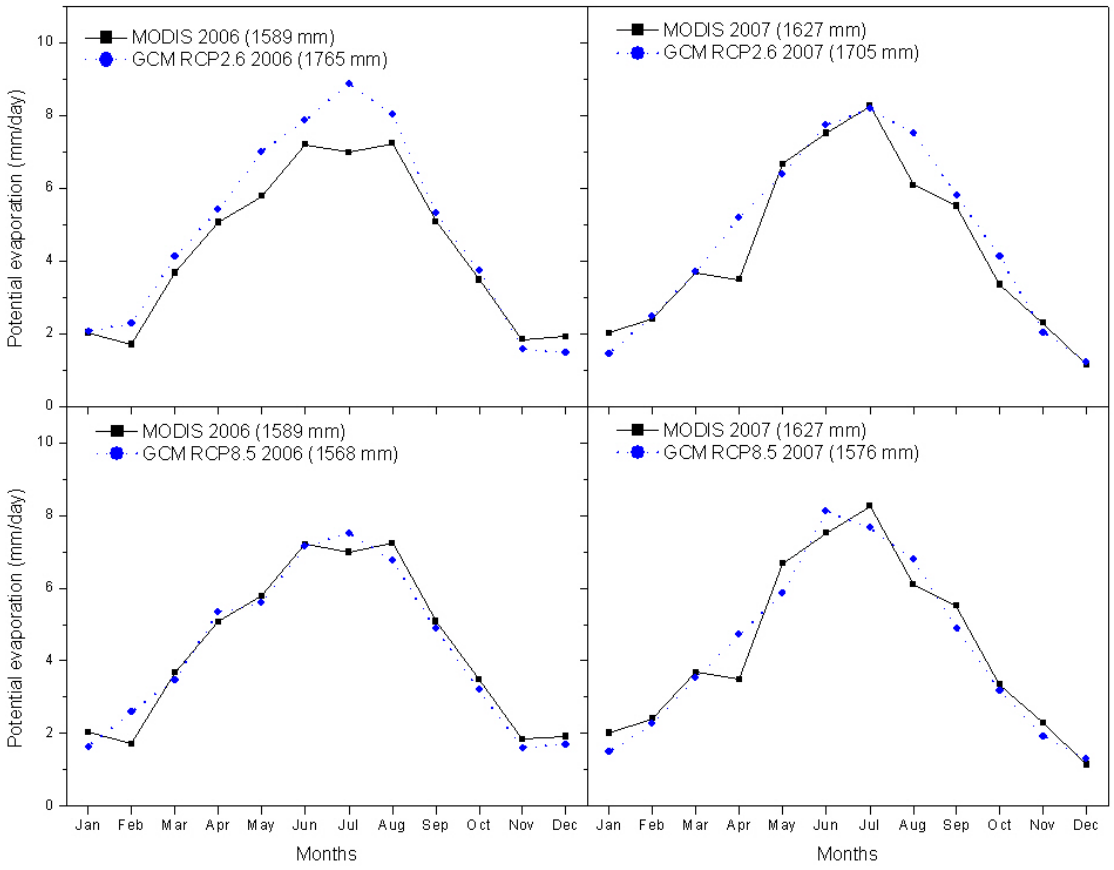

Figure 9.3: Mean monthly PE computed from the RCP2.6 and the RCP8.5 scenarios with mean monthly PE computed from MODIS data over the catchment, for the years 2006 and 2007. Numbers in parentheses represent mean annual values.

Table 9.3: The mean PE computed from the MODIS data (2002-2007) and the mean scaled PE for the two GCM scenarios and for the periods 2006/07-2015/16, 2030/31-2049/50 and 2080/81-2099/00, using the scaling factor SF1. The per cent difference with respect to the MODIS 2002-2007 mean PE is also shown.

Month	2002-2007	2006/07-2015/16				2030/31-2049/50				2080/81-2099/00			
	MODIS	RCP2.6		RCP8.5		RCP2.6		RCP8.5		RCP2.6		RCP8.5	
	mm/day	mm/day	%	mm/day	%	mm/day	%	mm/day	%	mm/day	%	mm/day	%
Oct	3.50	3.25	-6.98	3.52	0.62	3.16	-9.66	3.43	-1.97	3.04	-13.12	3.62	3.60
Nov	2.23	2.37	5.98	2.13	-4.40	2.19	-1.90	2.19	-1.86	2.22	-0.53	2.44	9.35
Dec	1.87	1.35	-27.87	1.48	-20.87	1.19	-36.36	1.38	-25.89	1.25	-33.12	1.42	-23.89
Jan	1.76	1.59	-9.84	2.01	14.27	1.70	-3.66	2.15	22.00	1.75	-0.51	2.27	28.60
Feb	2.22	2.16	-2.67	2.12	-4.65	2.08	-6.44	2.15	-3.23	2.17	-2.39	2.35	6.00
Mar	3.66	3.67	0.28	3.66	0.01	3.64	-0.60	3.80	3.85	3.72	1.41	4.11	12.19
Apr	4.62	4.25	-7.96	3.83	-17.08	4.13	-10.66	3.93	-14.89	4.23	-8.34	4.41	-4.56
May	6.16	6.02	-2.22	6.40	4.02	5.97	-2.96	6.41	4.14	6.26	1.78	6.89	11.87
Jun	7.09	7.41	4.56	7.02	-1.08	7.33	3.33	6.86	-3.21	7.35	3.66	7.29	2.76
Jul	7.49	7.26	-2.96	7.64	2.03	7.41	-0.99	7.62	1.82	7.50	0.14	7.66	2.37
Aug	6.60	6.36	-3.56	6.41	-2.87	6.40	-2.97	6.55	-0.64	6.33	-4.06	6.73	1.97
Sep	5.11	5.49	7.35	5.30	3.61	5.34	4.38	5.46	6.82	5.29	3.49	5.61	9.81
Annual (mm)	1600	1561	-2.5	1573	-1.8	1542	-3.7	1585	-1.0	1559	-2.6	1672	4.4

Table 9.4: The mean PE computed from the MODIS data (2002-2007) and the mean scaled PE for the two GCM scenarios and for the periods 2006/07-2015/16, 2030/31-2049/50 and 2080/81-2099/00, using the scaling factor SF2. The per cent difference with respect to the MODIS 2002-2007 mean PE is also shown.

Month	2002-2007	2006/07-2015/16				2030/31-2049/50				2080/81-2099/00			
	MODIS	RCP2.6		RCP8.5		RCP2.6		RCP8.5		RCP2.6		RCP8.5	
	mm/day	mm/day	%	mm/day	%	mm/day	%	mm/day	%	mm/day	%	mm/day	%
Oct	3.50	3.45	1.17	3.57	2.22	3.35	-4.0	3.48	-0.4	3.23	-7.69	3.68	5.2
Nov	2.23	2.34	4.87	2.18	2.20	2.17	-2.9	2.24	0.4	2.20	-1.57	2.50	11.9
Dec	1.87	1.88	0.60	1.81	2.80	1.66	-11.2	1.70	-9.0	1.74	-6.71	1.74	-6.5
Jan	1.76	1.60	9.47	1.67	5.14	1.71	-3.3	1.79	1.3	1.76	-0.10	1.88	6.8
Feb	2.22	2.22	0.27	2.27	2.25	2.14	-3.6	2.30	3.8	2.23	0.56	2.52	13.7
Mar	3.66	3.66	0.10	3.78	3.29	3.63	-1.0	3.93	7.3	3.70	1.02	4.24	15.9
Apr	4.62	4.76	3.12	4.46	3.43	4.62	0.1	4.58	-0.9	4.74	2.69	5.13	11.1
May	6.16	6.05	1.65	6.12	0.62	6.01	-2.4	6.12	-0.5	6.30	2.37	6.58	6.9
Jun	7.09	7.14	0.70	6.90	2.66	7.06	-0.5	6.75	-4.8	7.08	-0.16	7.17	1.1
Jul	7.49	7.28	2.71	7.36	1.68	7.43	-0.7	7.34	-1.9	7.52	0.40	7.38	-1.4
Aug	6.60	6.48	1.81	6.60	0.00	6.52	-1.2	6.75	2.3	6.44	-2.33	6.93	5.0
Sep	5.11	5.18	1.25	5.14	0.47	5.03	-1.5	5.30	3.6	4.99	-2.39	5.44	6.5
Annual (mm)	1600	1587	-0.9	1582	-1.2	1566	-2.2	1595	-0.4	1584	-1	1683	5.1

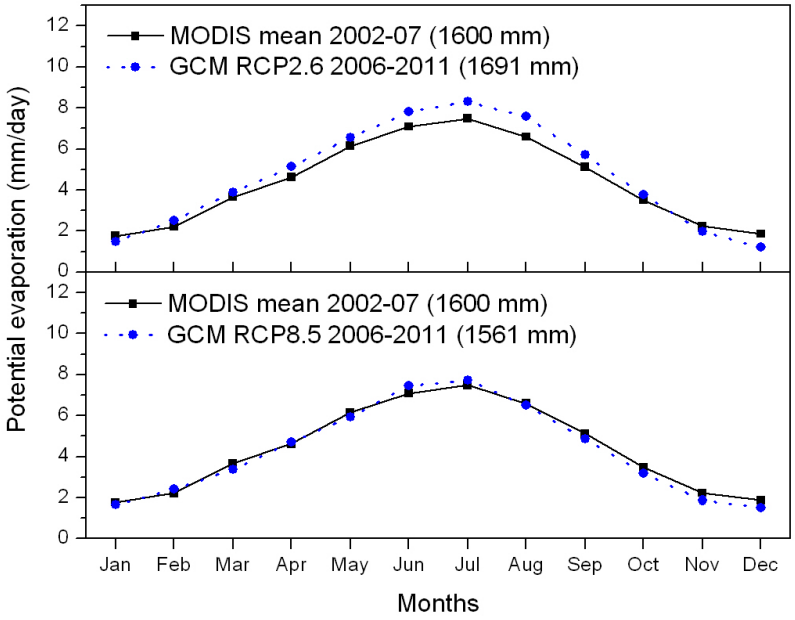

Figure 9.4: The five-year mean monthly PE (1/1/2006 to 31/12/2011) computed from the GCM data and the five-year mean monthly PE (period 1/1/2002 to 31/12/2007) computed from the observed climatological data. Numbers in parentheses represent mean annual values.

9.3 Future catchment water balance

The long-term averages for annual rainfall, runoff, actual evaporation and recharge are calculated running the model with: A- observed ground-based and MODIS satellite data for the period 1989/90-2008/09; B-GCM data for the period 2006/2007-2015/2016; C- GCM data for the period 2030/31-2049/50; and D- GCM data for the period 2080/81-2099/2100. The estimates for the scenarios RCP2.6 and RCP8.5 are shown in Tables 9.5 and 9.6, with the two different scaling factor for the potential evaporation. The difference in the estimated water fluxes, when using the SF1 and SF2 scaling factors, is less than 1.5% for the actual evaporation and the recharge for both GCM scenarios and for all time periods. For the discharge however, for the RCP2.6 scenario, there is an underestimation of about 6% for all periods when using SF2, whilst for the RCP8.5 scenario the corresponding underestimation is about 2.5% for all periods. For the RCP2.6 scenario and for the three time periods (B, C, D) the annual PE estimated from SF2 is about 1.6% overestimated compared to the annual PE estimated from SF1, whilst for the RCP8.5 scenario the corresponding value is about 0.6% higher for all periods. In the following discussion we use the SF1 results which give higher

Table 9.5: Long-term averages in Mm^3 of catchment annual rainfall, discharge, actual evaporation, recharge and net recharge. The total PE in mm/yr is also given. Present period A (1989/90-2008/09), and periods B (2006/2007-2015/2016), C (2030/31-2049/50) and D (2080/81-2099/100) for the two GCM scenarios. The scaling factor SF1 was used for scaling the PE.

Water Fluxes	Present	RCP2.6			RCP8.5		
Mm^3	A	B	C	D	B	C	D
Rainfall	174	172.5	173.4	161.81	176.68	153	132.22
Discharge	21.47	24.60	20.97	16.63	20.8	13.97	6.85
Evaporation	128.68	124.1	128.69	122.01	131.0	116.99	105.35
Recharge	23.82	23.8	23.8	23.16	24.9	22.0	20.00
Net Recharge	10.21	10.1	10.05	9.74	11.1	8.97	8.35
PE (mm/yr)	1617	1561	1542	1559	1573	1585	1672

Table 9.6: Long-term averages in Mm^3 of catchment annual rainfall, discharge, actual evaporation, recharge and net recharge. The total PE in mm/yr is also given. Present period A (1989/90-2008/09), and periods B (2006/2007-2015/2016), C (2030/31-2049/50) and D (2080/81-2099/100) for the two GCM scenarios. The scaling factor SF2 was used for scaling the PE.

Water Fluxes	Present	RCP2.6			RCP8.5		
Mm^3	A	B	C	D	B	C	D
Rainfall	174	172.5	173.4	161.81	176.68	153	132.22
Discharge	21.47	23.2	19.71	15.51	20.27	13.6	6.63
Evaporation	128.68	125.59	130.2	123.4	131.59	117.5	105.8
Recharge	23.82	23.68	23.5	22.92	24.82	21.9	19.8
Net Recharge	10.21	10.08	9.95	9.65	11.18	8.91	8.29
PE(mm/yr)	1617	1587	1566	1584	1582	1595	1683

discharge and lower PE compared to the corresponding values estimated from SF2.

The application of the model for the period 1989/90 to 2008/09 gave for precipitated water the following long-term partitioning: from a total of 174 Mm^3 per year rainfall and amount of 74% (128.68 Mm^3) returns to the atmosphere as actual evaporation, 12.3% (21.47 Mm^3) goes to surface runoff (12.5% is the observed) and 13.7% (23.82 Mm^3) goes to recharge of the groundwater store. If we take into account groundwater eventually lost to the atmosphere and the sea, the net recharge is 5.9% of rainfall and the total water lost is 81.8%. Thus, only 18.2% of precipitation is available for surface and groundwater resources. Assuming no change in the relative intensity of precipitation by the end of the 21^{st} century (2080/81 to 2099/00), the model predicts a lower amount of rainfall and lower percentage of this being available for surface runoff and recharge. More specifically, the amount of long-term mean annual rainfall would be reduced from 174 Mm^3 (1989/90-2008/09) to 161.8 Mm^3 for the

mild GCM scenario and to 132 Mm^3 for the extreme GCM scenario, i.e. a reduction of 7% and 24%, respectively. The reduction in rainfall most likely will be apparent by the middle of the 21st century; the RCP2.6 and RCP8.5 scenarios predict a 0.3% and 12.1% reduction, in the long-term average annual rainfall, respectively.

For the catchment discharge that inflows to the Kouris dam, the reduction is more severe, reduced from the present value of 21.47 Mm^3 to 16.63 Mm^3 for the mild scenario and to 6.85 Mm^3 for the extreme scenario. The worse case scenario results in the reduction by about 2/3 in the available water for storage in the Kouris dam. These findings are in agreement with other researchers who argue that rainfall reduction is amplified when translated to surface runoff (Chiew and MacMahon 2002; Ragab et al. 2010). The total inflow into the Cyprus dams is about 69.9 Mm^3 per year and the Kouris represents 31% of this amount, thus if the surface inflow into the other dams is similar, then by the end of the 21st century the water resources available in the current dams will fall to about only 21.67 Mm^3, under the extreme climate change scenario. Unless drastic planning takes place and associated engineering projects constructed, such as desalination, recycling and dam storage improvement, Cyprus might be faced with a massive water resource shortage.

The future percentage of rainfall that goes to water losses will be even higher compared to the present values. An amount of 83.7% (88.6%) of future annual rainfall will be lost via evaporation and sea losses, 10.3% (5.2%) will go to surface runoff and 6% (6.3%) for net recharge for the RCP2.6 scenario. Numbers in parentheses refer to the RCP8.5 scenario. Thus, the percentage of rainfall that is available for surface water and groundwater resources would be reduced to 16.3% (26.4 Mm^3) and 11.5% (15.2 Mm^3) for the two scenarios, without taking into consideration the external pumping of the aquifer. If we consider that the present annual water demand of the area is estimated to be about 10 Mm^3, with an increasing tendency, and this demand is mostly satisfied by pumping, then the amount of water supply falls dramatically. If the precipitation occurs in fewer, more extreme events, as some GCMs and regional models suggest (Christensen et al. 2007; Meehl et al. 2007; Vaze et al. 2011b), the reduction in the water supply will be further exacerbated.

Seasonal variability

We look for variations in the catchment monthly rainfall, discharge and evaporation by the end of the 21st century. RCP8.5 scenario predicts for the period 2080/81 to 2099/00, a reduction in the long-term mean monthly rainfall for all months except July, up to 38% (January), compared to the observed rainfall values of the period 1989/90 to 2008/09. RCP2.6 predicts a reduction up to 22% (January) for the rainy period from November to February.

The RCP8.5 GCM scenario predicts, for the end of the 21st century, a reduction in the long-term mean monthly discharge of all months, up to 75% (January) compared to the catchment simulated discharge of the period 1989/90-2008/09. The RCP2.6 predicts a reduction up to 40.7% (February) for all months except October. The change in the long-term mean monthly rainfall and discharge for both scenarios is shown in Figure 9.5.

The RCP8.5 scenario predicts for the period 2080/81-2099/00, an increase in the long-term mean monthly PE up to 33% (January) for most of the months, compared to the mean values of the period 1989/90-2008/09. The RCP2.6 scenario predicts, for the period 2080/81-2099/00, an increase up to 4.8% (May) but not for all months, compared to the values of the period 1989/90-2008/09 (Figure 9.6).

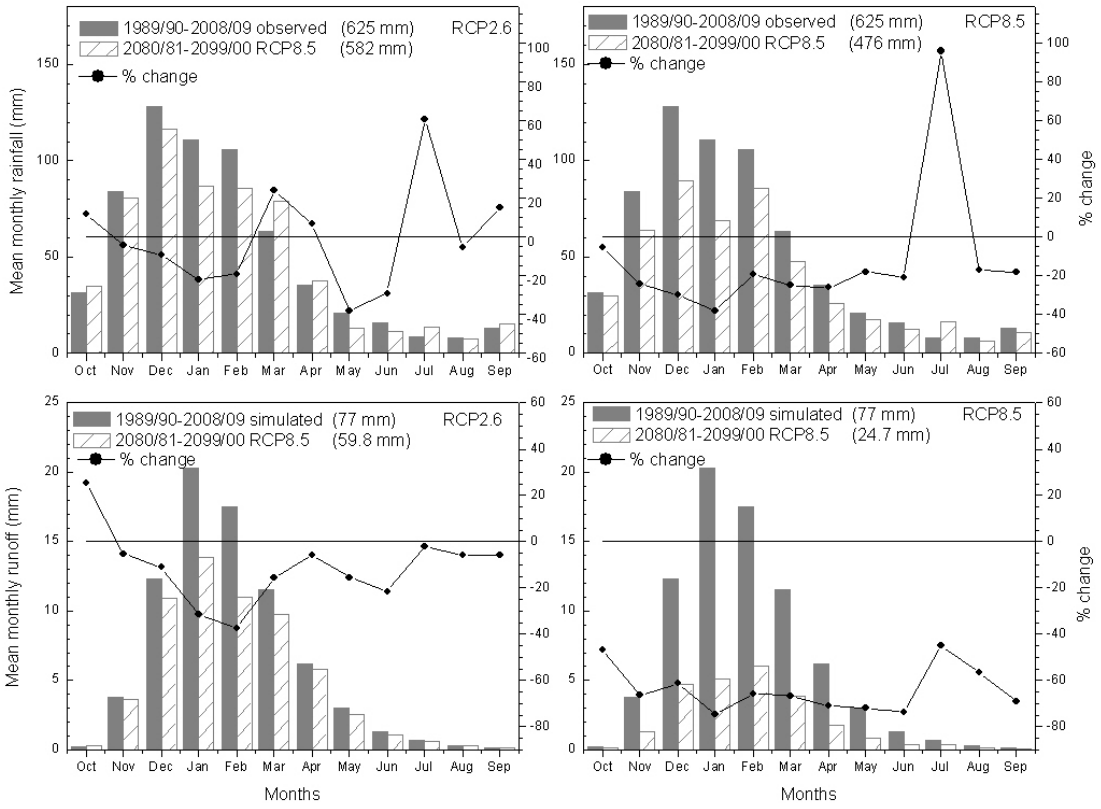

Figure 9.5: Long-term mean monthly rainfall and simulated discharge for the two GCM scenarios, for the periods 1989/90 to 2008/09 and 2080/81 to 2099/00. Numbers in parentheses represent mean annual values.

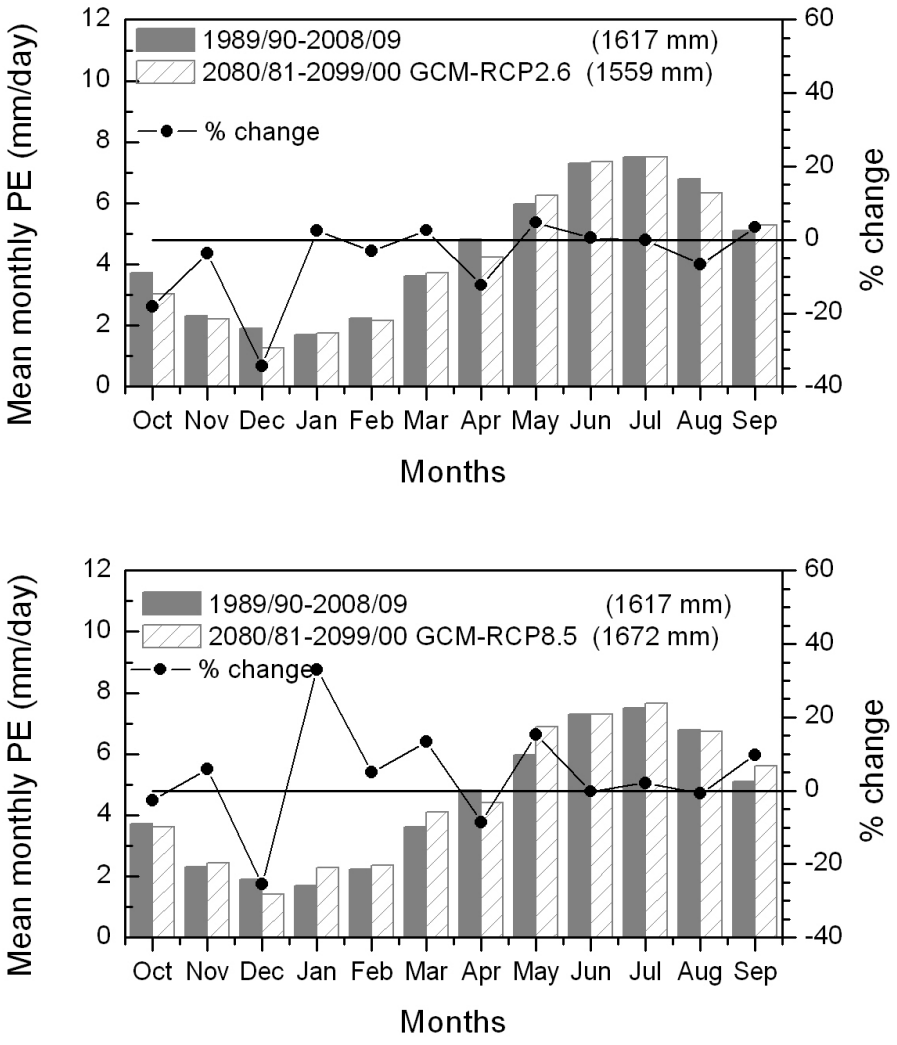

Figure 9.6: Long-term mean monthly catchment potential evaporation for the period 1989/90 to 2008/09 and for the period 2080/81 to 2099/00 for the two GCM scenarios. Number in parentheses represent mean annual values.

Bibliography

Chiew, F. and MacMahon, T.: Modelling the impacts of climate change on Australian streamflow, Hydrological Processe, 16, 1235-1245, 2002.

Christensen, J., Hewitson, B., Busuioc, A., Chen, A., Gao, X., Held, I., Jones, R., Kolli, R., Kwon, W., Laprise, R., Magaña, V., Rueda, L., Mearns, C., Menéndez, J., Räisänen, A., Rinke, A., Sarr, and Whetton, P.: Regional Climate Projections. In: Climate Change 2007: The Physical Science Basis. Contribution of Working Group I to the Fourth Assessment Report of the Intergovernmental Panel on Climate Change [Solomon, S., D. Qin, M. Manning, Z. Chen, M. Marquis, K.B. Averyt, M. Tignor and H.L. Miller (eds.)], Cambridge University Press, Cambridge, United Kingdom and New York, NY, USA., 2007.

Meehl, G., Stocker, T., Collins, W., Friedlingstein, P., Gaye, A., Gregory, J., Kitoh, A., Knutti, R., Murphy, J., Noda, A., Raper, S., Watterson, I., Weaver, A., and Zhao, Z.-C.: Global Climate Projections. In: Climate Change 2007: The Physical Science Basis. Contribution of Working Group I to the Fourth Assessment Report of the Intergovernmental Panel on Climate Change [Solomon, S., Qin, D., Manning, M., Chen, Z., Marquis, M., Averyt, K.B., Tignor, M., Miller, H.L., (eds.)], Cambridge University Press, Cambridge, United Kingdom and New York, NY, USA., 2007.

Mpelasoka, F. and Chiew, F.: Influence of Rainfall Scenario Construction Methods on Runoff Projections, Journal of Hydrometeorology, 10, 1168-1183, 2009.

Ragab, R., Bromley, J., Dorflinger, G., and Katsikides, S.: IHMS—Integrated Hydrological Modelling System. Part 2. Application of linked unsaturated, DiCaSM and saturated zone, MODFLOW models on Kouris and Akrotiri catchments in Cyprus, Hydrological Processes, 24, 2681-2692, 2010.

Vaze, J., Teng, J., and Chiew, F.: Assessment of GCM simulations of annual and seasonal rainfall and daily rainfall distribution across south-east Australia, Hydrological Processes, 25, 1486-1497, 2011b.

Chapter 10

Discussion & Conclusions

10.1 Study limitations

Modeling catchment hydrology and the climatic parameters that affect it, is a process that inevitably involves uncertainties, such as the uncertainty in the hydrological model due to its structure and its calibrated parameters, the uncertainty in downscaling climate parameters, such as the rainfall and the potential evaporation from a coarser GCM resolution to the catchment scale, the uncertainty associated with the GCM model and the scenarios of future emissions of greenhouse gases and other forcing agents.
We have used a well-tested and validated conceptual rainfall-runoff model (CREEK) and have put our model through reasonably rigorous testing by running the model on a daily basis and comparing the results with the observed values. Of course, this engenders more confidence in our climate impact assessment done on monthly and annual basis. The calculation of the potential evaporation was performed by using high resolution MODIS climatic data over the actual catchment and well-tested radiation transfer models. We have assessed the uncertainties sourced by the calibrated model parameters, the downscaling of GCM data over the catchment and the two GCM scenarios. We first discuss the uncertainty sourced by the model structure.

Model structure

Model limitations arise from the structure of the model and the assumptions that were made regarding the physical characteristics of the catchment. It is a conceptual model (CREEK) which considers the catchment as a homogeneous unit with the same physical characteristics across its entire area. Despite its simplicity, the CREEK captures the catchment hydrology well, considering the complexity of the catchment. The most powerful distributed models

which use a large amount of data, do not guarantee better description of the hydrology of a catchment (Beven 1989).
Several assumptions were made considering the initial condition and the physical characteristics of the catchment. The catchment consists of many small aquifers (Georgiou 2002) of different physical characteristics (different effective porosity, gradient etc) and the only realistic modeling approach is to consider them as one united aquifer having the characteristics of the majority of the aquifers. The model parameters though, are related to some extent to the physical characteristics of the catchment and their calibration ensures a good representation of the real catchment. As far as the estimation of the discharge is concerned, the fact that the model is optimized by using stream flow data, reduced considerably the uncertainty in its estimation. However, the model remains unreliable in the estimation of the absolute value of groundwater volume. To have a good estimation of the groundwater volume we should have data from an adequate number of boreholes, concerning characteristics such as the groundwater level, the aquifer's depth etc, which we do not have. Nevertheless, we can make estimates of the relative change in the groundwater level.

Rainfall distribution

The historical analysis of rainfall data (Saitas station) verifies the decreasing trend in annual rainfall, with very good agreement with the GCM predictions from 1956 to the present. During the last century there was no significant change in the number of dry or wet days per decade but rather a slight decrease in the number of very wet days. The model was calibrated using a dry year for the GCM scenarios, which is more representative of a future drier climate. There is also the question of a change in the rainfall intensity distribution. The effect of this on the historical data is implicitly included in the parameter values as the use of daily data precludes the possibility of having information on the diurnal variation in rainfall intensity. Basically, the model only sees the daily rainfall amount. The impact of rainfall intensity is only captured in the stream flow data, and hence this effect is implicitly included in the calibrated parameter values.

Rainfall-runoff model parameters

We have assumed that the model parameter values that represent the catchment response do not change with a changing climate. This may not be true for several reasons. First of all the increased level of greenhouse gases such as CO_2 may affect plant transpiration and vegetation cover, and hence surface albedo and evaporation losses. Further, the decrease in rainfall and the increase in temperature and potential evaporation will lead to a change in the amount

Table 10.1: Differences arising from calibration parameter sets: A - per cent difference between the mean annual simulated and observed discharge for the historical period 1989/90 to 2008/2009, for three different parameter sets. Also shown is the per cent change in the mean annual simulated discharge between the same historical period and the end of 21st century, for the two GCMs scenarios.

Parameters	Period of calibration	A	RCP2.6	RCP8.5
Set 1	1989/90	-1.5	-22.1	-67.8
Set 2	1991/92	-3.1	-21.7	-60.2
Set 3	1989/90-1994/95	-12.1	-20.9	-58.9

of water stored in the soil and aquifers, and may affect the type of vegetation cover and hence the interception store. In spite of the modellers best efforts during model development and calibration conditions, we cannot exclude the fact that models may suffer from some limitation in their "climatic extrapolation capacity", especially when the changes considered are greater than the historical variability (observed during calibration), as shown by (Vaze et al. 2010; Merz et al. 2011). The list is not exhaustive, and the evolving catchment would need to be monitored over the years.

In order to investigate the effect of the model parameter values on the future water fluxes we first used three different optimized parameter sets derived from: a) a dry year (1989/90), b) a wet year (1991/92), and c) a combination of dry and wet years (1989/90-1994/95). The difference between simulated and observed long-term annual discharge for the period 1989/90-2008/09 is shown in column 3 of Table 10.1. Model performance was better on the full record of data when the dry year 1989/90 (Set 1) was used as a calibration period. The lower predicted flows corresponding to this dry year calibration is consistent with the findings of Coron et al. (2012).

The per cent change of long-term annual simulated discharge between the periods 1989/90-2008/09 and 2080/81-2099/00 and for the two scenarios are shown in columns 4 and 5, respectively. The model, for the period 1989/90-2008/09, underestimates the long-term annual discharge by 1.5% up to 12.1% depending on the set of optimized parameters. The percent change between long-term annual historical and future simulated discharge is from 20.9% to 22.1% for the RCP2.6 scenario and from 58.9% to 67.8% for the RCP8.5 scenario, implying that different sets of parameter values give a different reduction in discharge. However, the worse case scenario is still for reductions in future discharge between about 60 and 70%, a significant reduction in water inflow into the Kouris dam, and by extension to the other dams of Cyprus.

Further, in order to explore the effect of uncertainties in the most sensitive parameters on

Table 10.2: The per cent change in the simulated discharge due to changes in key model parameters.

Parameter	+5%	+10%	-5%	-10%
L_{max}	-1.4	-2.8	1.3	2.9
S_{max}	-3.6	-7.2	3.8	8.3
p_0	-0.2	-0.4	0.1	0.5
γ	-2.5	-4.9	2.4	5.2
L_{max}, S_{max}, p_0	-5.2	-10.3	5.5	11.9
ALL	-7.8	-15.2	8.1	16.7

the simulated discharge (1989/90-2008/09) we performed a sensitivity analysis by changing their value by ±5% and ±10%. The effect on the simulated discharge is shown in Table 10.2. The most sensitive parameters are the interception store capacity L_{max}, the soil store capacity S_{max}, the percolation rate p_0 and γ the power law for contribution to flow from the soil store. The increase in the value of each one of the above parameters results in a reduction in the simulated discharge whilst a reduction in their value results in an increase in the simulated discharge. If more than one parameter changes then the effect in the simulated discharge is reinforced.

The 5% and 10% changes in the value of these parameters results in a change in the simulated discharge that ranges from -0.2% to -15.2% (when parameter values increase) and from 0.1% to 16.7% (when parameter values decrease). Whether a parameter value will change or not under changing climatic conditions is an open question that will need to be continuously assessed in coming years by more sophisticated evolving models designed to monitor the trends in water resource availability. We should mention though that several attempts have already been made in order to investigate parameter instability with changing climate (Coron et al. 2012; Brigode et al. 2013). Under a more arid climate the vegetation cover, and hence L_{max}, might be reduced and from Table 10.2 we see that the discharge will increase, due to a reduction in evaporation losses, however, this could be more than compensated by an increase in the surface albedo. A subsequent increase in erosion, coupled with a possible increase in rainfall intensity because of more extreme events, might lead to a reduction also in the soil storage, S_{max}. Percolation might also increase in a more arid climate as fractures and fissures increase as the top soil is lost.

Downscaling factors and scenarios

There is also the question of how well the downscaled GCM data are representative of the catchment. The per cent difference between the long-term GCM historical annual rainfall

Table 10.3: Per cent change from the present (1989/90-2008/09), to the periods C (2030/31-2049/50) and D (2080/81- 2099/100) for the two GCM scenarios, in long-term average annual surface runoff, actual evaporation, recharge, net recharge and annual PE.

Water Fluxes	RCP2.6				RCP8.5			
	C		D		C		D	
	SF1	SF2	SF1	SF2	SF1	SF2	SF1	SF2
Discharge	-2.3	-8.2	-22.5	-27.8	-35	-36.7	-68.1	-69.1
Evaporation	0	1.2	-5.2	-4.1	-9.1	-8.7	-18.1	-17.8
Recharge	-0.2	-1.2	-2.8	-3.8	-7.7	-8.3	-16.1	-16.9
Net Recharge	-1.6	-2.6	-4.6	-5.5	-12.2	-12.8	-18.3	-18.9
Annual PE	-3.7	-2.2	-2.6	-1.3	-1.0	-0.4	4.4	5.1

and the corresponding average annual rainfall observed by the ground-based Saitas gauge in the catchment varies from -2.3% (1955/56- 1974/75) to -0.6% (1985/86-2004/05), so the uncertainty in the catchment rainfall due to downscaling should be small.

We have also looked at the uncertainty due to the downscaling of the GCM physical conditions over Cyprus to the catchment scale that are used to compute potential evaporation. By using the two different monthly scaling factors SF1 (the average for the years 2006 and 2007) and SF2 (the five-year mean for the period 2002/2003-2007/2008), we estimated the effect on the water fluxes. In Table 10.3 the per cent change from the present (1989/90-2008/09) for the various modelled water fluxes is given for the two GCM scenarios. We see that, the estimated reduction in the water fluxes is not significantly different whether the SF1 or SF2 scaling factors are used.

Further, we also see in Tables 9.5 and 9.6 that the water fluxes for the period 2006/2007-2015/2016 computed from the GCM mild scenario data are in good agreement with those given by the model for the present period 1989/90-2008/2009, based on the observed climatic data.

10.2 Recommendations for further work

The present study assessed the impact of climate change on the water resources of the most important catchment of Cyprus. The application of the model to other important catchments of Cyprus will strengthen the conclusions we draw about the impact of climate change to Cyprus water resources. Also, the use of more than one hydrological models to assess the climate change impact will add value to the prediction and reduce the uncertainty sourced from the hydrological model. The largest uncertainty though in climate change impact studies is attributed to the type of GCM that is used (Prudhomme et al. 2003), so the use of several

GCM models and scenarios will help in assessing better the impact of climate change on Cyprus water resources.

10.3 Conclusions

The focus of the present work was to assess the historical and future water resource trends of Cyprus. To achieve this we used a modeling approach that is a synthesis of models and data to simulate trends in catchment water fluxes, an approach applicable to any catchment. The set of models comprises a conceptual daily rainfall-runoff model, radiation transfer models and GCM scenarios downscaled to the catchment level. The rainfall-runoff model was adapted to the Kouris catchment of Cyprus and model input data included rainfall, potential evaporation and discharge for validation. The radiation models used MODIS climatological data at high resolution (10 × 10 km) over the catchment. For the historical period, the model was run using daily rainfall data from a network of ground-based stations within the catchment. Monthly potential evaporation was estimated from high resolution satellite climatic data over the catchment and ground-based wind data. We focused on annual and monthly values of the water fluxes and we found that surface runoff is very sensitive to rainfall and a reduction in rainfall is amplified in runoff by two to three times. Both the historical trends and the GCM predictions strongly point towards a future drier climate for Cyprus. The historical analysis of the annual rainfall of the catchment shows a reduction of 2 mm per year for the 20^{th} century. For the 21^{st} century, the catchment annual rainfall is expected to follow a decreasing trend of about 1.73 mm/yr. For the period 1969/70 - 2008/09 (forty years) the reduction in long-term mean annual rainfall and discharge was about 7% and 38%, respectively. We note that there has been also a local warming over Cyprus of about 1.3 °C (rise in mean annual temperature) over the 20^{th} century (Price et al. 1999), which is double the global average. By the end of the 21^{st} century, the reduction in long-term mean annual values is expected to be from 7% to 24% for the rainfall and from about 22% to 68% for the discharge, for the range of climate changes predicted by the mild and extreme emission scenarios, respectively.

Bibliography

Beven, K.: Changing Ideas in hydrology-The case of physically-based models, Journal of Hydrology, 105, 157-172, 1989.

Brigode, P., Oudin, L., and Perrin, C.: Hydrological model parameter instability: A source of additional uncertainty in estimating the hydrological impacts of climate change?, Journal of Hydrology, 476, 410-425, 2013.

Coron, L., Andreassian, V., Perrin, C., Lerat, J., Vaze, J., Bourqui, M., and Hendrickx, F.: Crash testing hydrological models in contrasted climate conditions: An experiment on 216 Australian catchments, 48, doi:http://dx.doi:10.1029/2011WR011721, 2012.

Georgiou, A.: Reassessment of the island's water resources and demand, Objective 1 - Output 1.4.2, Assesssment of Groundwater Resources of Cyprus, Ministry of Agriculture, Natural Resources and Environment of the Republic of Cyprus, 2002.

Merz, R., Parajka, J., and Blöschl, G.: Time stability of catchment model parameters: Implications for climate impact analyses, Water Resources Research, 47, 2011.

Price, C., Michaelides, S., Pashiardis, S., and Alpert, P.: Long term changes in diurnal temperature range in Cyprus, Atmospheric Research, 51, 85-98, 1999.

Prudhomme, C., Jakob, D., and Svensson, C.: Uncertainty and climate change impact on the flood regime of small UK catchments, Journal of Hydrology, 277, 1-23, 2003.

Vaze, J., Post, D., Chiew, F., Perraud, J.-M., Viney, N., and Teng, J.: Climate non-stationarity-validity of calibrated rainfall-runoff models for use in climate change studies, Journal of hydrology, 394, 447-457, 2010.

Appendices

Appendix A

Penman Potential Evaporation

Potential evaporation depends on the available energy for evaporation and the water vapour transfer from the surface to the atmosphere. The available energy is defined as the difference between the net solar energy entering the earth-atmosphere system and the thermal energy re-radiated back to space from the system. It is computed using atmospheric radiation transfer models (Hatzianastassiou and Vardavas 2001a,b; Pavlakis et al. 2007; Vardavas and Taylor 2011) developed from a radiative-convective model (Vardavas and Carver 1984). The evaporation due to water vapour transfer is estimated by using satellite derived climatic data of humidity, air temperature and air pressure, and wind speed data obtained from a representative meteorological station (Agros station) within the catchment. The climatological data were obtained from the Moderate Resolution Imaging Spectroradiometer (MODIS), on board NASA's Terra and Aqua satellites which pass over the catchment from 11 a.m. to 1 p.m.and 1 p.m. to 3 p.m., respectively. The potential evaporation of the catchment is then the average potential evaporation computed using Terra and Aqua data.

Analytically (Vardavas 1987), assuming that there is no heat advection or storage, the Penman potential evaporation rate E (in mm/day) is given as the weighted average of the evaporation rate E_s due to solar heating and the aerodynamic evaporation rate E_a due to the wind (Penman 1948) so as

$$E = \left(\frac{\Delta}{\Delta + \gamma}\right) E_s + \left(\frac{\gamma}{\Delta + \gamma}\right) E_a \tag{A.1}$$

where Δ is the slope of the saturation water vapour pressure curve with respect to the air temperature T (it is computed at T_a the atmospheric temperature above the water surface) and γ is the psychrometric constant in mbar K^{-1} and it is given by Brutsaert (1984) as

$$\gamma = \frac{c_p p M_d}{L M_v} \tag{A.2}$$

with c_p=0.24 cal g^{-1} K^{-1} the specific heat of moist air, p the surface atmospheric pressure in mbar, M_d and M_v the mean molecular weights of dry air and water vapour respectively with M_v/M_d=0.622 and L the latent heat of evaporation in cal g^{-1} which is given by

$$L = 597.3 - 0.553\,(T - T_o) \tag{A.3}$$

with T_o=273.15 K.

Estimation of E_s

E_s (in mm/day) depends on the available energy and it is given by

$$E_s = \frac{239 Q_n}{L\rho} \tag{A.4}$$

where ρ=1 g cm^{-3} is the density of water, L was defined above and Q_n is the net all-wave flux (MJ m^{-2} day^{-1}) above the water surface given by

$$Q_n = \bar{F}^{\downarrow}_{sol} - \bar{F}^{\uparrow}_{tr} \tag{A.5}$$

where $\bar{F}^{\downarrow}_{sol}$ and $\bar{F}^{\uparrow}_{tr}$ represent the net downward flux and the net upward terrestrial flux at the water surface, respectively.

Estimation of E_a

E_a depends mainly on the wind speed and the water vapour pressure deficit and it is given by (Penman 1948)

$$E_a = f(\bar{u})\,[e_s\,(T_a) - e\,(T_a)] \tag{A.6}$$

where $f(\bar{u})$ is the wind function and $\bar{u}$ is the mean wind speed, $e_s\,(T_a)$ is the saturation vapour pressure at the water surface, evaluated at the air temperature T_a and $e(T_a)$ is the vapour pressure at some height above the water surface. The wind function is either empirically determined or evaluated theoretically from similarity profile functions (Brutsaert 1984), which for neutral conditions is given by:

$$f(\bar{u}) = \left[\frac{M_v}{M_d}\right] \frac{a_v k^2 \bar{u}}{D} \tag{A.7}$$

with

$$D = R_d T_a \ln\left[\frac{z_2 - d_0}{z_{0v}}\right] \ln\left[\frac{z_1 - d_0}{z_{0m}}\right] \tag{A.8}$$

where k=0.42 is the Von Karman constant, a_v=1.13 (Pruitt et al. 1973) is the ratio of the eddy diffusivity for water vapour and the eddy viscosity, M_v/M_d =0.622, R_d is the gas constant for dry air, z_1 is the level of the wind speed measurement and z_2 that for the water vapour pressure. For a smooth surface, such as a water surface, d_0 =0 and the momentum roughness can be evaluated from:

$$z_{0m} = \frac{0.135v}{u_*} \tag{A.9}$$

with the roughness length for water vapour given by:

$$z_{0v} = \frac{0.624v}{u_*} \tag{A.10}$$

The friction velocity u_* can be evaluated using the logarithmic wind profile law for mean wind speed:

$$\bar{u} = \frac{u_*}{k} \ln\left[\frac{z_2 - d_0}{z_{0m}}\right] \tag{A.11}$$

which from equation 9 reduces to:

$$\bar{u} = \frac{u_*}{k} \ln\left[\frac{z_2 u_*}{0.135v}\right] \tag{A.12}$$

The above equation can be solved for u_* using the Newton-Raphson iteration given a wind speed measurement at height z_2. In the above, v is the kinematic viscosity (m^2s^{-1}) of air, which can be computed with reasonable accuracy from:

$$v = 2.964 \times 10^{-6} \frac{T_a^{3/2}}{p} \tag{A.13}$$

where p the atmospheric pressure in mbar and the temperature T_a in K. If

$$C_w = \frac{3966}{T_a \ln\left[\frac{z_2}{z_0}\right] \ln\left[\frac{z_1}{z_{0m}}\right]} \tag{A.14}$$

$$E_a = C_w \bar{u} (1 - r_H) e_s (T_a) \tag{A.15}$$

where E_a is measured in mm/day, $\bar{u}$ in m/s, $e_s(T_a)$ in mbar and r_H the relative humidity.
Once the E_s and E_a are evaluated the potential evaporation rate E can be computed from equation 10.1. Thus, the long-term mean monthly potential evaporation for the period 2002

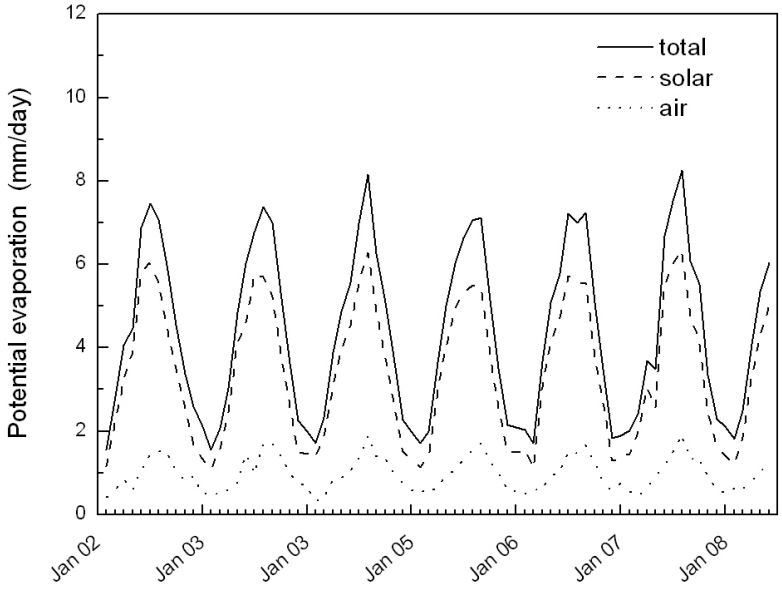

Figure A.1: Mean solar, air and total potential evaporation for the period 1/1/2002 to 31/12/2007.

to 2007 can be estimated. The contribution of the wind component (second term of equation A.1), to the total potential evaporation, is on average 24% for the period 2002-2007 implying that solar heating is more important than the wind in estimating the potential evaporation over the catchment (see Figure A.1). Thus, using wind data from only one station within the catchment for estimating potential evaporation does not introduce great errors and we expect the potential evaporation to be insensitive to the surrounding topography.

Bibliography

Brutsaert, W.: Evaporation in the Atmosphere: Theory, History and Applications, D. Reidel, Dordrecht, The Netherlands, 299, 1984.

Hatzianastassiou, N. and Vardavas, I.: Shortwave radiation Budget of the Southern Hemisphere using ISCCP C2 and NCEP-NCAR climatological data, Journal of Climate, 14, 4319-4329, 2001a.

Hatzianastassiou, N. and Vardavas, I.: Longwave radiation Budget of the Southern Hemisphere using ISCCP C2 climatological data, Journal of Geophysical Research, 106, 17 785-17 798, 2001b.

Pavlakis, K. G., Hatzidimitriou, D., Drakakis, E., Matsoukas, C., Fotiadi, A., Hatzianastassiou, N., and Vardavas, I.: ENSO surface longwave radiation forcing over the tropical Pacific, Atmospheric Chemistry and Physics, 7, 2013-2026, 2007.

Penman, H., L.: Natural evaporation from open water, bare soil and grass, Proc. R. Soc. London Ser. A, 193, 120-145, 1948.

Pruitt, W., Morgan, D., and Laurence, F.: Momentum and mass transfers in the surface boundary layer, Quarterly Journal of the Royal Meteorological Society, 99, 370-386, 1973.

Vardavas, I. and Carver, J.: Solar and terrestrial parameterizations for radiative-convective modelsWater resources in the desertification-threatened Messara Valley of Crete: estimation of potential lake evaporation, Planet. Space Sci., 32, 1307-1325, 1984.

Vardavas, I. and Taylor, F.: Radiation and Climate: Atmospheric Energy Budget from Satellite Remote Sensing, International Series of Monographs on Physics, OUP Oxford, 2011.

Vardavas, I. M.: Modelling the seasonal variation of net all-wave radiation flux and evaporation in a tropical wet-dry region, Ecological Modelling, 39, 247-268, 1987.

List of Figures

1.1 The East Mediterranean with the island of Cyprus shown near the Middle East coast. . . . 9
1.2 A geological map of Cyprus. . . . 10
1.3 Cyprus annual precipitation since the beginning of the 20^{th} century. The regression line is also shown. . . . 12

2.1 The Kouris catchment with the river network and a map of Cyprus with an outline of the catchment boundary. Also shown is the location of Cyprus in the Eastern Mediterranean region. . . . 18
2.2 The Kouris dam . . . 18
2.3 Wild vegetation of Troodos. . . . 19
2.4 Troodos cedar forest. . . . 19
2.5 Vineyards on the south slopes of Troodos. . . . 20
2.6 Outcrop of harzburgite (background) and gabbro (foreground) in a tectonic contact at the Troodos ophiolite. . . . 21
2.7 Sheeted dykes of Troodos ophiolite. . . . 22
2.8 Outcrop of pillow lavas of Troodos ophiolite. . . . 22
2.9 Chalks and marls in the sedimentary complex. . . . 23

3.1 Annual rainfall of the 16 stations plotted against elevation for the hydrological years 1989/90 to 1992/93. . . . 29
3.2 Annual rainfall of the 16 stations plotted against elevation for the hydrological years 1993/94 to 1996/97. . . . 30
3.3 Annual rainfall of the 16 stations plotted against elevation for the hydrological years 1997/98 to 2000/01. . . . 31
3.4 Annual rainfall of the 16 stations plotted against elevation for the hydrological years 2001/02 to 2004/05. . . . 32

3.5 Annual rainfall of the 16 stations plotted against elevation for the hydrological years 2005/06 to 2008/09. 33
3.6 Annual rainfall distribution for the period 1989/90 to 2008/09. 36
3.7 Diversion of Diarizos river via Arminou tunnel (from the WDD). 38
3.8 Seasonal variability of rainfall and discharge for the period 1989/90 to 2008/09. 39
3.9 Lag in months between peak rainfall and peak discharge for the period 1989/90 to 2008/09. Annual rainfall is also shown. 40
3.10 Distribution of annual discharge for the period 1989/90 to 2008/09. 40
3.11 Annual pan evaporation for the Kouris, Saitas and Agros meteorological station for the period 1989/90 to 2008/09. 42
3.12 Long-term mean monthly pan evaporation for the period 1989/90 to 2008/09. 42
3.13 Annual variation of rainfall, discharge, pan and potential evaporation. Numbers in parentheses refer to long-term mean values for the period 1989/90 to 2008/09 for the rainfall, the discharge and the pan evaporation and for the period 2002/03 to 2006/07 for the potential evaporation. 44
3.14 Seasonal variation of rainfall, discharge, pan and potential evaporation. . . . 44
3.15 Monthly pan and potential evaporation for the period 1/1/2002 to 31/12/2007. 45
3.16 Pan coefficient long-term averages for the period 1/1/2002 to 31/12/2007. . . 46

4.1 A flow diagram of the conceptual rainfall-runoff model. 51

5.1 Daily simulated and observed discharge at the catchment outlet for low-flow hydrological years 1989/90, 1990/91, 1993/94, 1995/96, 1996/97, 1997/98. Hydrological year begins on 1st October and ends 30th September. 64
5.2 Daily simulated and observed discharge at the catchment outlet for low flow hydrological years 1998/99, 1999/00, 2000/01, 2004/05, 2005/06, 2006/07, 2007/08 and 2008/09. 65
5.3 Daily simulated and observed discharge at the catchment outlet for high flow hydrological years 1991/92, 1992/93, 1994/95, 2001/02, 2002/03 and 2003/04. 66
5.4 Annual and monthly simulated and observed discharge at the catchment outlet. 67
5.5 Normal and logarithmic transformation of simulated and observed flow (bin data) duration curves for the period 1989/90 to 2008/09. 68
5.6 Scatter diagram with regression line and 95% confidence band of annual simulated and observed discharge. Numbers in parentheses represent the hydrological years with big divergences between model and observed flow. 71

5.7 Scatter diagram with regression line and 95% confidence band of monthly simulated and observed discharge. Numbers in parentheses represent the months of a specific year with big divergences between model and observed flow. 72
5.8 Scatter diagram with regression line and 95% confidence band of monthly simulated and observed discharge without the values of January and February 2004. 72
5.9 Runoff coefficient derived from Fourier analysis of rainfall and discharge data (simulated and observed), demonstrating the quick response of the catchment and the one day delay in the peak flow after the last rainfall, with DEL_0=0.5 obtained by model optimization. 73
5.10 Runoff coefficient derived from Fourier analysis of rainfall and discharge data (simulated and observed), demonstrating the quick response of the model catchment to the rainfall event if DEL_0 parameter is set equal to 1, no delay. . 74

6.1 Long-term monthly rain and potential evaporation for the period 1989/90 to 2008/09. 78
6.2 Long-term mean monthly simulated actual, soil and interception plus surface evaporation for the period 1989/90 to 2008/09. 79
6.3 Simulated soil water content with years. 79
6.4 Mean monthly simulated soil and actual evaporation with years. 80
6.5 Long-term mean monthly potential, actual and pan evaporation for the period 1989/90 to 2008/09. 81
6.6 Variation of potential, actual and pan evaporation with years. Numbers in parentheses represent long-term mean annual values of the period 1989/90 to 2008/09. The actual evaporation is 463 mm or 74% of the mean annual rainfall of 623 mm for the same period. 81
6.7 Long-term mean monthly fast and slow discharge. Numbers in parantheses represent mean annual values. 82
6.8 Scatter diagrams of observed and simulated annual discharge versus annual rainfall, for the period 1989/90 to 2008/09. Linear and quadratic fits valid only for the rainfall range 400-900 mm. 83
6.9 Scatter diagrams of observed and simulated annual discharge versus annual rainfall, for the 15 years, of period 1989/90 to 2008/09, with annual rainfall from 400 to 600 mm. 84

6.10 Scatter diagrams of observed and simulated annual discharge versus annual rainfall, for the 15 years, of period 1989/90 to 2008/09, with annual rainfall from 400 to 700 mm. 85
6.11 Scatter diagrams of runoff coefficient versus annual rainfall, for the observed and the simulated discharge data and for the period 1989/90 to 2008/09. . . . 86
6.12 Simulated groundwater level for the period 1989/90 to 2008/09, expressed as meters below surface 88
6.13 Simulated and observed (from boreholes tests) groundwater level, for the month April, expressed as meters below surface 89
6.14 Long-term annual means of rainfall, discharge, actual evaporation and net recharge from the rainfall-runoff model for the period 1989/90 to 2008/09. . 90

7.1 Catchment annual rainfall and Saitas annual rainfall with years, for the period 1986/87 to 2009/10. Numbers in parantheses are mean values for the above period. 96
7.2 Scatter diagram of the Saitas annual rainfall versus catchment annual rainfall for the period 1986/87 to 2009/10. 96
7.3 Scatter diagram of annual rainfall at Saitas station for the period 1916/17 to 2009/10. 97
7.4 Long-term decadal rainfall of Saitas station for the period 1919/20 to 2008/09. 98
7.5 Frequency of dry and wet years in every decade. 99
7.6 Frequency of winter days per decade, with no rain and with rain exceeding 20 mm/day. 99
7.7 Scatter diagram of January rainfall at Saitas station. 100
7.8 Scatter diagram of February rainfall at Saitas station. 100
7.9 Long-term monthly rainfall at Saitas station for the periods 1916/17 to 1945/46 and 1980/81 to 2009/10. 101
7.10 Scatter diagram of mean annual temperature with years at Lefkosia station, for the period 1901 to 2004. 102
7.11 Catchment annual discharge and Saitas annual rainfall for the period 1969/70 to 2008/09. 102

8.1 The ECHAM6 grid cells of 1.9-degree grid resolution that cover Cyprus. . . 106
8.2 Comparison of the long-term decadal observed rainfall (Saitas station) and GCM historical rainfall for the period 1916/17 to 2004/05, showing the good agreement from the decade starting in 1956. 108

8.3 Long-term decadal rainfall for Cyprus from GCM data for the period 1856 to 2095. 108
8.4 GCM historical mean annual rainfall and January mean rainfall, over Cyprus, for the period 1850/51 to 2004/05. Linear regression lines are also shown. . . 109
8.5 Twenty-year long-term monthly rainfall from GCM historical data. Numbers in parantheses represent mean annual values. 110
8.6 Mean annual rainfall and January mean rainfall, over Cyprus for the GCM RCP8.5 scenario, for the period 2006/07 to 2099/00. Linear regression lines are also shown. 111
8.7 Long-term mean monthly rainfall over Cyprus, for the RCP2.6 and the RCP8.5 scenarios, for the periods 2006/07 to 20015/16 and 2080/81 to 2099/00. Numbers in parentheses represent mean annual values. 113
8.8 Mean annual temperatures over Cyprus for the RCP2.6 and the RCP8.5 scenarios, for the period 2006/07 to 2099/00. Regression lines are also shown. . 114
8.9 Decadal mean monthly temperatures over Cyprus for the RCP2.6 and the RCP8.5 scenarios for the periods 2006/07 to 2015/16 and 2090/91 to 2099/00. Number in parentheses represent long-term mean annual values. 115
8.10 Mean annual and mean monthly for the month April, potential evaporation over Cyprus, for the period 2006/07 to 2099/00, for the RCP8.5 scenario. . . 117
8.11 Long-term decadal annual potential evaporation and temperature over Cyprus, for the period 2006/07 to 2095/96, for the RCP2.6 scenario. 118
8.12 Long-term decadal annual potential evaporation and temperature over Cyprus, for the period 2006/07 to 2095/96, for the RCP8.5 scenario. 118
8.13 Long-term mean monthly potential evaporation over Cyprus for the RCP2.6 and RCP8.5 scenarios. Numbers in parentheses represent mean annual values. 119

9.1 Scatter diagrams of mean monthly PE computed from the RCP2.6 and the RCP8.5 scenarios with mean monthly PE computed from MODIS data over the catchment, for the years 2006 and 2007. Regression lines are also shown. 126
9.2 Scatter diagrams of the five-year mean monthly PE (1/1/2006 to 31/12/2011) computed from the GCM data and the five-year mean monthly PE (period 1/1/2002 to 31/12/2007) computed from the observed climatological data. Regression lines are also shown. 127
9.3 Mean monthly PE computed from the RCP2.6 and the RCP8.5 scenarios with mean monthly PE computed from MODIS data over the catchment, for the years 2006 and 2007. Numbers in parentheses represent mean annual values. 128

9.4 The five-year mean monthly PE (1/1/2006 to 31/12/2011) computed from the GCM data and the five-year mean monthly PE (period 1/1/2002 to 31/12/2007) computed from the observed climatological data. Numbers in parentheses represent mean annual values. 131
9.5 Long-term mean monthly rainfall and simulated discharge for the two GCM scenarios, for the periods 1989/90 to 2008/09 and 2080/81 to 2099/00. Numbers in parentheses represent mean annual values. 134
9.6 Long-term mean monthly catchment potential evaporation for the period 1989/90 to 2008/09 and for the period 2080/81 to 2099/00 for the two GCM scenarios. Number in parentheses represent mean annual values. 135

A.1 Mean solar, air and total potential evaporation for the period 1/1/2002 to 31/12/2007. 152

List of Tables

3.1 Characteristics of rainfall stations 27

3.2 Annual rainfall at the 16 stations 34

3.3 Weights of rainfall stations 35

3.4 Characteristics of discharge stations 37

3.5 Characteristics of pan evaporation stations 41

4.1 The set of model parameters 50

4.2 Values of model parameters, search range and sensitivity of the objective function to a 10% change in a parameter value. 60

5.1 Values on a daily basis of the objective function χ^2 , relative error ε and Nash-Sutcliffe efficiency *NSE* for each hydrological year. Also shown are the *NSE* values on a monthly basis. The total number of days with no flow is also shown 70

6.1 The percentage of rainfall that goes to discharge, evaporation and recharge. . 91

9.1 The scaling factors for the RCP8.5 GCM scenario period 2080/81 to 2099/00 and for the four different historical reference periods. 124

9.2 The rainfall scaling factor used for the two GCM scenarios and for the periods 2006/07-2015/15, 2030/31-2049/50 and 2080/81-2099/00. The reference GCM historical period is the period 1985/86-2004/05. 125

9.3 The mean PE computed from the MODIS data (2002-2007) and the mean scaled PE for the two GCM scenarios and for the periods 2006/07-2015/16, 2030/31-2049/50 and 2080/81-2099/00, using the scaling factor SF1. The per cent difference with respect to the MODIS 2002-2007 mean PE is also shown. 129

9.4 The mean PE computed from the MODIS data (2002-2007) and the mean scaled PE for the two GCM scenarios and for the periods 2006/07-2015/16, 2030/31-2049/50 and 2080/81-2099/00, using the scaling factor SF2. The per cent difference with respect to the MODIS 2002-2007 mean PE is also shown. 130
9.5 Long-term averages in Mm^3 of catchment annual rainfall, discharge, actual evaporation, recharge and net recharge. The total PE in mm/yr is also given. Present period A (1989/90-2008/09), and periods B (2006/2007-2015/2016), C (2030/31-2049/50) and D (2080/81-2099/100) for the two GCM scenarios. The scaling factor SF1 was used for scaling the PE. 132
9.6 Long-term averages in Mm^3 of catchment annual rainfall, discharge, actual evaporation, recharge and net recharge. The total PE in mm/yr is also given. Present period A (1989/90-2008/09), and periods B (2006/2007-2015/2016), C (2030/31-2049/50) and D (2080/81-2099/100) for the two GCM scenarios. The scaling factor SF2 was used for scaling the PE. 132

10.1 Differences arising from calibration parameter sets: A - per cent difference between the mean annual simulated and observed discharge for the historical period 1989/90 to 2008/2009, for three different parameter sets. Also shown is the per cent change in the mean annual simulated discharge between the same historical period and the end of 21^{st} century, for the two GCMs scenarios. 141
10.2 The per cent change in the simulated discharge due to changes in key model parameters. 142
10.3 Per cent change from the present (1989/90-2008/09), to the periods C (2030/31-2049/50) and D (2080/81- 2099/100) for the two GCM scenarios, in long-term average annual surface runoff, actual evaporation, recharge, net recharge and annual PE. 143